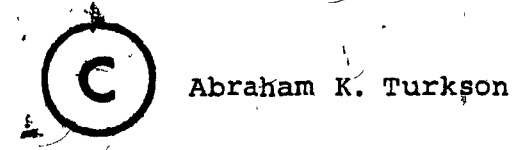
### TANGENTIAL FLOW ELECTROFILTRATION

hv



A Thesis Submitted to the Faculty of Gradua Studies
and Research in Partial Fulfillment of the
Requirements for the Degree of
Master of Engineering

Department of Chemical Engineering McGill University
Montreal, Canada

#### ABSTRACT

In the tangential flow electrofilter, a membrane is supported on a porous cylinder which rotates inside a larger, stationary cylinder. The cylinders are insulated so that an electric field can be applied across the annular gap. The suspension flows axially between the cylinders while the filtrate is removed from the inner cylinder. In this device, the growth of a cake at the membrane surface is minimized by the transport of particles away from the membrane by fluid turbulence, centrifugal force and electrophoresis and by removal of the cake by shear at the rotating surface.

Experiments were conducted with an aqueous latex suspension with 0.02 kg/m<sup>3</sup> particle concentration and 0.60 µm particle diameter and a zeta potential of -60 mV. Filtrate fluxes increased with pressure difference, rotation rate and field strength.

Above a critical field strength, the flux declined. Particle rejections were always above 94%.

A mathematical model was derived to predict the time variation of filtrate flux. The model included cake build-up as well as the four mechanisms acting to minimize cake formation.

#### RESUME

Dans l'électro-filtre à alimentation tangentielle une menbrane est fixée sur un cylindre poreux qui tourne à l'intérieur d'un cylindre stationnaire de plus grande dimension. Les cylindres sont isolés de telle façon qu'un champ électrique peut être appliqué dans l'espace interannulaire. La suspension s'écoule axialement entre les cylindres pendant que le filtrat est recueilli dans le cylindre intérieur. Dans ce montage, la croissance du gâteau à la surface de la menbrane est minimisée par le transport des particulés loin de la menbrane par turbulence, force centrifuge et électrophorèse ainsi que par les forces de cisaillements exercées sur le gâteau à la surface de la menbrane.

Une série d'expériences a été accomplie utilisant une solution aqueuse de latex, concentration des particules 0.02 kg/m³, diamètre des particules 0.60 µm, potential zéta -60 mV. Le taux de filtrat peut être augmenter suivant la différence de pression, la vitesse de rotation et la force du champ. Au dessus d'une certaine valeur du champ, le taux de filtrat diminue à nouveau. Le pourcentage de rejet des particules était maintenu au-dessous de 94%.

Un modèle mathématique a été développé pour prédire la variation du filtrat en fonction du temps. Ce modèle inclus la formation et la croissance du gâteau ainsi que l'effet des quatres mécanismes minimisant la formation du gâteau.

### ACKNOWLEDGEMENTS

The author wishes to express his sincere appreciation and gratitude to:

- Professors M.E. Weber and J.A. Mikhlin, for their advice and support throughout the course of this project.
- Messrs. Andy Krish and Herb Alexander, for speedy attention during equipment breakdowns.
- Ms. Pat Fong, for flawlessly typing this thesis.

To my wife, Florence, for her immeasurable moral support from afar and near, I say a big "thank you".

TO

DAD

WHO MADE IT ALL POSSIBLE

# TABLE OF CONTENTS

	•		_					1					,		_	_
		-						`	,				-	-		Page
ABS	raci		<i>.</i>		•		• •	•	• •			•		٠	•	i
ACKN	OWLE	DGEMENT	s.		(.)	/		•	• •		• •	•	• •	•	• ,	iii
TABI	E OF	CONTEN	ITS .	• •	• •	• • • ,		•		٠.		•	• •	•	<u>ر</u>	<b>v</b>
LIST	OF	FIGURES	• • .		•• •	• •		•			•	٠	• •	•	4 •	viii
LIST	OF	TABLES	• • •	• •	• •	· •		• (	• •	, <b>-</b> •	•	٠		•	•	xi
1.	INTR	ODUCTIO	N		·						ر. پر	•	• •	•	•	1-1
,	1.1	Types	of Fil	ltra	tion	Proc	cess	es .	•		•	•		•	•	1-2
		1.1.1 1.1.2 1.1.3 1.1.4	Depth Cake	Fil.	ltrat trati	ion on		• ' •	•		•	•		•	•	1-3 1-3
		Tangen Object														
2.	REVI	EW OF R	ELATED	), FII	rerat	URE	• •	• •	•	. :	, •	•		.•	•	2-1
	2.1	Cross-	Flow F	'iltı	ratio	n.			•	•, •		•		٠	<i>,</i> •	2-1
, /	/	2.1.1	Conce	ntra	ation	Pol	ari.	zati	lon	Mod	lel	•		•	•	2-1
	2.2	Electr	ofiltr	atio	on .				•		•	•		•	•	2-6
,		2.2.1	Elect	rofi	iltra	tion	Мо	del	•		•	•	• •	•	•	2-8
	2.3	Flow B	etween	Rot	atin	g Cy	lin	ders			•	•		•	•	2-10
,		2.3.1 2.3.2	Rotat Rotat													
3. '	EXPE	RIMENTA	L APPA	RATU	JS AN	D PR	OCE.	DURE			•	•		•	, •	3-1
,	3.2 3.3	Descriper Proper Defini	ical A ation	rrar of E	geme:	nt tyre	ne	 Late	x S	 usp	ens	:10)	n.	•	•	3-1 3-5 3-5 3-7 3-9

•	•	<u> </u>	Page
	3.6 3.7	Procedure for a Run	3-10 3-11
4.	EXPE	ERIMENTAL REŞULTS	4-1
	4.2 4.3	Introduction  Effect of Electric Field on Filtrate Flux	4-1 4-6
	4.5 4.6	Rejection of Particles by the Filter	1-9 1-9
5.	MODE	EL FOR-THE ELECTROFILTER	5-I
	5.1 5.2	Derivation of the Model	5-2 5-5
,	-	5.2.1 Cake Filtration	5-5 5-8 5-10
•	5.3	Expressions for Slip Velocity, U <sub>s</sub> 5	i <b>-</b> 10
А		5.3.1 Velocity Due to Turbulence 5 5.3.2 Velocity Due to Centrifugal Force 5 5.3.3 Velocity Due to Electric Force 5	5-13
<i>(</i> }	5.4 5.5	Cake Removal Rate, $\phi_R$	-14 -15
6.	DISC	CUSSION OF RESULTS	-1
	6.1 6.2	Introduction	-1 -1
		6.2.1 Specific Cake Resistance	-7
	6.3	Behavior at Long Times	-12
	4	6.3.1 Effect of Rotation Rate 6 6.3.2 Effect of Field Strength 6	-14 -17
	6.4	Power Consumption and Flux 6	-20
7.	CONC	LUSIONS	-1
MON	ENCLA'	TURE	-1

## LIST OF FIGURES

<i>→</i> ·		-4
Figure	Caption	Page
1.1	Conventional Filtration	1-1
1.2	Axial/Cross-Flow Filtration	1-5
1.3	Tangential Flow Filtration	\\\\\\\\\\\\\\\\\\\\\\\\\\\\\\\\\\\\\
1.4	Tangential Flow Electrofiltration	1-7
2.1	Macrosolute Concentration Polarization Model	2-2
2.2	Cross-Flow/Electrofiltration Concept	2-9
2:3	Pressure Profile Between Rotating Cylinders	2-14
3.1	Cross-Section of the Tangential Flow Electro-filter	3-2
3.2	Schematic Diagram of Tangential Flow Electro- filtration Flow Loop	3-4
3.3	Electrical Circuit in Tangential Flow Electrofiltration	3~6
4.1	Variation of Flux with Time Showing Effect of Field Strength on Flux, APm 68.9 kPa, N = 0.0 rpm	4-2
4.2	Variation of Flux with Time Showing Effect of Field Strength on Flux, $\Delta P_m = 68.9$ kPa, N = 2000 rpm	4-3
4.3	Variation of Flux with Time Showing Effect of Field Strength on Flux, $\Delta P_m = 137.8 \text{ kPa}$ , N = 1200 rpm	<b>4:-4</b>
4.4	Variation of Flux with Time Showing Effect of Field Strength on Flux, $\Delta P_m = 137.8 \text{ kPa}$ , N = 2800 rpm	4-5
4.5	Variation of Flux with Time Showing Effect of Rotation Rate on Flux, $\Delta P_m = 68.9$ kPa, E = 0.0 and 87.5 V/cm	. 4-7
<b>4.</b> 6	Variation of Flux with Time Showing Effect of Rotation Rate on Flux, $\Delta P_{\rm m} = 137.8$ kPa, E = 0.0 and 87.5 V/cm	4-8

,	Figure.	Caption	Page
ē	4.7	Variation of Flux with Time Showing Effect of Pressure Drop on Flux, E = 0.0 V/cm, N = 0.0 rpm and E = 131 V/cm, N = 2000 rpm	4-10
	4.8	Variation of Rejection with Time Showing Effect of Rotation Rate on Rejection, $\Delta P_m = 68.9 \text{ kPa}$ , $E = 0.0 \text{ V/cm}$	4-11
	4.9	Variation of Rejection with Time Showing Effect of Rotation Rate on Rejection, $\Delta P_m = 137.8 \text{ kPa, E} = 131 \text{ V/cm}$	4-12
	4.10	Reproducibility of Results in Tangential Flow Electrofilter Depicted by Variation of Flux and Rejection with Time, $E=0.0 \text{ V/cm}$ , N= 2000 rpm, $\Delta P_{\text{m}}=68.9 \text{ kPa}$	4-13
	4.11	Reproducibility of Results in Tangential Flow Electrofilter Depicted by Variation of Flux and Rejection with Time, $E = 45 \text{ V/cm}$ , N = 1200 rpm, $\Delta P_{\text{m}} = 137.8 \text{ kPa}$	4-14
	5.1	Cross-Section of Tangential Flow Electrofil-	5-1
	5.2	Variation of Flux with Time Predicted by Model	5-6
	5.3	Cake Filtration Plot of Model Predictions. "	5-7
	5.4	Pressure Variation in the Radial Direction with Inner Cylinder Empty	5-17
	6.1	Plot of $(1/J^2 - 1/J_0^2)$ Versus Time Depicting Small Time Solution to Model, $\Delta P_m = 68.9$ kPa, $E = 0.0$ V/cm	6-2
	6.2	Plot of $(1/J^2 - 1/J_0^2)$ Versus Time Depicting Small Time Solution to Model, $\Delta P_m = 68.9$ kPa, $E = 25$ V/cm	6-3
	6.3	Plot of $(1/J^2 - 1/J_0^2)$ Versus Time Depicting Small Time Solution to Model, $\Delta P_m = 137.8$ kPa, E = 0.0 V/cm	6-4
	6.4	Plot of $(1/J^2 - 1/J_0^2)$ Versus Time Depicting Small Time Solution to Model, $\Delta P_m = 137.8$ kPa, E = 25 V/cm	6-5

Figure	Caption	Page
119410		1490
6.5	Plot of $(1/J^2 - 1/J_0^2)$ Versus. Time Depicting Small Time Solution to Model, $\Delta P_m = 137.8$ kPa, E = 87.5 V/cm	6-6
6.6	Variation of Specific Cake Resistance with Pressure Driving Force	6-9
6.7~	Variation of Specific Cake Resistance with Field Strength, $\Delta P_{m} = 68.9 \text{ kPa}$	6-11,
6.8	Variation of Ratio of Cake Resistance with Field, Strength	6 <b>-13</b>
6.9	Variation of Flux with Rotation Rate Raised to the 0.9 Power, $\Delta P_m = 68.9 \text{ kPa}$	6-15
6.10	Variation of Flux with Rotation Rate Raised to the 0.9 Power, $\Delta P_m = 137.8 \text{ kPa}$	6-16 <sup>°</sup>
6.11	Variation of Flux with Field Strength, ΔP <sub>m</sub> = 68.9 kPa	6-18
6.12	Variation of Flux with Field Strength, $\Delta P_{m} = 137.8 \text{ kPa}$	6-19
6:13	Variation of Filtrate Flux with Total Power Consumed, ΔP <sub>m</sub> = 68.9 kPa	6-23
6.14	Plot of Total Power Per Unit Flux Versus Field Strength, $\Delta P_m = 68.9$ kPa	6-25
.A3.1	Pressure Variation in Radfal Direction with Inner Cylinder Full	A3-2
A4.1°	Plot of Rotation Rate Versus Power Per Unit Length for Tangential Flow Electrofilter	A4-2
A4.2	Plot of Rotation Rate Versus Power Per Unit Length for Margaritis and Wilke Rotorfer- mentor	· A4-3
	at the state of th	1

### LIST OF TABLES

0

Table	<u>Title</u> .	Page
}.1	Properties of Feed System (25°C)	3-8
6.1	Slopes from Plots of J <sub>90</sub> Versus E	6-17
0.2	Calculated Power Requirements	, 6-22
A1-1	Small Time Slopes from Cake Filtration Plots, $\Delta P_{m} = 68.9 \text{ kPa}$	<b>A1-1</b> ,
A1-2	Small Time Slopes from Cake Filtration Plots, $\Delta P_{m} = 137.8 \text{ kPa}$	A1-2
A3-1 .	Filtration Pressure Difference, ΔP <sub>f</sub>	A3-4
A3-2	Fluxes for Distilled Water	<u>A</u> 3−5
A4-1	Power Requirements for Rotorfermentor (RF) and the Tangential Flow Electrofilter (TFE);	A4-1

#### CHAPTER 1

### INTRODUCTION

Filtration is the process in which dispersed particles are separated from a fluid by means of a porous medium. The main features of a conventional filter are shown in Fig. 1.1. The

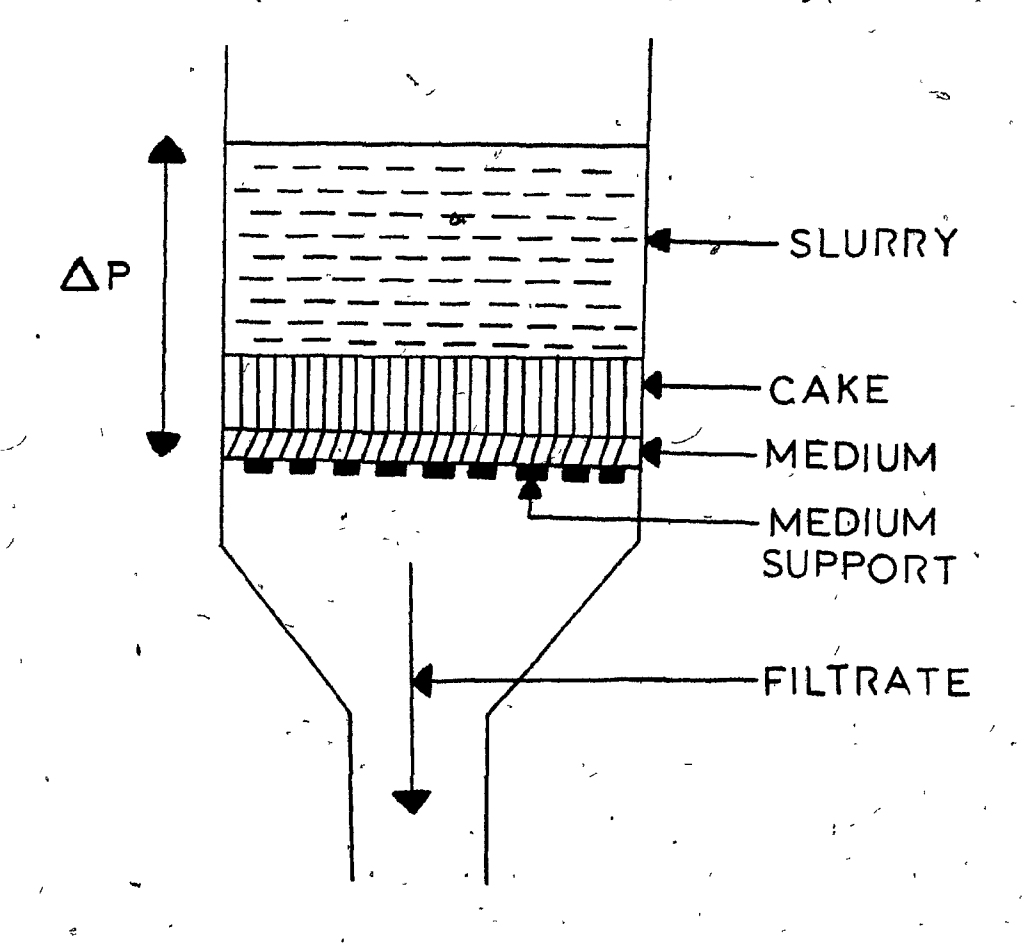


FIGURE 1.1. Conventional Filtration

porous medium is held in place by a support through which the filtrate can easily pass. Particles may be retained either in

the pores of the medium or as a cake on top of the medium or by , a combination of these.

Not all of the features shown in Fig. 1.1 are distinguishable in every filter. For example, in many cartridge filters using paper media, the paper is self-supporting. The choice of a filter design for a given process depends on many factors, among which are the properties of the solid particles such as size, density and compressibility, the concentration of particles, the properties of the suspending fluid such as density and viscosity, the quantity of material to be handled, whether the material to be retained is the solid or the liquid, and whether the process is batch or continuous. Another important factor in the design of a filter is the source of the driving force, which may be gravity, suction on the filtrate side of the medium, pressure on the slurry side of the medium, the application of a centrifugal force or a combination of these. This choice will also depend upon the factors listed above.

#### 1.1 Types of Filtration Processes

Filtration processes are conventionally divided into classes for convenience. However, in virtually all industrial filtration processes more than one of these mechanisms takes part.

### 1.1.1 Medium Filtration

In medium filtration, the particles are retained because they are larger than the holes in the filter medium. The filter

behaves as a sieve.

#### 1.1.2 Depth Filtration

In depth filtration, the particles are retained within the medium even though they are smaller, often very much smaller, than the pores of the medium. (For filtration to occur, the particles must impact on the walls of the pores, hence the particles must leave the fluid streamlines. The rate at which this is achieved depends on the balance of inertial and drag forces experienced by the particles. The medium may be either a bed of granular material or a porous solid. Examples of the former include deep-bed sand filters and precoat filters where, the medium is a bed of diatomageous earth or similar material supported on a coarse screen; and of the latter, felt and sintered metal filters.

### 1.1.3 Cake Filtration

In cake filtration, the solid material accumulates on the surface of the medium, so that after a short initial period, the bed of deposited solid acts as the filter medium. This process continues until the pressure drop across the cake exceeds the maximum permitted by economic or technical considerations or until the space available for the cake is filled. The most important factor in cake filtration is the permeability or resistance of the filter cake. This may be controlled, to some extent, by altering the particle size distribution of the material, sometimes by adding another solid to it.

As stated above, real filtration processes are often composite in nature, several or all of the filtration mechanisms occurring simultaneously or consecutively. For example, in cake filtration, the very important initial layer of the cake must be retained on the surface of the medium by medium filtration. If the pores are larger than the particles, depth filtration must occur until the sizes of the pores are reduced to the point where medium filtration can occur and, subsequently, cake filtration.

### 1.1.4 Axial/Cross-Flow Filtration

The inherent time variation of the filtrate flux under a constant driving force in conventional filtration can be eliminated if the slurry flows parallel to the filter medium rather than perpendicular to it. This mode of operation is called axial or cross-flow filtration. The process is shown in Fig. 1.2.

The movement of the permeate causes particle transport toward the filter medium and leads to an aggregation of particles at the medium. This is counteracted by the sweeping motion of the fluid parallel to the medium. A gradient in the particle concentration is established in the direction perpendicular to the filter medium. This phenomenon, called "concentration polarization", decreases the rate at which permeate or filtrate can be obtained. To reduce concentration polarization, turbulence promoters are sometimes installed on the feed side of the medium.

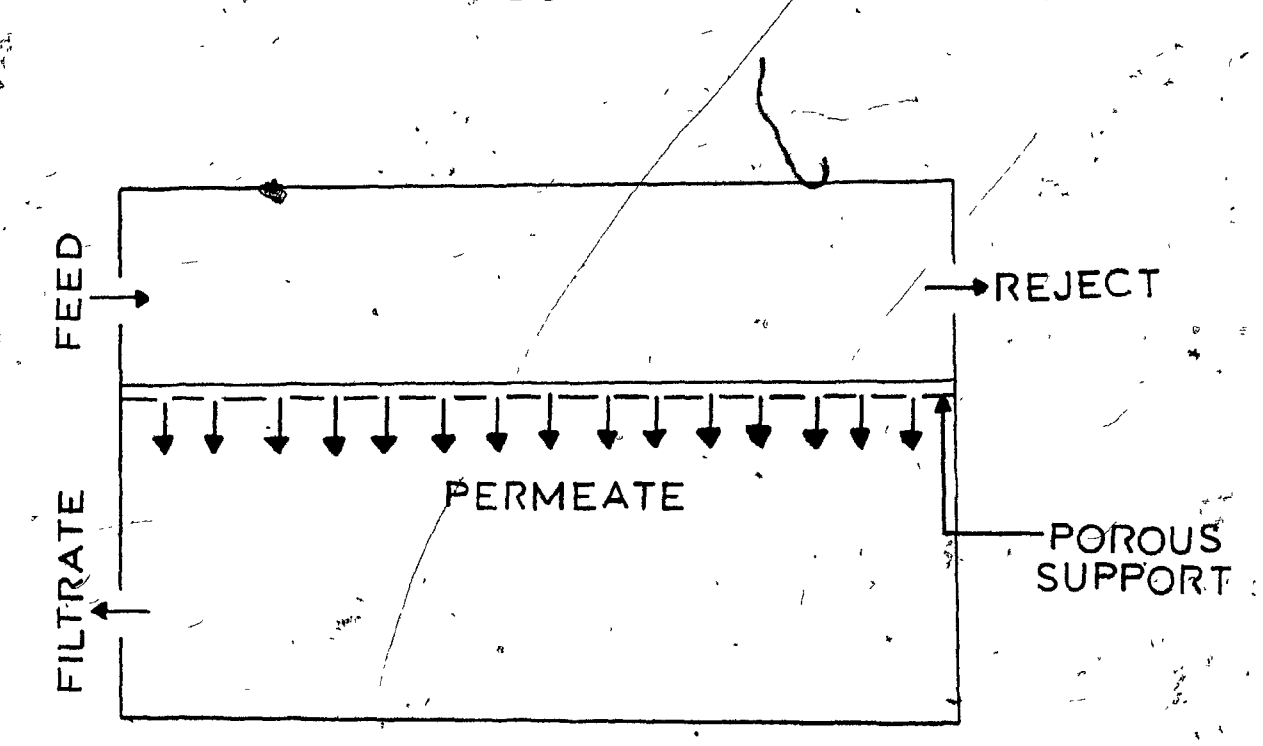


FIGURE 1.2. Axial/Cross-Flow Filtration

Mikhlin (1976) has devised the novel filter sketched in Fig. 1.3. In this device, the filter medium is supported on a porous cylinder which rotates inside a larger, stationary cylinder. The slurry flows in the annular gap between the cylinders while the filtrate is removed from the inside of the rotating cylinder. This process may be called "tangential flow filtration". The superposition of the rotating turbulent flow and centrifugal force upon the axial flow is effective in reducing concentration polarization (Mikhlin and Tanny, 1979). In addition, the rotation increases the shear force on the surface of the cake. This prevents the cake from growing too thick and may actually shear "chunks" of the cake from the medium.

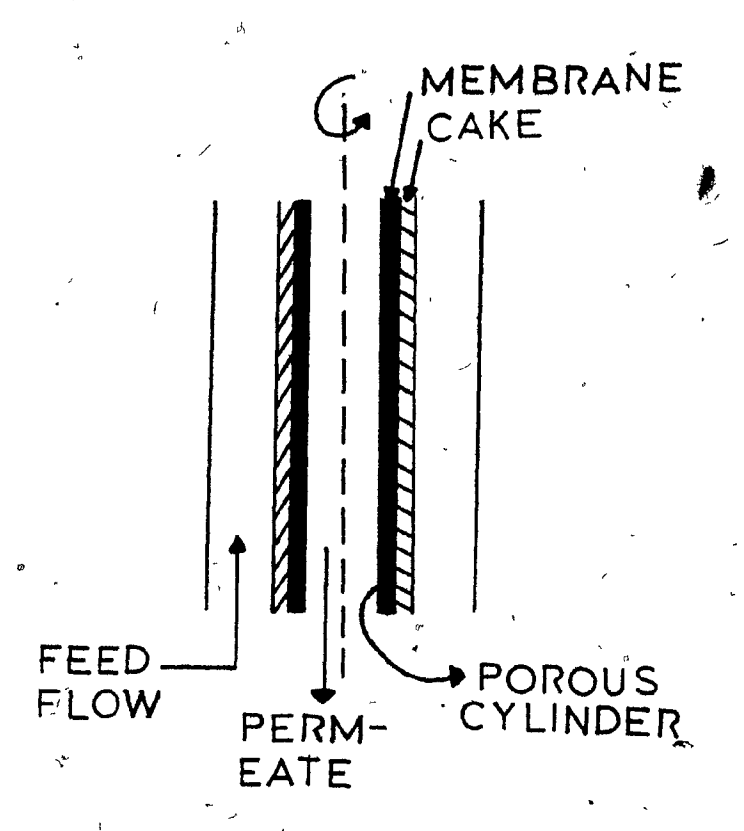


FIGURE 1.3. Tangential Flow Filtration

## 1.2 Tangential Flow Electrofiltration

The present study involves a modification of Mikhlin's tangential flow filter. The basic idea is to add an electrical force directed away from the medium to the forces already present. With the electrical force added, the proposed process may be called "tangential flow electrofiltration". It is hypothesized that the addition of the electrical force will permit larger filtration rates for charged particles. The proposed process combines particle migration away from the filter due to centrifugal forces and fluid turbulence generated by the rotating membrane support and electrophoretic migration due to a DC electrical field applied normal to the medium - see Fig. 1.4.

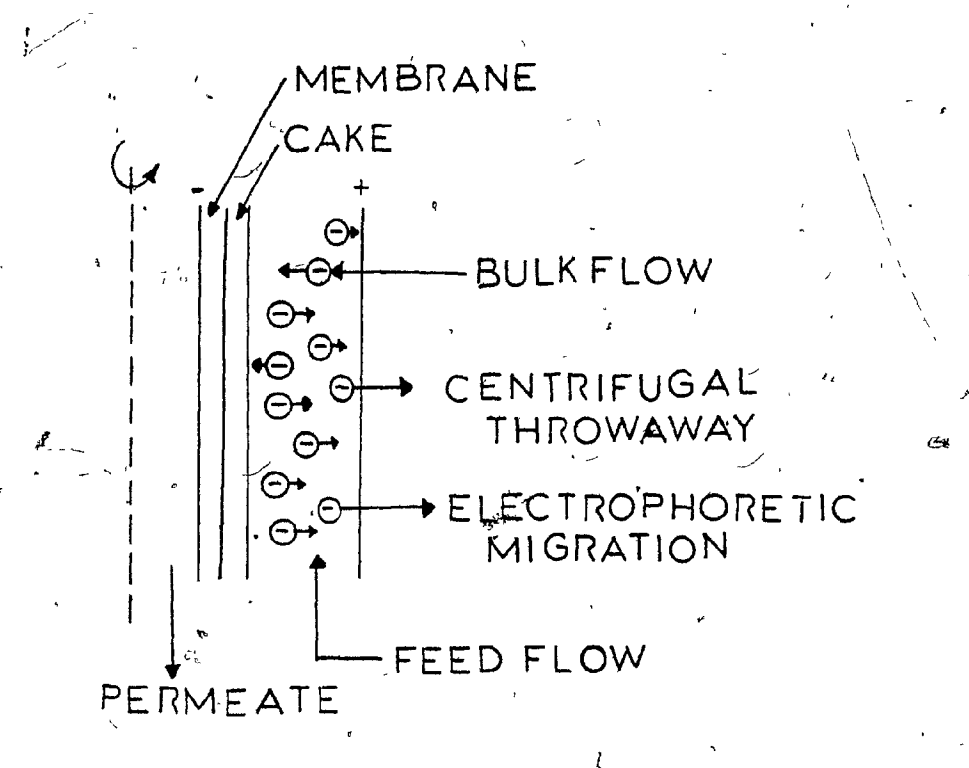


FIGURE 1.4. Tangential Flow Electrofiltration

Dahlheimer et al. (1970) have used cross-flow filtration to dewater suspended solids such as kaolin clay slurries. Henry and Allred (1977) used the cross-flow filtration process to concentrate bacterial cells. Reis and Lightfoot (1976) employed a process known as electropolarization chromatography to fractionate protein mixtures. Owing to the fact that the kaolin particles, bacterial cells and protein mixtures were negatively charged in aqueous suspensions, a DC electric field should improve all of these processes. Tangential flow electrofiltration with its added rotating membrane surface should find application in the filtration, concentration, clarification and fractionation of charged particles suspended in fluids of low electrical conductivity.

### 1.3 Objectives

The objectives of the present work were the following:

- (i) To determine if the application of a DC electric field improves the separation of particles in the tangential flow fulter.
- (ii) To determine the influence of electrical field strength, rotational speed and transmembrane pressure drop on filter performance.
- (iii) To derive a model for the tangential flow electrofilters which includes all important filtration
  mechanisms and includes the variation of flux with
  time.

The experiments were performed on a polystyrene latex suspension. The individual particles were negatively charged and slightly denser than the water in which they were suspended.

#### CHAPTER 2

#### REVIEW OF RELATED LITERATURE

#### 2.1 Cross-Flow Filtration

Henry (1972) has discussed the status of cross-flow filtration module development, reviewed many applications of the cross-flow filter and discussed various mathematical models which have been used to interpret cross-flow filtration data. Virtually all mathematical models for the cross-flow filtration process are based on a representation of the particle concentration polarization phenomenon that occurs in the suspension adjacent to the filter medium. The models assume 100% rejection of solute by the membrane.

### 2.1.1 Concentration Polarization Model

During filtration, a layer of solids is formed at the surface of the filter medium. A gradient in suspended solids concentration is established in the direction perpendicular to the membrane. The particles are transported back into the bulk, stream by convective diffusion. This phenomenon, called concentration polarization, was found to be of importance in ultrafiltration of macromolecules like proteins. With these materials, a gel layer forms at the membrane surface due to precipitation of the macromolecules when the concentration exceeds the solubility limit, C<sub>s</sub>.

A model for concentration polarization during filtration of macrosolutes has been derived by Blatt et al. (1970) and de Fillippi and Goldsmith (1970). The mechanism is illustrated below.

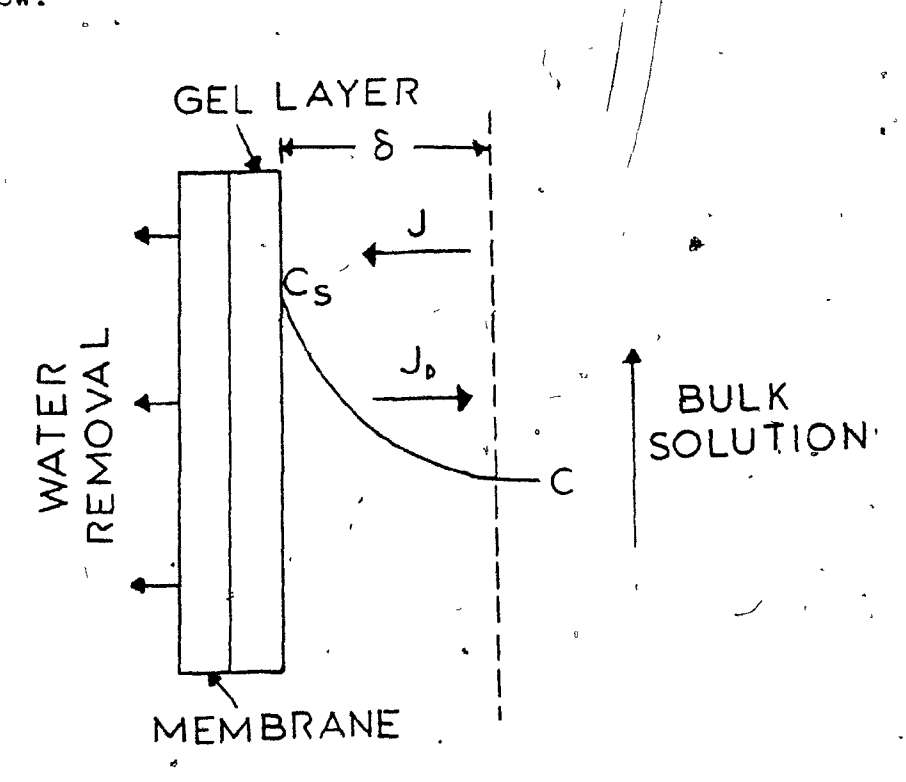


FIGURE 2.1. Macrosolute Concentration Polarization Model

Solute is carried toward the filter by the bulk flow of permeate, J, and is carried away from the filter by diffusion, represented by a flux J<sub>D</sub>. At steady state, the net solute flux is zero. Using the stagnant film theory of mass transfer to describe the diffusion flux, the following relationship is obtained for the permeate flux.

$$J = \frac{D}{\delta} \ln \frac{C_s}{C}$$
 (2-1)

where D = diffusion coefficient

 $\delta$  = thickness of stagnant film

C = bulk concentration of solute

The quantity  $(D/\delta)$  can be equated to the mass transfer coefficient, k. Consequently,

$$J = k \ln \frac{C_s}{C} \qquad (2-2)$$

If C<sub>s</sub> is not too much larger than the logarithm can be expanded and Eq. (2-2) can be written

$$J = \frac{k}{C} (C_s - C)$$
 (2-3)

This form has been derived by Porter and Nelson (1972). When particles are filtered,  $C_{\rm S}$  is taken to be the concentration of particles at the surface of the cake.

To reduce concentration polarization and increase the permeate flux, much effort has been expended to increase k, usually by increasing the fluid velocity past the membrane or adding turbulence promoters on the slurry side of the membrane.

When particles are filtered rather than macromolecular solutes, Eq. (2-2) underpredicts the filtrate flux and does not describe the flux-concentration relationship found experimentally (Blatt et al., 1970; Porter, 1972a). Several reasons have been proposed for this. Blatt et al. (1970) hypothesized that the major difference between the filtration of molecules and of solutes was the permeability of the gel layer or cake.

( }

The gel layer, which results from the precipitation of macro-molecules, is much less permeable than the cake formed from the accumulation of particles on the membrane. This argument is incorrect, however, as Porter has shown.

Forter (1972a) pointed out that the filtrate flux was also equal to the transmembrane pressure drop,  $\Delta P_F$ , divided by the sum of the hydraulic resistances of the membrane  $(R_M)$  and cake or gel  $(R_C)$ :

$$J = \frac{\Delta P_F}{R_M + R_C} \tag{2-4}$$

At steady state, the flux from Eq. (2-4) must equal that from Eq. (2-2):

$$k \ln \frac{C_s}{C} = \frac{\sqrt{\Delta P_F}}{R_M + R_C}$$
 (2-5)

For a sufficiently high value of  $\Delta P_F$ , the cake resistance at steady state adjusts itself so that Eq. (2-5) is satisfied. If  $\Delta P_F$  is low enough so that

$$\ln \frac{C_s}{C} > \frac{1}{k} \left( \frac{\Delta P_F}{R_M} \right)$$
 (2-6)

with the maximum physically attainable value of  $\mathbf{C}_{\mathbf{S}}$ , then no cake or gel layer forms and

$$J = \frac{\Delta P_{\mathbf{F}}}{R_{\mathbf{M}}}$$

At low  $\Delta P_F$ , no cake is present and the flux is proportional to  $\Delta P_F$  through Eq. (2-7). At high  $\Delta P_F$ , a cake forms and the flux is given by Eq. (2-2). In the latter case, the steady state flux is the same regardless of the magnitude of the resistance of the cake.

Since Eq. (2-2) underpredicted the steady state flux and Blatt's explanation was incorrect, Porter (1972a) hypothesized that there was an additional mechanism for transport of particles away from the membrane. This mechanism was the so-called "tubular pinch effect" in which particles migrate away from the walls of a tube in laminar flow, e.g. see Karnis et al. (1966). Although qualitatively correct, quantitative predictions were not good. The effect of turbulent flow has not yet been treated theoretically.

Trettin and Doshi (1979) and Doshi and Trettin (1980) allowed for the growth of a cake with time by writing a transient solute mass balance in differentiated form with distance measured outward from the surface of the cake rather than from the surface of the membrane. They obtained solutions of the transient mass balance for an unstirred cell in which the only mechanism of macromolecule or particle transport away from the medium was Fickian diffusion. They also included the resistance of the cake in their analysis. In their unstirred system, the flux was inversely proportional to the square root of time. At any given time, the flux was much larger than the prediction of the film theory model.

### 2.2 Electrofiltration

The processes of electrophoresis and electroosmosis were combined to purify colloids by Beechold in 1926 utilizing a batch cell/he called an electro-ultrafilter. / By measuring the time required to reduce the concentration of contaminant in a hydrosol by a specific amount, Manegold (1937) was able to study the effectiveness of filtration, dialysis, electrolysis and their intercombinations. Much later, Bier (1959) developed a membrane technique using an electrical field to dewater colloidal suspensions. He was the first to study the process of electrofileration under cross-flow conditions. In his experiments, Bier used transmembrane pressure differences in the range of 1400-4000 kPa in conjunction with a stationary membrane. Moulik et al. (1967) and Bier (1971) modified the batch filtration. equations to include the effect of the particle mobility in the slurry adjacent to the filter medium. They neglected the effect of fluid shear tangential to the filter medium and did not incorporate concentration polarization concepts in their mathematical models. "

Grushka et al. (1973) investigated field flow fractionation with an electrical field added. The field flow fractionation concept involves establishing a laminar flow between parallel plates and imposing an electric field normal to the direction of flow. The electrical field causes charged solutes to concentrate near one of the walls. The lower velocity of the laminar flow in the region near the wall means that solutes in that region will be retarded, while solutes near the center-line will

move down the duct with a higher velocity. This process is like conventional chromatographic separation because solute (or particle) bands can be developed and eluted from the flow channel.

Grushka et al. did not investigate the effect of turbulence on the process.

Henry et al. (1977), using suspensions of kaolin clay and oil in water, investigated the effects of electric field strength, axial velocity and transmembrane pressure difference on filtrate flux in a parallel plate cross-flow filter. The electric field strength varied from 0-50 V/cm, Reynolds number from 1200-3600 and transmembrane pressure difference from 7-28 kPa. They found a "critical voltage", Ec, at which the net particle migration velocity toward the filter medium was zero, i.e. at the critical voltage there was a balance between the electrical migration away  $^\circ$  from the medium/and the velocity at which the particles are swept toward the medium by bulk flow. Henry et al. observed that at E < E, the filtrate flux increased with Reynolds number. There was a net migration of particles toward the filtration medium and a cake was formed. The concentration of the particles was higher at the filter medium than in the bulk, causing diffusion of particles away from the medium. The overall effect was an increase in flux as Reynolds number increased. When  $E = E_c$ , there was no tendency for particles to concentrate at any point in the liquid film. Consequently, there was no concentration gradient and the Reynolds number did not affect the flux. For E > E, the concentration of particles in the bulk was higher than at the filter medium, causing particle diffusion toward the

100

medium and resulting in a decrease in flux as Reynolds number increased.

Cooper et al. (1965) noted another effect of the electric field which has been largely ignored by more recent workers. In experiments conducted with dissolved organics, they discovered that the solute rejection increased with field strength to an upper limit beyond which a continued increase in the field strength had no effect. They failed, however, to offer any explanation for this.

### 2.2.1 Electrofiltration Model

Henry et al. (1977) presented a model for steady state cross-flow/electrofiltration. The cross-flow/electrofilter is illustrated in Fig. 2.2. The process combines particle migration away from the filter due to fluid shear and to electrophoretic migration.

Henry et al. (1977) expressed the flux of particles as the sum of a diffusive contribution and an electrophoretic contribution. The electrophoretic velocity of a charged particle in a DC electric field is conventionally written as K<sub>e</sub>E, where K<sub>e</sub> is the electrophoretic mobility and E is the field strength. The mobility is the velocity of a particle under an electric field strength of 1 V/cm. It can be measured experimentally in a micro-electrophoresis cell. For the diffusive contribution, they used the stagnant film theory. At steady state, the filtrate flux is given by

$$J = k \ln \frac{C_s}{C} + K_e E$$
 (2-8)

Neglecting electroosmotic effects in the membrane and cake, the flux is also given by Eq. (2-4).

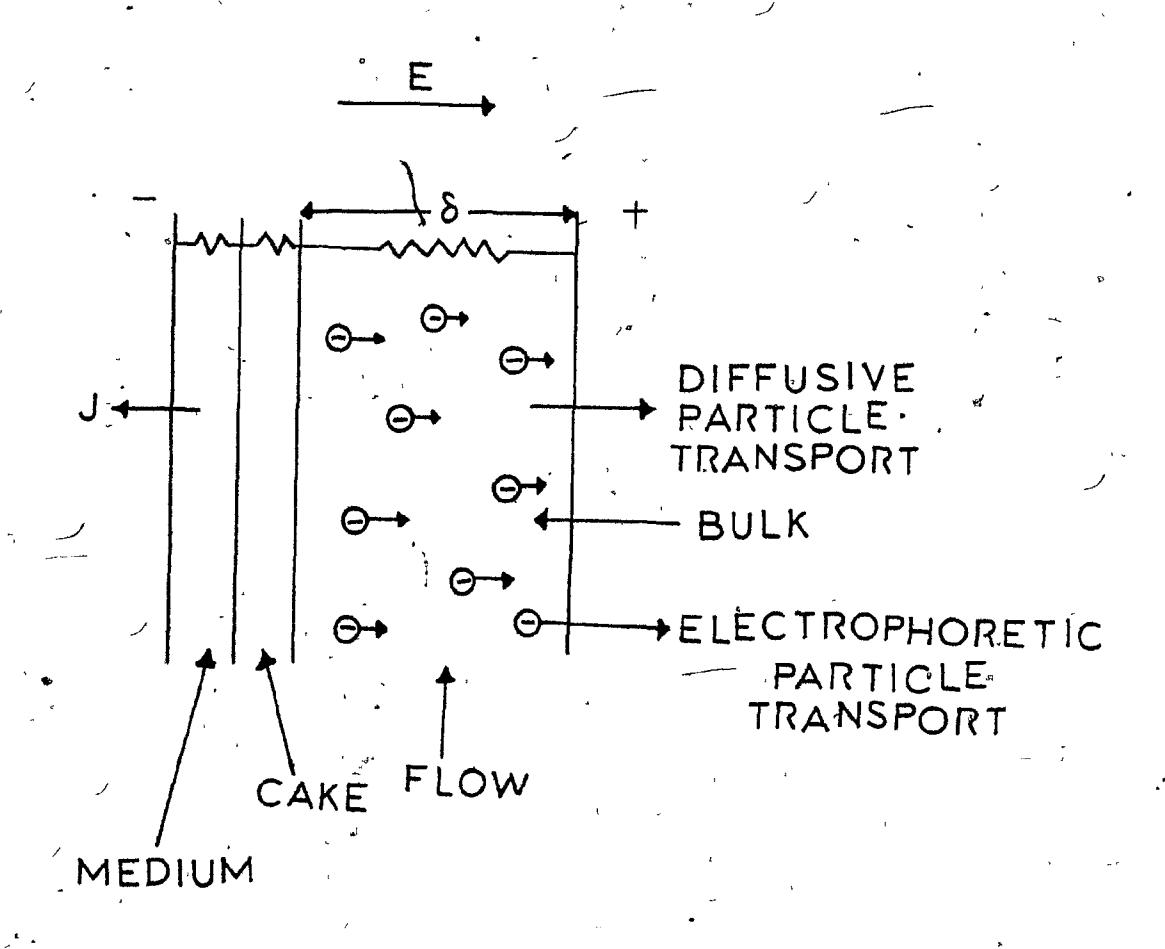


FIGURE 2.2. Cross-Flow/Electrofiltration Concept

There is an error in the Henry et al. derivation. They put Eq. (2-8) into the form "flux  $-\Delta P_F/r$ esistance" to derive an expression for the "film resistance" and then added this resistance to the cake and medium resistances. This is incorrect because Eq. (2-8) is valid only when a steady state flux J exists. Establishing a surface concentration of  $C_S$  and a field E will not produce a flux of permeate equal to J.

If  $E > E_c$ , no cake forms and the flux (including electro-osmosis in the membrane) was assumed by Henry et al. to be given by

$$J = \frac{\Delta P_F}{R_M^{o_f}} + K_M E \qquad (2-9)$$

Equating Eqs. (2-8) and (2-9) gives

$$(K_e - K_M)E + kln \frac{C_s}{C} = \frac{\Delta P_F}{R_M}$$
 (2-10)

At the critical field strength,  $E=E_{\rm c}$ ,  $C_{\rm s}=C$  and Eq. (2-10) yields

$$E_{C} = \frac{\Delta P_{F}/R_{M}}{K_{e} - K_{M}} \tag{2-11}$$

The critical field strength is proportional to the transmembrane pressure difference. For clay suspensions at  $\Delta P_{\rm F} \sim 7$  kPa, Henry et al. (1977) found that  $E_{\rm C} \sim 20$  V/cm which was in good agreement with the value predicted by Eq. (2-11). For E > E\_c, the flux increases linearly with field strength as given by Eq. (2-9).

### 2.3 Flow Between Rotating Cylinders

Only the characteristics of the flow between a pair of coaxial cylinders in which the inner rotates and the outer is stationary are considered.

### 2.3.1 Rotating Cylinders without Axial Flow

Much of the early experimental and theoretical work was provided by G.I. Taylor. In 1923, he analyzed the stability of incompressible viscous flow in the annular gap between concentric rotating cylinders of infinite length in the absence of axial flow. He assumed small perturbations of the velocity components in the Navier-Stokes equations and solved for the lowest rate of rotation for which the perturbations would grow. At this critical rate of rotation,  $\Omega_{\rm C}$ , the purely tangential flow breaks down with the formation of a series of transverse vortex pairs, the Taylor vortices. Taylor's result for the critical rate was

$$\Omega_{c}^{2} = \frac{\pi^{4} v^{2} (R_{i} + R_{o})}{2Ab^{3} R_{i}^{2}}$$
 (2-12)

where  $R_i$  = outside radius of inner cylinder  $R_o$  = inside radius of outer cylinder

 $b = gap width, R_o - R_i$ 

with

$$A = 0.0571 \left(1 - 0.652 \frac{b}{R_i}\right) + 0.00056 \left(1 - 0.652 \frac{b}{R_i}\right)^{-1}$$
 (2-13)

Taylor (1923) confirmed this result experimentally.

For b << R<sub>1</sub>, Eq. (2-12) can be put in the form of a critical Taylor number. The Taylor number is defined as (Schlichting, 1968):

1)

$$Ta = \frac{\Omega R_i^2}{v} \left(\frac{b}{R_i}\right)^{3/2} \tag{2-14}$$

With  $b \ll R_i$ , Eqs. (2-12) to (2-14) can be combined to yield

$$Ta_{c} = \frac{\pi^{2}}{\sqrt{0.0433}} = 47.4 \tag{2-15}$$

Schlichting (1968) suggested that the flow between the cylinders becomes turbulent for Ta > 400.

The power required to rotate the inner cylinder (per unit area of inner cylinder) is given by

$$P_{\mathbf{r}} = \tau_{\mathbf{r}} \Omega R_{\mathbf{i}} \tag{2-16}$$

where  $\tau_{\mathbf{r}}$  is the shear force per unit area of the inner cylinder. This force is written in terms of a drag coefficient defined by

$$\operatorname{er}_{\mathbf{r}} = \frac{C_{\mathbf{D}}}{2} \, \rho \left( \Omega R_{\mathbf{i}} \right)^{2} \tag{2-17}$$

where  $\Omega$  is the angular velocity. Hence,

$$P_{r} = \frac{c_{D}}{2} \rho \left(\Omega R_{i}\right)^{3} \tag{2-18}$$

The drag coefficient is a function of  $R_i/R_o$  and a Reynolds number, Re, defined as follows

$$Re = \frac{2\rho\Omega R_1^2}{\mu}$$
 (2-19)

For the laminar regime (Ta < 41.3), Taylor derived

$$c_{D} = \frac{8}{Re} \left[ 1 - \left( \frac{R_{i}}{R_{o}} \right)^{2} \right]^{-1}$$
 (2-20)

The turbulent flow (Ta > 400), experiments yield

$$C_{\rm D} = aRe^{-0.2}$$
 (2-21)

where the constant a is a function of  $R_{1/R_{0}}$ . Taylor (1936) also measured drag coefficients in this regime.

Taylor (1935) measured the variation of the pressure between the rotating cylinders. Since the outer cylinder is stationary, the fluid does not rotate as a rigid body and the pressure distribution is not hydrostatic. A sketch of the variation of pressure with radial position as found by Taylor (for Re ~ 105) is sketched in Fig. 2.3. Near the rotating inner cylinder the pressure rises rapidly, reaches a plateau over most of the gap and then rises rapidly again near the stationary outer cylinder. An approximate fit to Taylor's data yields the following

$$Ta = \frac{Re}{2} \left( \frac{b}{R_i} \right)^{3/2}$$

Comparing Eqs. (2-19) and (2-14) shows that

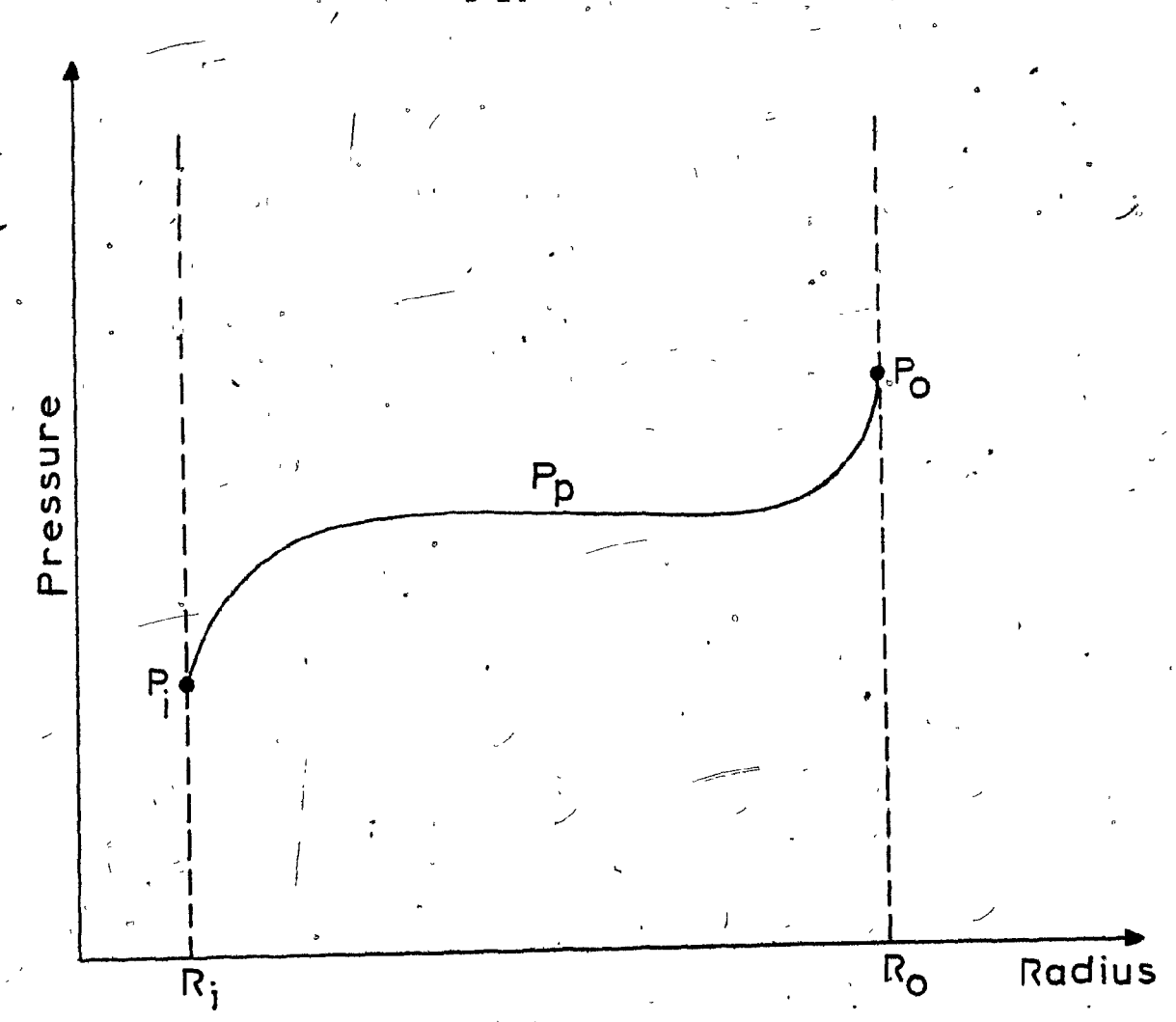


FIGURE 2.3. Pressure Profile Between Rotating Cylinders
expressions for the pressure difference between the cylinders

$$P_{o} - P_{i} = 0.27 \frac{\rho (\Omega R_{i})^{2}}{2} \left[ 1 - \left( \frac{R_{i}}{R_{o}} \right)^{2} \right]$$
 (2-23)

and between the pressure at the outer cylinder and the plateau pressure

$$P_{O} - P_{p} = 0.27 \frac{\rho (\Omega R_{i})^{2}}{2} \left[ \frac{(R_{i}/R_{O})^{2}}{0.9 + 0.1 (R_{O}/R_{i})} \right]_{a}$$
 (2-24)

Taylor also found that the mean tangential velocity,  $v_{\theta}$ , was inversely proportional to the radial position over the central 80% of the gap. His data are well approximated by

$$v_{\theta}r = 0.52 \Omega R_i^2$$
 (2-25)

## 2.3.2 Rotating Cylinders with Axial Flow

Four regimes have been distinguished for axial flow through concentric cylinders with the inner one rotating - see Strong and Carlucci (1976). These flow regimes are:

- (a) Purely laminar flow for low axial Reynolds numbers and low Taylor numbers.
- (b) Laminar-plus-Taylor vortex flow for low axial Reynolds' numbers and moderate Taylor numbers.
- (c) Purely turbulent flow for large axial Reynolds numbers and small Taylor numbers.
- (d) Turbulent-plus-Taylor vortex flow for large axial

  Reynolds numbers and large Taylor numbers. The boundaries between these regimes are not well established.

  In addition, the region of small axial Reynolds numbers and large Taylor numbers, say larger—than 10<sup>3</sup>,
  has not been explored.

#### CHAPTER 3

### EXPERIMENTAL APPARATUS AND PROCEDURE

### 3.1 pescription of System and Operation

The tangential flow electrofiltration set-up consisted of a rotatable cylinder with a perforated surface (1600 holes of Q.10 cm diameter over the central 5.0 cm). This central portion of this cylinder was covered by a 0.2 µm Acropor polymeric membrane. A. The membrane was held in place along its length by a retaining clamp which fitted into a slot 0.2 cm deep and 5.5 cm The retaining clamp was screwed to the rotating cylinder by four screws, one in each corner. The ends of the membrane were held by tape (Scotch No. 898-3H1-17). The membrane area was approximately 100 cm<sup>2</sup>. The exact value was determined for each new membrane from the measured length of membrane between the end tapes and the outside diameter of the inner cylinder. The inner cylinder, which had an inner diameter of 6.1 cm, an outer diameter of 6.5 cm and a length of 18.2 cm rotated coaxially in a motionless cylinder of inner diameter 8.1 cm. rotating seals were made by special rings which prevented electrical contact between the inner and outer cylinders. section of the filtration unit is shown in Fig. 3.1. The rotate able cylinder was coupled to a motor which was fitted with a

Acropor is a registered trademark of Gelman Instruments Inc., Ann Arbor, MI, U.S.A.

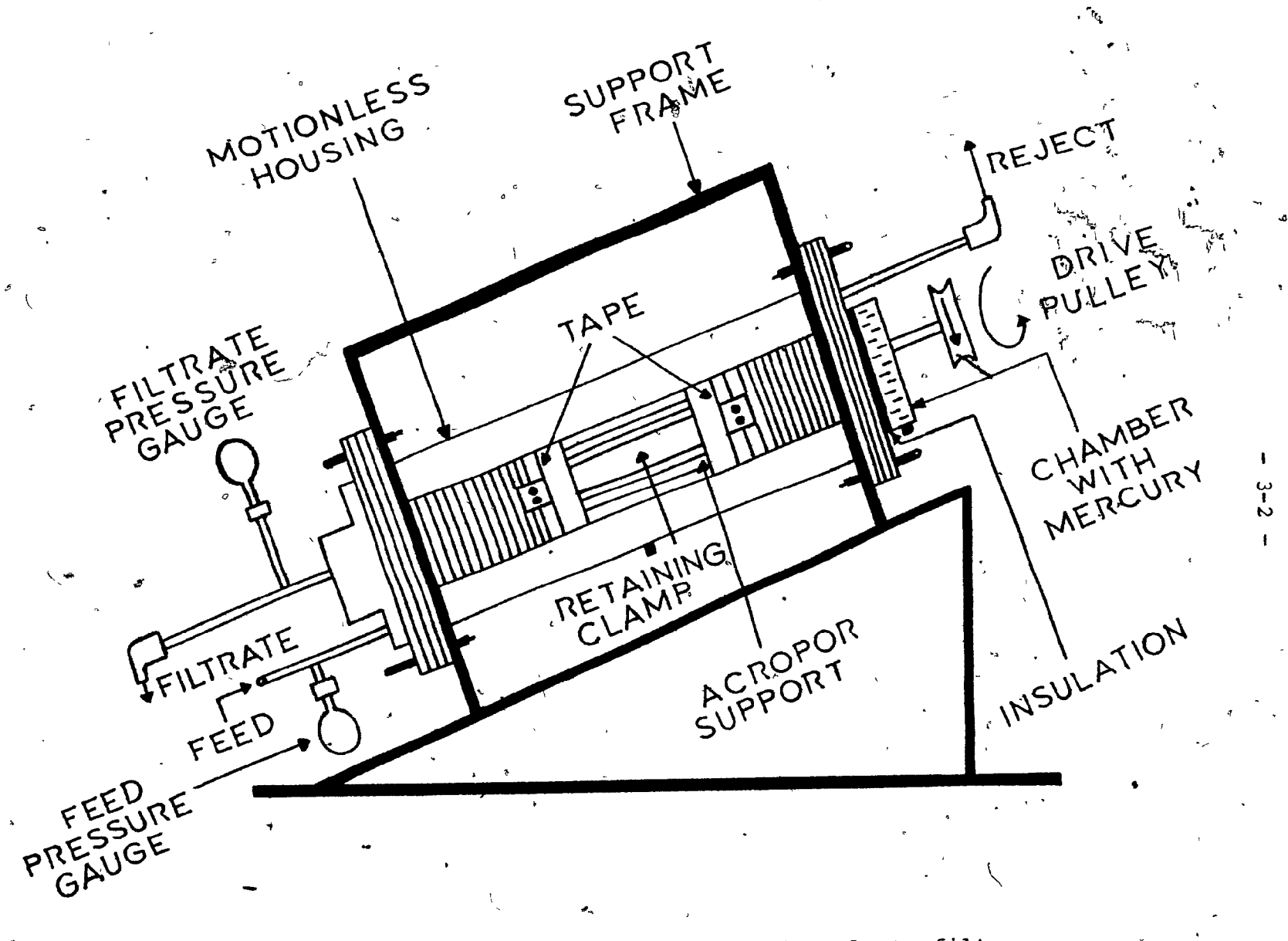


FIGURE 3.1. Cross-Section of the Tangential Flow Electrofilter

regulator to maintain constant rates of rotation.

A schematic diagram of the flow loop is shown in Fig. 3.2. The feed was circulated along the gap between the motionless cylinder and the rotor. A pressure gauge was installed on the feed line to measure the pressure of the feed as it entered the gap. To avoid a possible mechanical influence of the pump on the particle size distribution in the feed, a peristaltic pump was used for feed circulation. A stabilizer was also employed to damp pulsations in the flow. Rejected suspension was collected in a vessel separate from the feed in order to maintain constant feed concentration. The rejectaline was fitted with a sample line which allowed collection of samples during a run.

The transmittances of the feed and filtrate were measured with a spectrophotometer (Baush and Lomb, Model DB). The spectrophotometer was first zeroed with distilled water in the two cleaned cells. A sample of the original feed solution was scanned to determine the wavelength that gave the maximum percentage transmittance. This wavelength was maintained throughout. The maximum percentage transmittance for the present latex was obtained at a wavelength of 700 nm. In all measurements, the reference cell contained distilled water. Before each measurement, the sample was allowed to attain equilibrium (30 s) before the transmittance was recorded. After each measurement, the cells were cleaned with a dilute solution of hydrochloric acid and rinsed with distilled water.

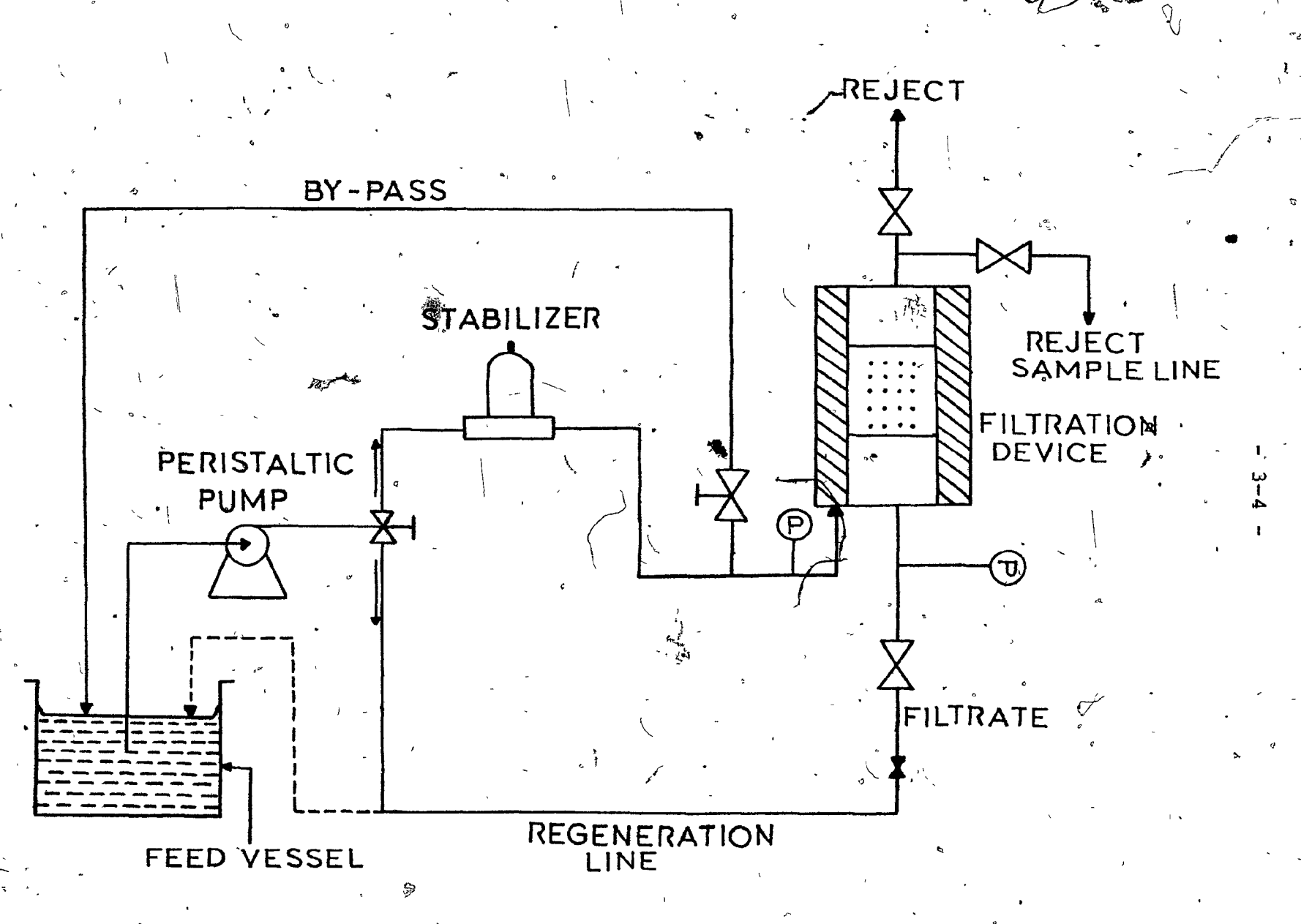


FIGURE 3.2. Schematic Diagram of Tangential Flow Electrofiltration Flow Loop

#### 3.2 Electrical Arrangement

The special ring on the upper portion of the filtration unit was insulated from a chamber containing mercury (see Fig. 3.1).. The shaft connecting the rotor to the pulley passed through this chamber making contact with the mercury. A bolt at the bottom of the chamber served as the first electrical contact point. Since the motionless cylinder was made of stainless steel, a bolt on it served as the second electrical contact point. Dead end insulation between the special rings and the screws that held them in place prevented short-circuiting.

The circuit used in supplying electrical power to the filtration unit is illustrated in Fig. 3.3. A variac transformer (Superior Electric Co., Type 1168) received power at a voltage of 115 V from a voltage source. To minimize power dissipation, transformed energy was stored in a capacitor (General Radio Co., Model KBPC). Alternating voltage was converted into direct voltage by three rectifiers (P.R. Mallory and Co., Model TC 78) connected in parallel. The use of three rectifiers made it possible for two to act in concert to achieve full wave rectification while the third acted as filter to smooth the time variations resulting in a more nearly time invariant output voltage. The polystyrene latex suspension served as the resistance load. The current was measured with an ammeter (Simpson, Model C464).

# 3.3 Preparation of Polystyréne Latex Suspension

A method for preparation of monodisperse polystyrene

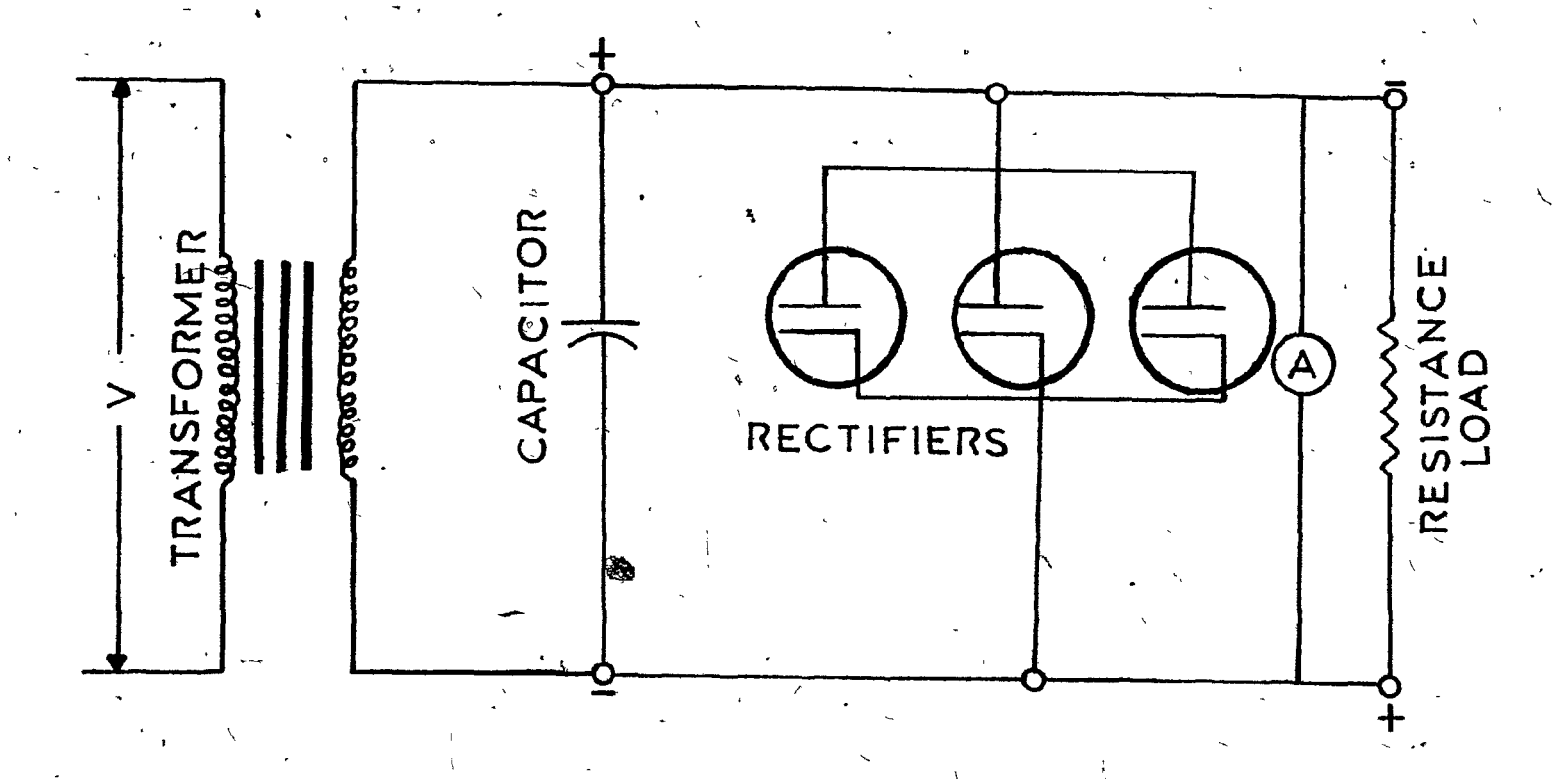


FIGURE 3.3. Electrical Circuit in Tangential Flow Electrofiltration

latices has been perfected by Kotera et al. (1970). The procedure as applied in this project is the following:

- (1) Styrene monomer (Aldrich Chemical Co., Milwaukee, WI, U.S.A.) was purified by washing three times with portions of 1.0 M NaOH and rinsing with distilled water. This removed activated alumina which otherwise would have acted as an inhibitor.
- (2) 1000 cm<sup>3</sup> of a mixture of distilled water and reagent grade methanol prepared in a volumetric ratio of 2:1 was poured into a bomb reactor.
- (3) 180 cm<sup>3</sup> of purified styrene was then added to the reactor.
- (4) 4.75 g of potassium persulphate was added to the reactor as the initiator.
- (5) Immediately after the addition of the potassium persulphate, oxygen-free nitrogen gas was bubbled into the reactor and the mixture stirred. The temperature was maintained at  $60^{\circ}$ C.
- (6) The system was then left for 18 hrs in a fume hood at  $60^{\circ}$ C with constant stirring and nitrogen bubbling.

The latex was poured out of the reactor and left to cool in storage vessels. The latex was filtered through No. 16 filter paper before dilution to the desired concentration.

# 3.4 Properties of Materials

The following instruments were employed to measure the properties of the feed system indicated in Table 3.1.

TABLE 3.1 Properties of Feed System (25°C)

Distilled Wa	ter	Polystyrene Latex Particles				Latex Suspension			
Specific Conductivity	pН	Density,	Mean Diameter, d	Hobility, K <sub>e</sub>	Zeta Potential, Ç	Density,	Viscosity,	Conductivity	Particle Concentration, C <sub>f</sub>
7x10 <sup>-6</sup> niho cm	5.7	1060 kg	0.60 um	4.22x10 <sup>-4</sup> cm/V cm	~60 mV	982 <u>kg</u>	8.91x10 <sup>-4</sup> kg	26.5x10 <sup>-6</sup> mho cm	$2.0 \times 10^{-2} \frac{kg}{m}$

η = dielectric constant

- 7.87x10<sup>-4</sup>

- (1) pH was measured with a pH meter (Fisher Scientific, Model 140A).
- (2) Electrical conductivity was measured with a conductivity meter (Leeds and Northrup Co., Model 4905-0-33-09).
- (3) Mobility was measured with a micro-electrophoresis cell (Carl Zeiss, Model 4325449).

# 3.5 Definitions of Flux and Rejection

The filtrate flux in the tangential flow electrofilter is defined as the volumetric flow rate through the membrane per unit area of the membrane.

The rejection measures the effect of the filter in removing particles. Seoud (1980) has shown that these latices obey Beer's law at low concentrations. According to Beer's law,

$$T = e^{-KC} (3-1)$$

where T = fractional transmittance

.C = concentration

K = constant dependent on wavelength and particle
size

From Eq. (3-1):

$$C = \frac{-\ln T}{K} \tag{3-2}$$

The percentage rejection is the percentage particles in the feed rejected by the membrane:

$$R = \left(1 - \frac{C_p}{C_f}\right) \times 100 \tag{3-3}$$

where  $C_p$  = concentration of particles in permeate  $C_f$  = concentration of particles in feed

Substituting Eq. (3-2) into (3-3) yields

$$R = \left(1 - \frac{\ln T_{\overline{p}}}{\ln T_{f}}\right) \times 100 \tag{3-4}$$

where  $T_p$  = fractional transmittance of permeate  $T_f$  = fractional transmittance of feed

## 3.6 Procedure for a Run

Before filtration of latex, distilled water was run through the apparatus at N = 2000 rpm and  $\Delta P_m = 68.9$  kPa. The distilled water flux was measured ( $J_f$ ) and compared to the flux when the Acropor support was freshly put in place ( $J_i$ ). Experience had shown that when  $J_f < 0.75$   $J_i$  ( $J_i \approx 0.1$  cm/s), the support was clogged beyond regeneration. In such a case, it was removed and a new one inserted. On the other hand, if  $J_f > 1.2$   $J_i$ , the filtration device was investigated for leakage. To begin a run, feed was circulated through the apparatus with the rotor stationary and no applied voltage. The rotor was kept stationary until the gap between the cylinders was full ( $\approx 5$  s). An excessively high transmembrane pressure difference was created when the rotor was rotated while the cylinder was empty or partially full. The time when the run was began was recorded and

the rotor set to the desired speed. The transformer was then set to the desired voltage.

The time of first appearance of filtrate was recorded and samples collected at 10-minute intervals. The time required to collect a volume of the filtrate was recorded. Samples of the rejected suspension were collected simultaneously. The transmittances of the filtrate and reject were measured during the time between the collection of samples. After 90 minutes, filtration was stopped and the support regenerated.

#### 3.7 Procedure for Regeneration

Regeneration of the Acropor membrane was accomplished by washing away the cake of accumulated particles. The technique involved the flow of a cleaning solution through the Acropor in the direction opposed to the filtrate flux using the regeneration line shown in Fig. 3.2. This backwash employed a solution of 1.0 M NaOH for 20 minutes at a transmembrane pressure difference of 0.5 kPa. During the backwash and subsequent rinse, the rotation rate was 2000 rpm. The temperature of the caustic solution was maintained at 30°C. The backwashing was stopped after 20 minutes because the caustic solution became ineffective after this time. A second, fresh portion of 1.0 M NaOH was then used in backwashing for another 10 minutes. Distilled water was then run through the apparatus in the normal direction until the pH of the filtrate approached that of the distilled water.

#### CHAPTER 4

#### EXPERIMENTAL RESULTS

#### 4.1 / Introduction

In the tangential flow electrofilter, the permeate flux is expected to be high at start-up and then to decrease with time to a steady state value as a cake builds up. Sample flux-time curves are presented in Fig. 4.1. The flux decays with time as expected. Steady state is not reached in 90 minutes which was the duration of the experiments. Long transients have been found by others. For example, Henry (1972), in a study of cross-flow filtration, achieved steady state only after 18 hrs of operation employing a transmembrane pressure difference of 414 kPa.

# 4.2 Effect of Electric Field on Filtrate Flux

Since the latex particles are negatively charged, a DC electric field directed away from the surface of the membrane causes the particles to be repelled from the membrane surface. Cake build-up should decrease with increasing electric field strength yielding an increasing flux as electric field strength increases. Figures 4.1, 4.2, 4.3 and 4.4 show the effect of electric field strength on filtrate flux for the tangential flow electrofilter at different rates of rotation and measured trans-

A flux of 0.01 cm/s corresponds to 212 gal (U.S.)/ft2.day.

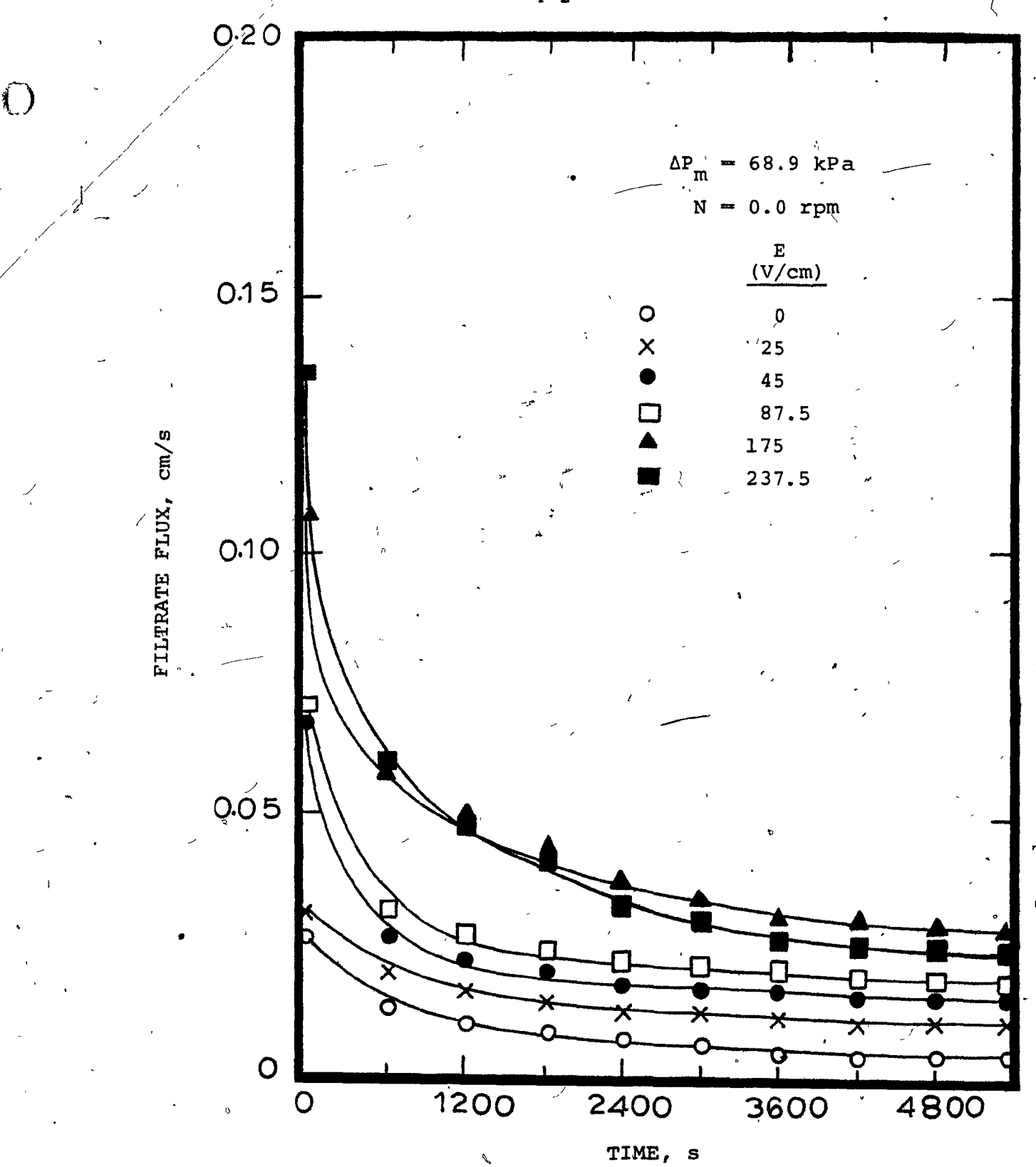


FIGURE 4.1. Variation of Flux with Time Showing Effect of Field Strength on Flux

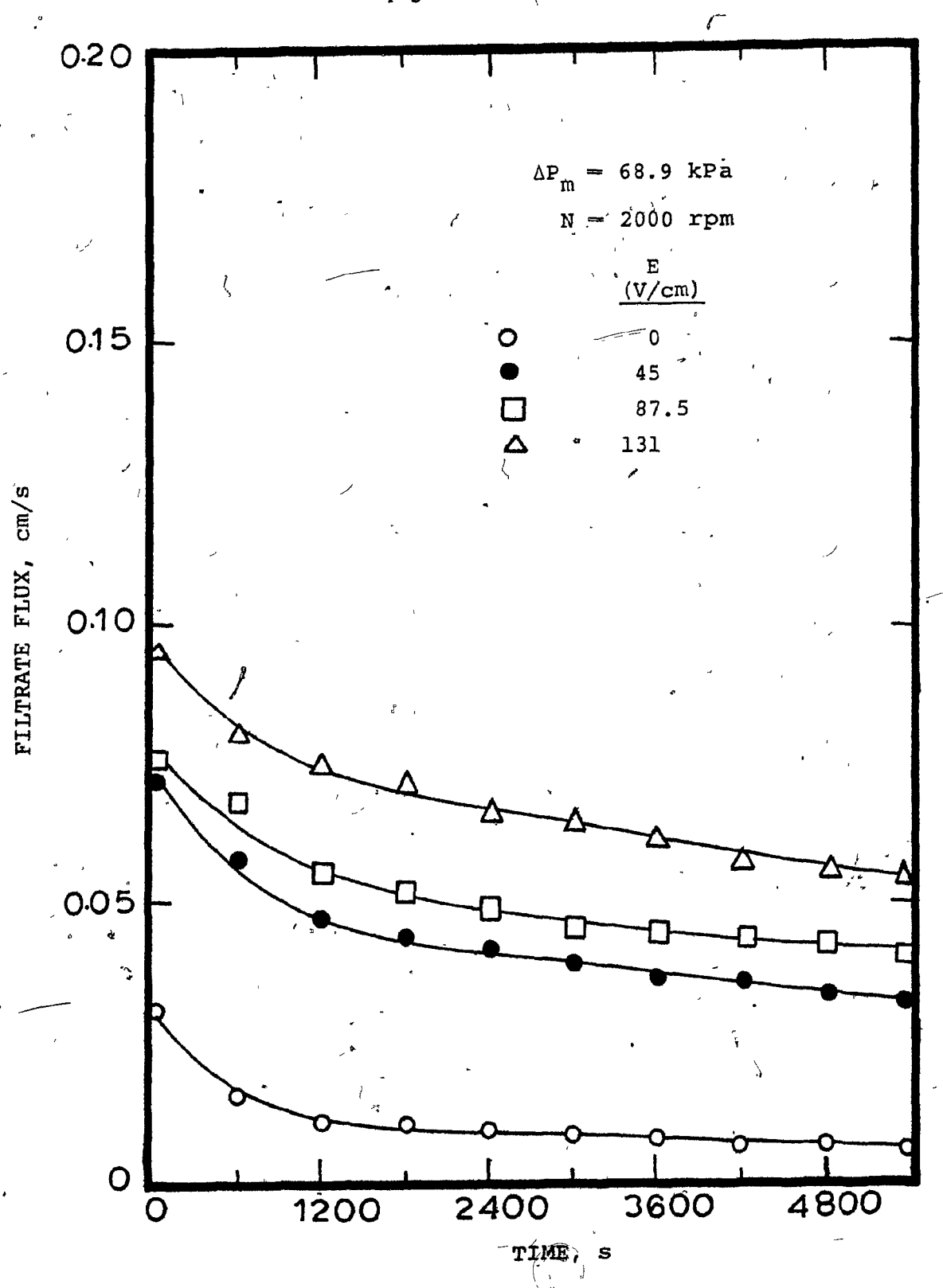
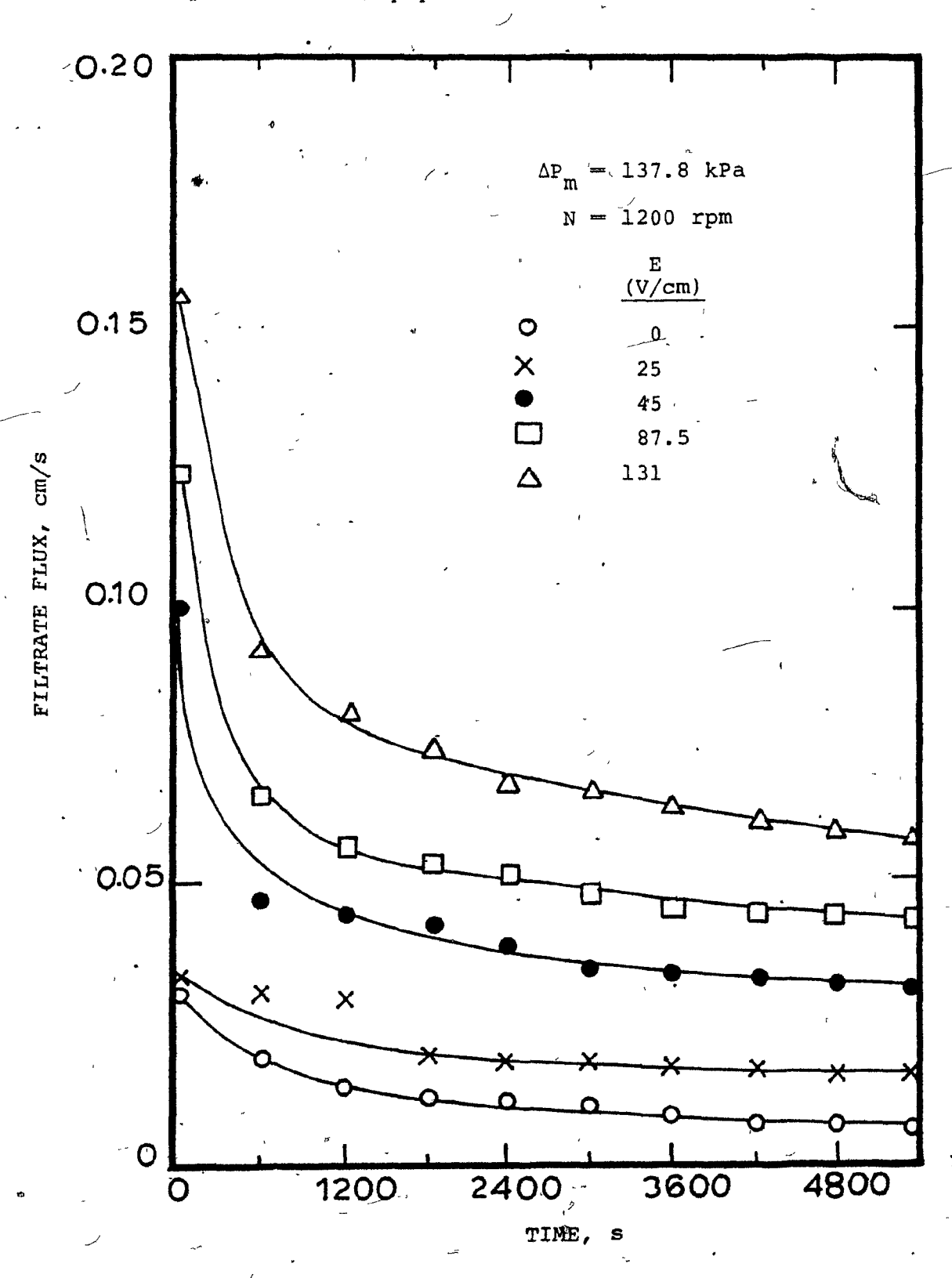


FIGURE 4.2. Variation of Flux with Time Showing Effect of Field Strength on Flux



Variation of Flux with Time Showing Effect of Field Strength on Flux FIGURE 4.3.

 $\tilde{()}$ 

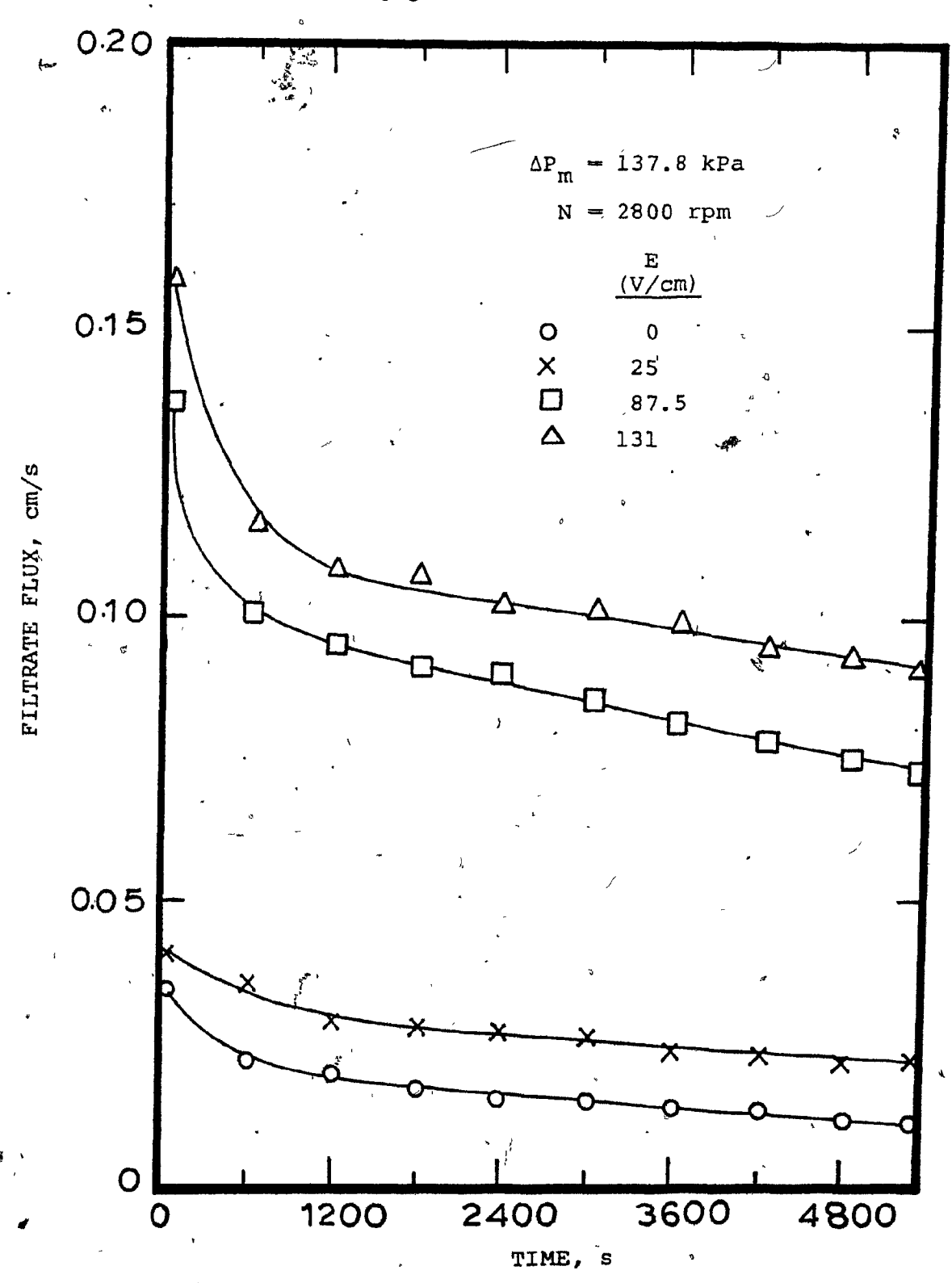


FIGURE 4.4. Variation of Flux with Time Showing Effect of Field Strength on Flux

membrane pressure drops. The flux increases with electric field strength for any value of the time up to E = 131 V/cm.

From Fig. 4.1, the flux for E = 175 V/cm is higher than that for E = 237.5 V/cm for any value of the time after 20 minutes.

This suggests an optimum electric field strength beyond which the flux starts to decrease with increasing electric field strength. This optimum electric field strength is determined in Chapter 6. The decrease of flux with electric field strength at high fields is attributed to the production of hydrogen bubbles which either increase the resistance between the cake and the membrane or clog the pores of the membrane.

Figures 4.1, 4.2, 4.3 and 4.4 contain only sample runs.

The same observations apply to all runs conducted with the tangential flow electrofilter.

# 4.3 Effect of Rotation on Filtrate Flux

Figures 4.5 and 4.6 illustrate the effect of rotation rate on filtrate flux. The flux increases with rotation rate for any value of the time at different electric fields and measured pressure drops. The increase of flux with rotation is greater for those cases with an electric field than those without an electric field (Figs. 4.5 and 4.6) suggesting a possible interaction between electric field strength and rotation. The mechanisms responsible for the increase of flux with rotation rate are discussed in Chapters 5 and 6.

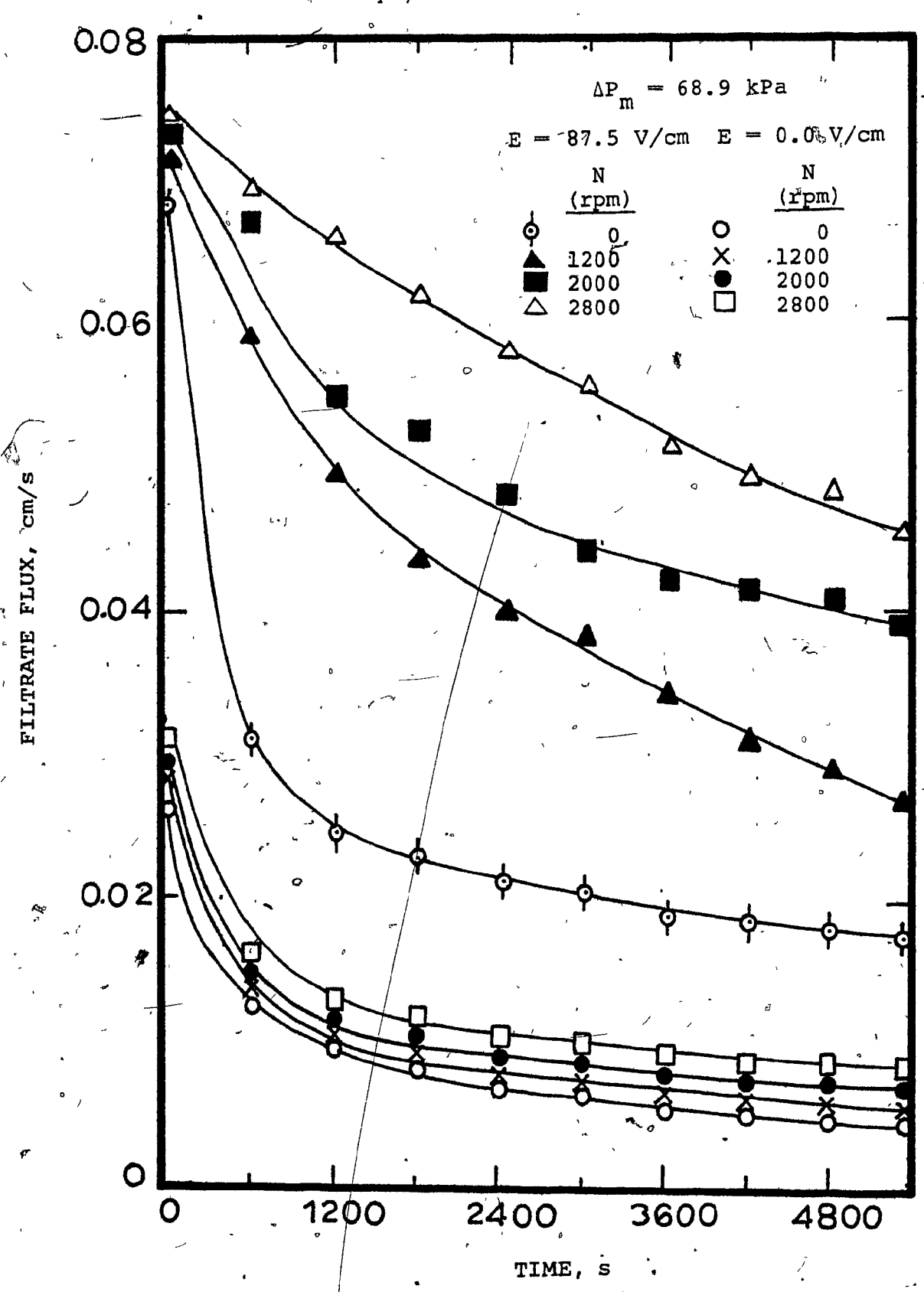


FIGURE 4.5. Variation of Flux with Time Showing Effect of Rotation Rate on Flux

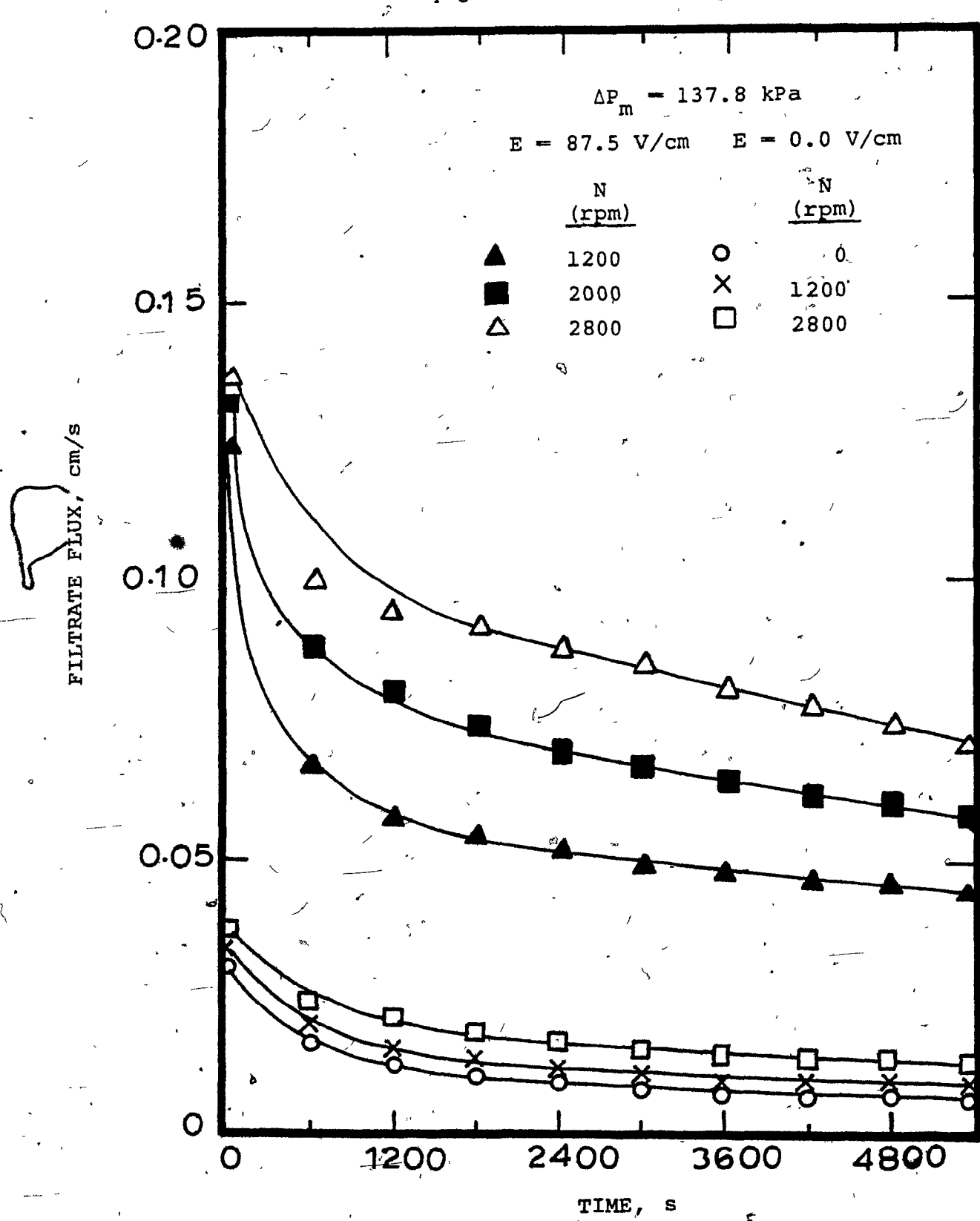


FIGURE 4.6. Variation of Flux with Time Showing Effect of Rotation Rate on Flux

## 4.4 Effect of Pressure Difference on Filtrate Flux

Figure 4.7 illustrates the effect of pressure difference on filtrate flux. The flux increases with  $\Delta P_{\rm m}$  for any value of the time. The effect of  $\Delta P_{\rm m}$  on the flux at a fixed time is greater when the inner cylinder is rotated and an electric field is applied (see Fig. 4.7). When  $\Delta P_{\rm m}$  is doubled from 68.9 kPa to 137.8 kPa, the flux after 90 minutes increases by 51% with a field of 150 V/cm and only 33% without a field.

# 4.5 Rejection of Particles by the Filter

Figures 4.8 and 4.9 contain sample plots of percent rejection, see Eq. (3-4), versus time for various operating conditions. The degree of rejection of particles is better than 94% for all conditions. The rejection decreases somewhat with increasing rotation rate. The larger fluxes at higher rotation rates evidently carry some particles through the membrane. The effect of electric field strength on rejection is negligible when there is no rotation. With rotation, application of electric field reduces the rejection of particles by a maximum of 2-3%. The larger fluxes obtained at higher rotation rates are again responsible for carrying particles through the membrane.

# 4.6 Reproducibility

Figures 4.10 and 4.11 illustrate the extent to which the experimental results are reproducible. Figure 4.10 contains the fluxes from runs conducted during stages of the project with different Acropor supports and the corresponding rejections.

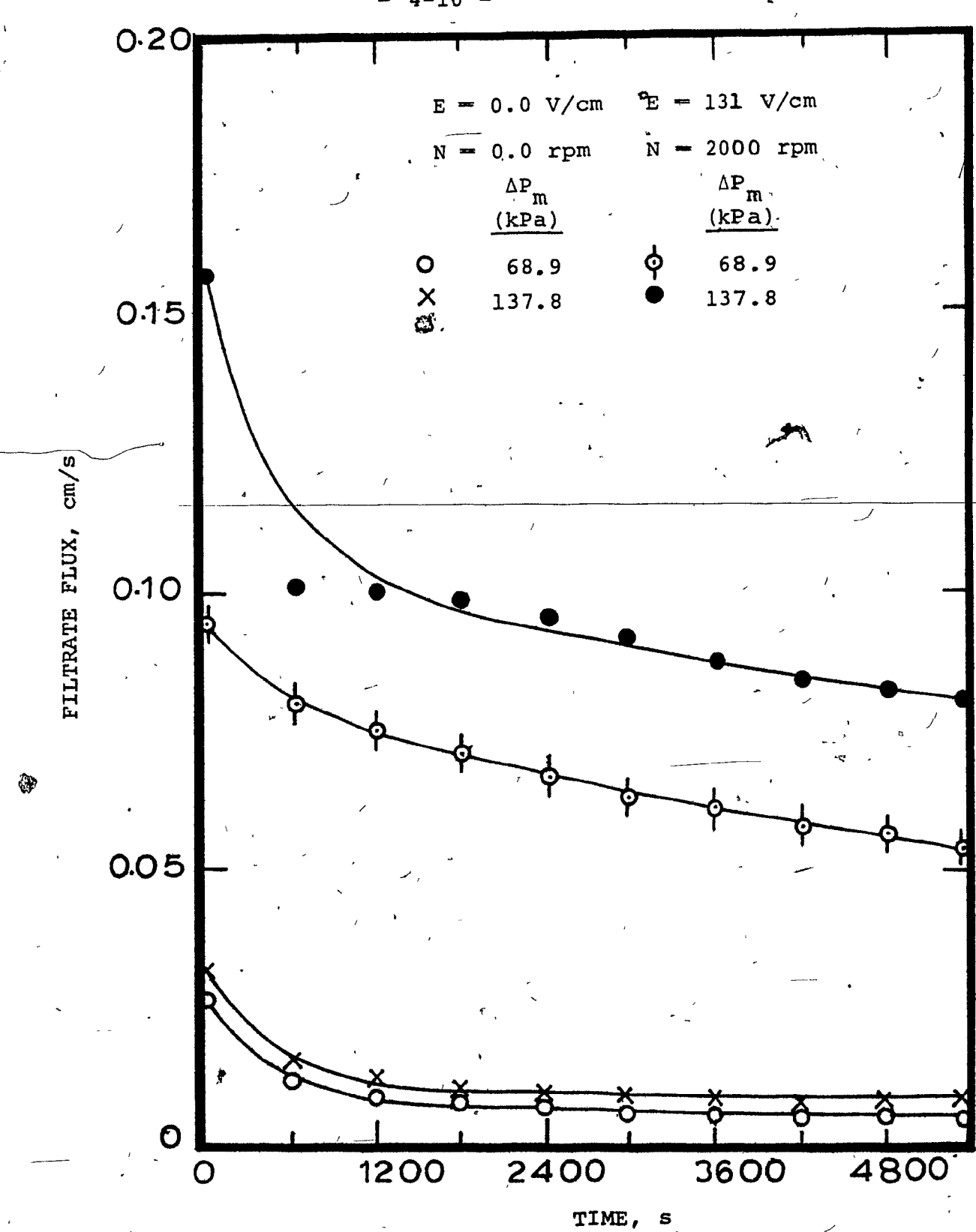


FIGURE 4.7. Variation of Flux with Time Showing Effect of Pressure Drop on Flux

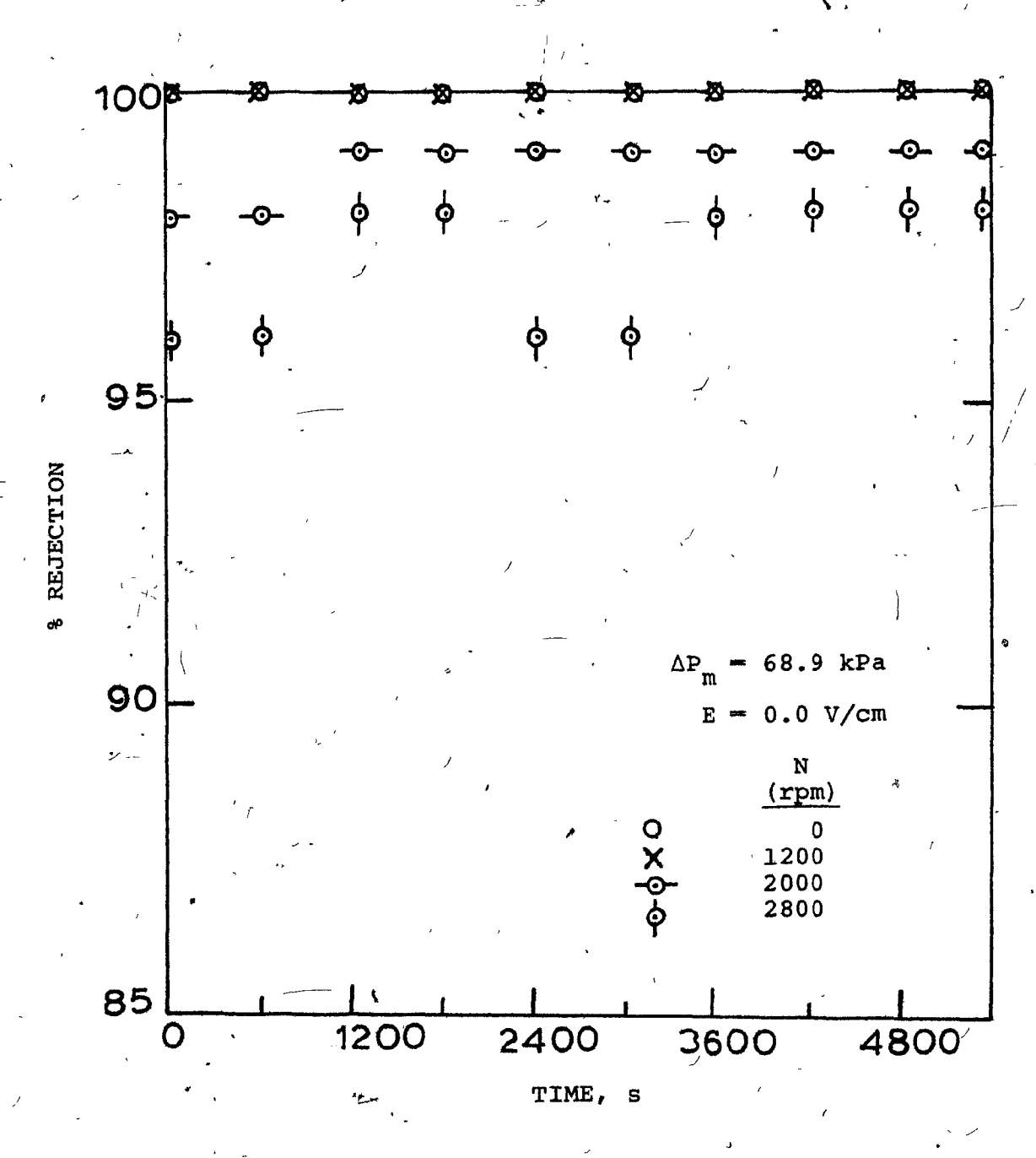


FIGURE 4.8. Variation of Rejection with Time Showing Effect of Rotation Rate on Rejection

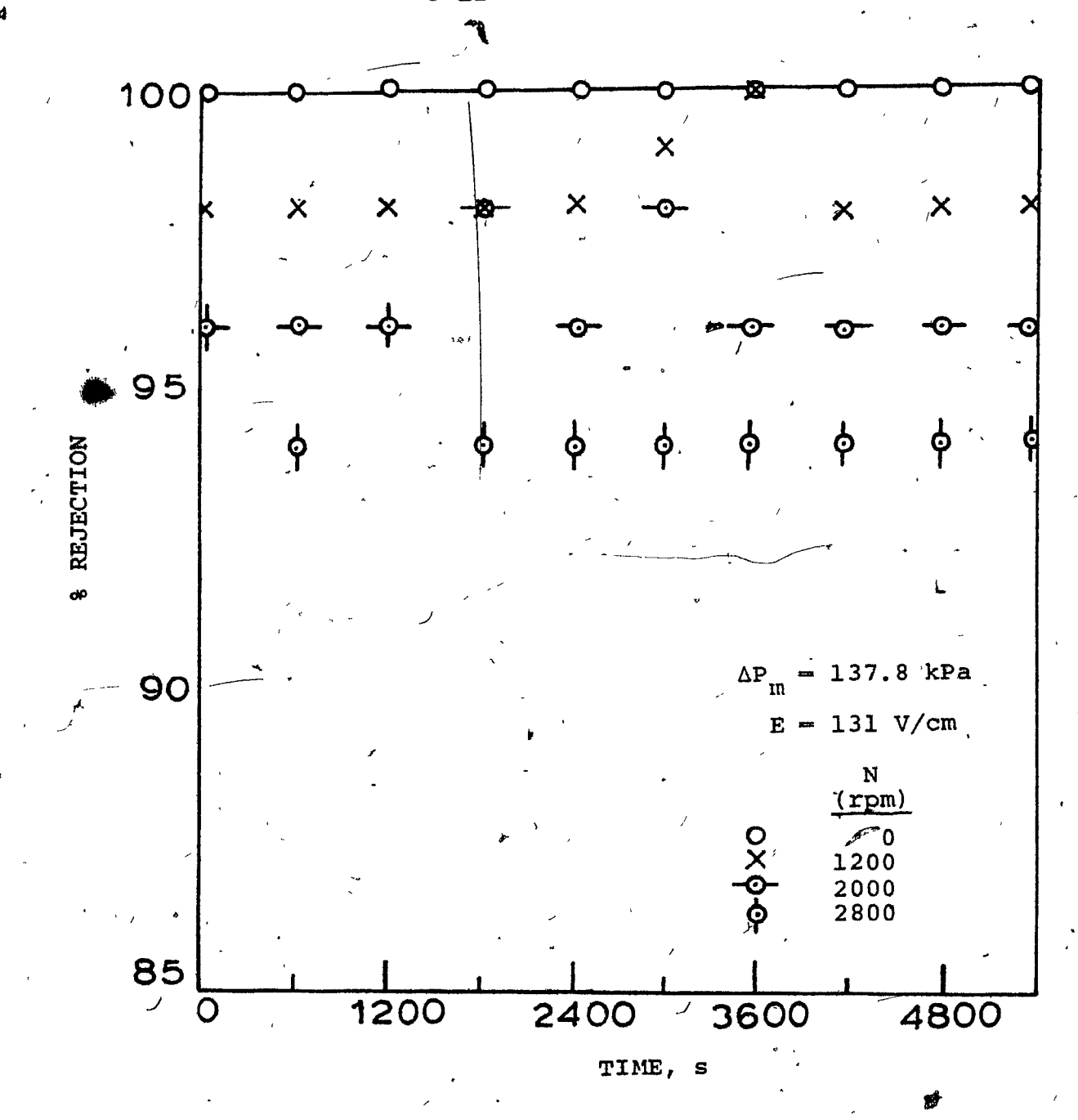


FIGURE 4:9. Wariation of Rejection with Time Showing Effect of Rotation Rate on Rejection

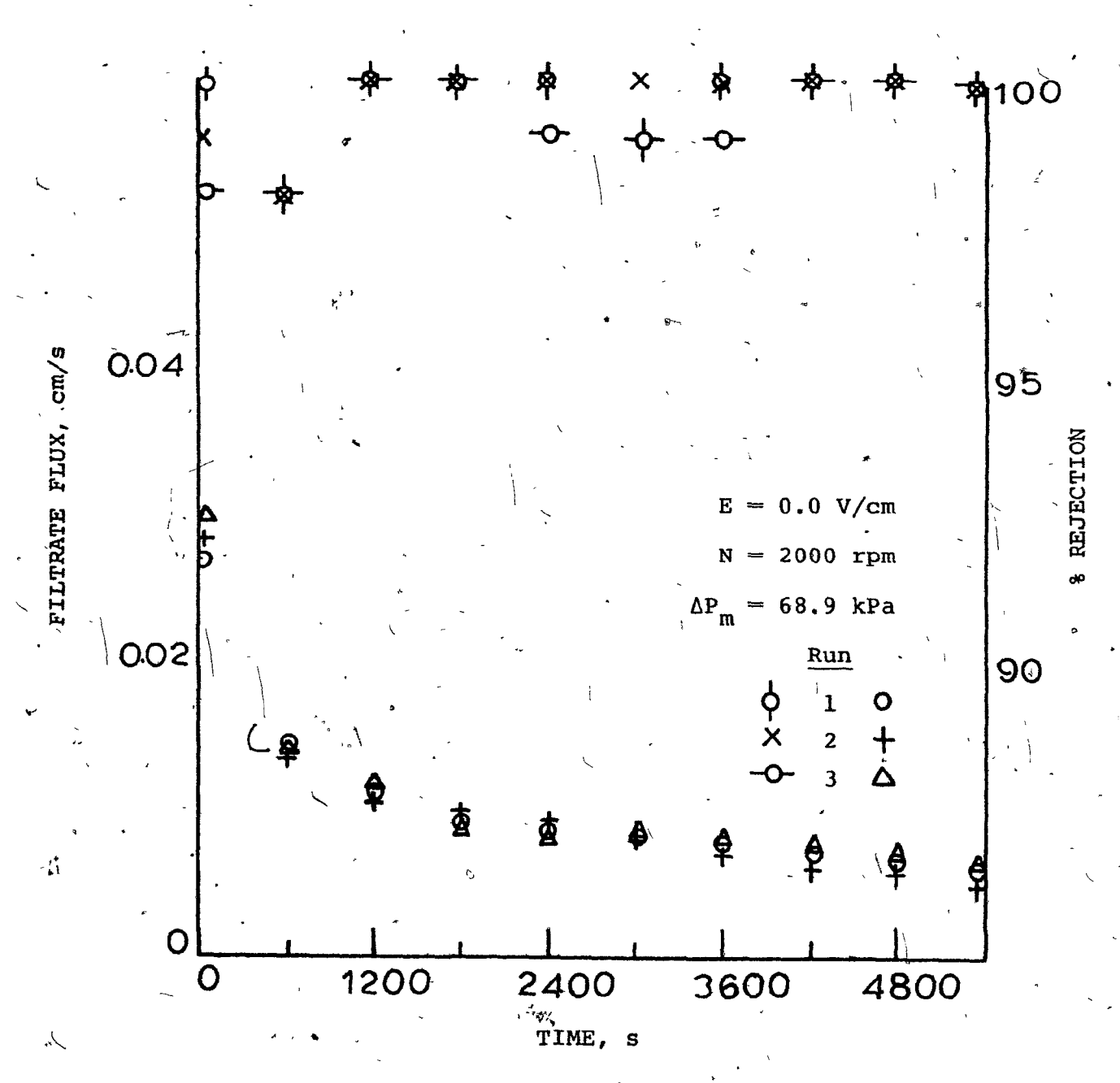


FIGURE 4.10. Reproducibility of Results in Tangential Flow Electrofilter Depicted by Variation of Flux and Rejection with Time

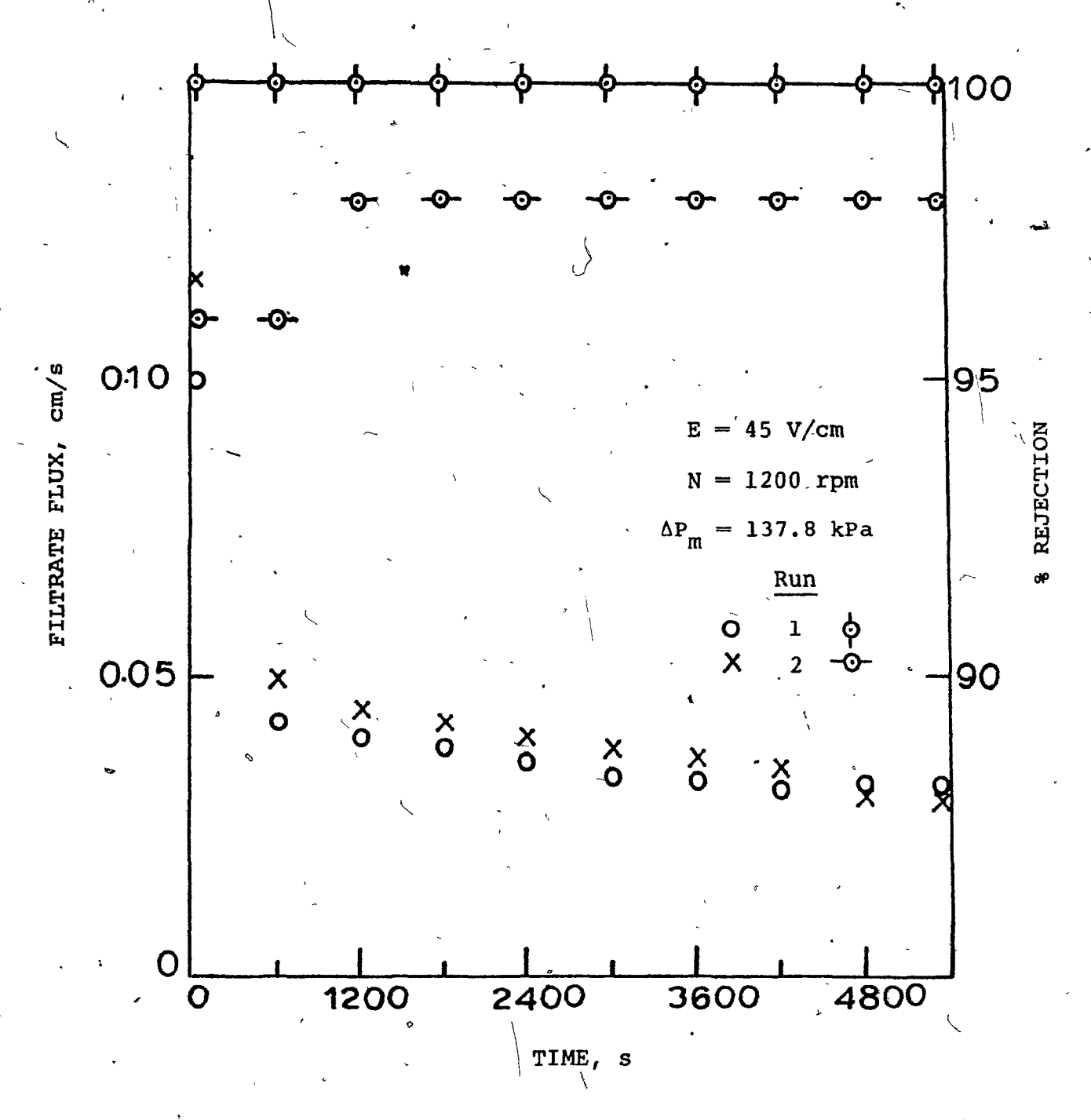


FIGURE 4.11. Reproducibility of Results in Tangential Flow Electrofilter Depicted by Variation of Flux and Rejection with Time

The agreement between the runs is very good. Agreement between the percent rejections from the runs is within 2%. In both Fig. 4.10 and Fig. 4.11, the greatest difference between runs occurs at the beginning. This is due to the fact that the time spent in setting the rotating cylinder to the correct rotation rate was not the same for each run.

#### CHAPTER 5

#### MODEL FOR THE ELECTROFILTER

The tangential flow electrofiltration process employs four particle transport mechanisms to minimize accumulation of particles on the filter medium. These transport mechanisms are fluid turbulence, centrifugal force, electrophoresis and skear stress. Turbulence, centrifugal force and electrophoresis serve to move individual particles away from the medium while shear on the surface removes chunks or layers of the cake. Figure 5.1 shows a cross-section of the tangential flow electrofilter. The

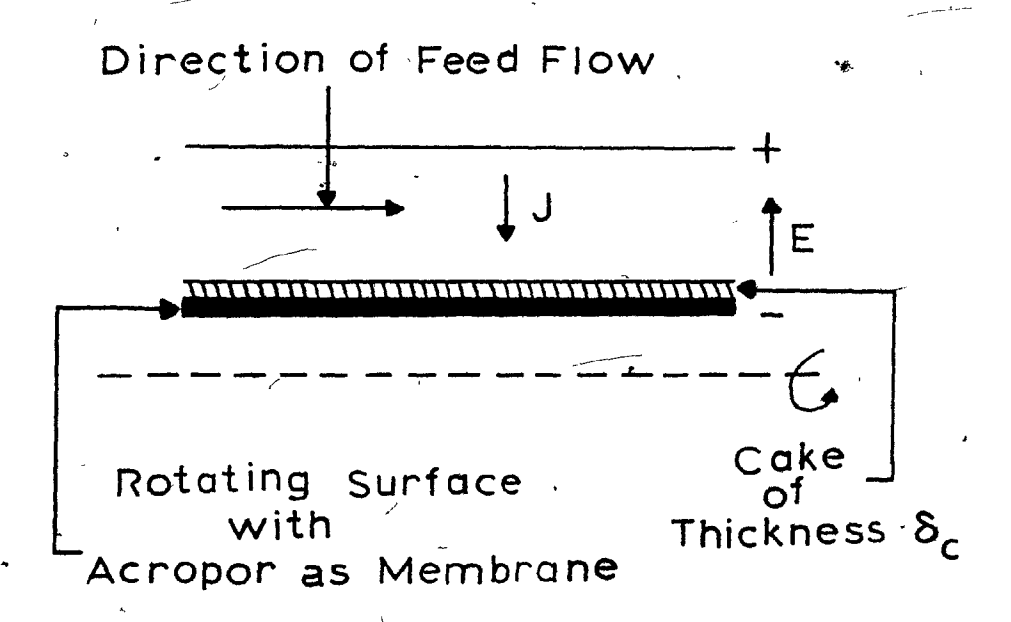


FIGURE 5.1. Cross-Section of Tangential Flow Electrofilter cake filtration mechanism is assumed to apply. All particles reaching the membrane are assumed to be retained.

# 5.1 Derivation of the Model

The fluid velocity normal to the cake equals the permeate flux and is denoted by J, the volumetric flow rate per unit filter area. Because of turbulence, centrifugal forces and electrical forces, the particles do not move toward the cake (or medium) at this velocity. The particles are assumed to have a velocity relative to the fluid,  $U_{\rm S}$ , directed opposite to J, hence the velocity of the particles relative to the cake is  $J-U_{\rm S}$ . The rate of cake removal (mass per unit area per unit time) due to shear is denoted by  $\phi_{\rm R}$ . Assuming that the particle concentration is uniform, a mass balance on the cake yields

$$\rho_{p}(1-\epsilon)\frac{d\delta_{c}}{dt} = (J-U_{s})C-\phi_{R} \qquad (5-1)$$

where

 $\delta_{c}$  = thickness of cake .

ρ - density of particles 💃 \*

 $\varepsilon$  = void fraction within the cake

C = particle concentration in the bulk

 $\phi_{R}^{}$  = rate of cake removal by shear forces at the cake surface

Denoting the resistance of the membrane as  $R_{\mathrm{M}}$  and the resistance of the cake as

$${}_{-}^{R}{}_{C} = {}^{K}{}_{C} \delta_{C} \tag{5-2}$$

where K is a constant, the flux is given by

$$J = \frac{\Delta P_F}{R_M + K_C \delta_C} \tag{5-3}$$

where  $\Delta P_F$  = pressure drop across the cake plus membrane which drives the flux

When no cake is present, the flux is  $J_{o}$ . Assuming  $\Delta P_{F}$  is constant,

$$J_{O} = \frac{\Delta P_{F}}{R_{M}}$$
 (5-4)

or

$$R_{\mathbf{M}} = \frac{\Delta P_{\mathbf{F}}}{J_{\mathbf{O}}} \tag{5-5}$$

Substituting Eq. (5-5) into Eq. (5-3) and rearranging gives

$$\frac{1}{J} = \frac{1}{J_O} + \frac{K_C^{\delta} c}{\Delta P_F}$$
 (5-6)

From (5-6):

$$\delta_{C} = \frac{\Delta P_{F}}{K_{C}} \left( \frac{1}{J} - \frac{1}{J_{O}} \right) \tag{5-7}$$

Differentiating Eq. (5-7) with respect to time and assuming again that  $\Delta P_{\rm F}$  is constant yields

$$\frac{d\delta_{\mathbf{C}}}{dt} = -\frac{\Delta P_{\mathbf{F}}}{K_{\mathbf{C}}\mathbf{J}^2} \frac{d\mathbf{J}}{dt}$$
 (5-8)

Substituting Eq. (5-8) into Eq. (5-1) and rearranging yields the following differential equation for the variation of the permeate flux with time

$$-\frac{1}{J^2}\frac{dJ}{dt} = K\left[J - \left(U_S + \frac{\phi_R}{C}\right)\right]$$
 (5-9)

where

$$K = \frac{K_C^C}{\rho_D (1 - \epsilon) \Delta P_F}$$
 (5-10)

The initial condition is the following.

at 
$$t = 0$$
,  $J = J_{0}$  (5-11)

Equations (5-9) to (5-11) complete the model.

Since  $U_S$  and  $\phi_R$  are constant, Eq. (5-9) can be rearranged as follows. At steady state, dJ/dt=0 and the steady state flux,  $J_\infty$ , is

$$J_{\infty} = U_{S} + \phi_{R}/C \qquad (5-12)$$

Hence, Eq. (5-9) can be written

$$-\frac{1}{J^2}\frac{dJ}{dt} = K(J - J_{\infty})$$
 (5-13)

The solution of Eq. (5-13) subject to Eq. (5-11) is

$$\frac{1}{J_{\infty}} \ln \left( \frac{\frac{1}{J_{\infty}} - \frac{1}{J_{0}}}{\frac{1}{J_{\infty}} - \frac{1}{J}} \right) + \frac{1}{J_{0}} - \frac{1}{J} - KJ_{\infty}t$$
 (5-14)

Equation (5-14) can be rearranged to the following dimensionless form:

$$\left(\frac{J_{o}}{J_{\infty}}\right)^{2} \ln \left[\frac{1-\left(\frac{J_{\infty}}{J_{o}}\right)}{1-\left(\frac{J_{\infty}}{J_{o}}\right)\left(\frac{J_{o}}{J_{\infty}}\right)}\right] - \left(\frac{J_{o}}{J_{\infty}}\right)\left(\frac{J_{o}}{J_{\infty}}-1\right) - KJ_{o}^{2}t \qquad (5-15)$$

Figure 5.2 gives the predictions of the model from Eq. (5-15) in terms of a dimensionless flux,  $J/J_{\rm O}$ , versus a dimensionless time,  $KJ_{\rm O}^2$ t, for several values of  $J_{\rm w}/J_{\rm O}$ . When  $J_{\rm w}/J_{\rm O}=0$ , the model predicts the standard cake filtration flux decay curve. As  $J_{\rm w}/J_{\rm O}$  is increased, the steady state flux is reached more quickly. Hence, any force which increases  $J_{\rm s}$  shortens the time required to achieve steady state.

Figure 5.3 shows the predictions of Eq. (5-15) plotted as  $(J_{\rm O}/J)^2-1$  versus dimensionless time. On these coordinates, classical cake filtration  $(J_{\rm w}/J_{\rm O}=0)$  yields a straight line. The curves approach the origin with a slope given by Eq. (5-17) - see below. For  $J_{\rm w}/J_{\rm O}>0$ , the flux function approaches asymptotic values for large times.

#### 5.2 Special Cases

#### 5.2.1 Cake Filtration

In classical cake filtration, the feed flows perpendicular to the filter medium resulting in the retention of all solute particles and the cake builds up until the filtrate flux reduces to zero. In Eq. (5-13), therefore,  $J_{\infty} = 0$  and

$$-\frac{1}{T^2}\frac{dJ}{dt} - KJ$$
 (5-16)

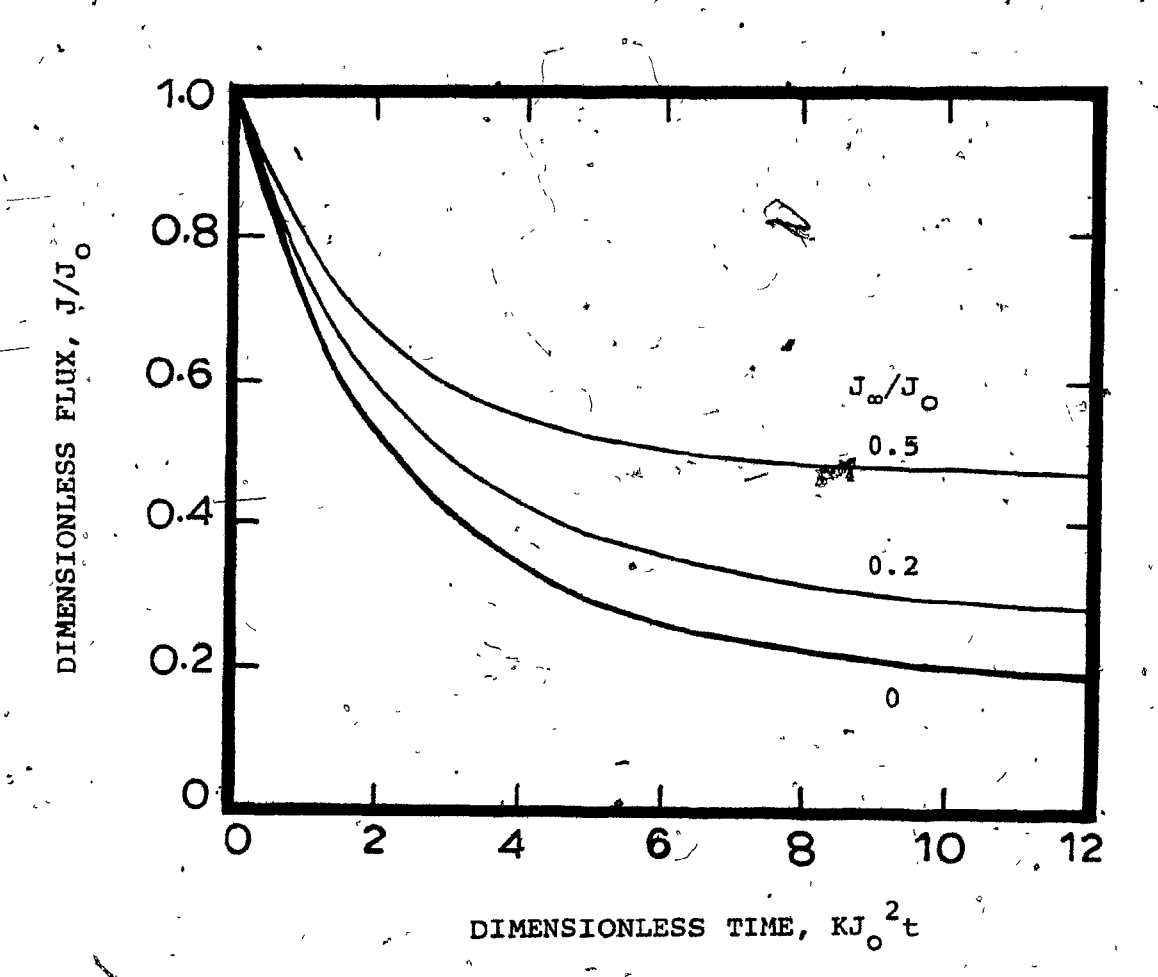


FIGURE 5.2. Variation of Flux ith Time Predicted by Model

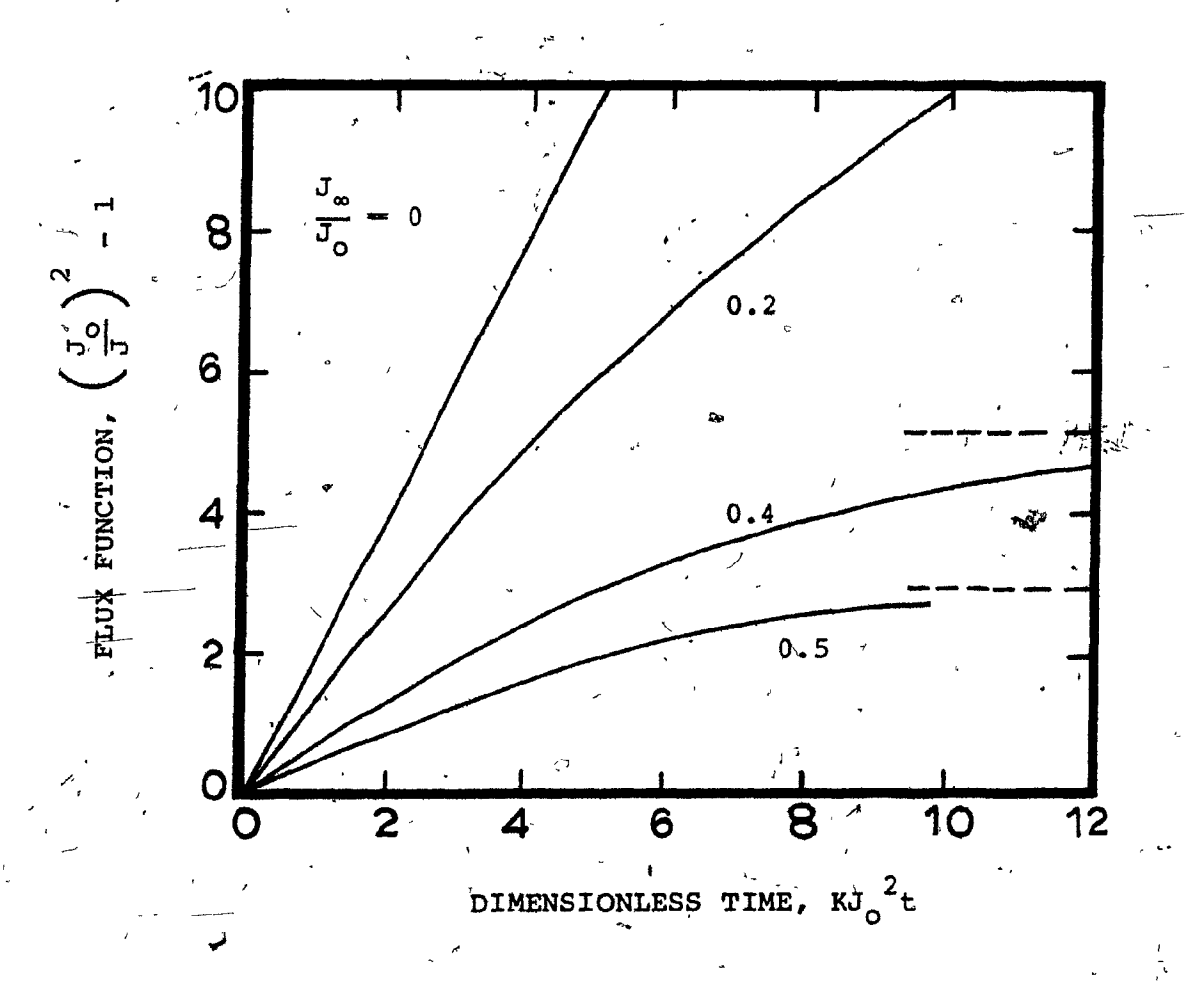


FIGURE 5.3. Cake Filtration Plot of Model Predictions

with Eq. (5-11) as the initial condition. Integration of Eq. (5-16) yields

$$\frac{1}{J^2} - \frac{1}{J_0^2} - 2Kt$$
 (5-17)

By assuming negligible membrane resistance, a similar result was obtained by Kraus (1974) for cross-flow filtration.

Mikhlin and Tanny (1979) also presented a classical cake filtration model which reduces to a form similar to Eq. (5-17) with the assumption of negligible membrane resistance.

# 5.2.2 Small Time Solution, $t \rightarrow 0$

By employing Taylor series expansion, a small time solution can be obtained for Eq. (5-14) in a form that can be compared to Eq. (5-17).

Equation (5-14) can be rewritten as

$$\frac{1}{J_{\infty}^{2}} \ln \left( \frac{1 - \frac{J_{\infty}}{J_{o}}}{1 - \frac{J_{\infty}}{J}} \right) + \frac{1}{J_{\infty}} \left( \frac{1}{J_{o}} - \frac{1}{J} \right) = Kt$$
 (5-18)

Let

$$Y = \frac{1}{\sqrt{2}}$$
 (5-19)

then

(5-20)

where

$$f(Y) = \frac{1}{J_{\infty}^{2}} \ln \left( \frac{1 - \frac{J_{\infty}}{J_{O}}}{1 - J_{\infty}\sqrt{Y}} \right) + \frac{1}{J_{\infty}} \left( \frac{1}{J_{O}} - \sqrt{Y} \right) \qquad (5-21)$$

The Taylor series representation for f(Y) as  $J + J_0$  is

$$f(Y) = f(Y_0) + \left(\frac{df}{dY}\right)_{Y_0} (Y - Y_0)$$
 (5-22)

where

$$Y_{0} = \frac{1}{J_{0}^{2}}$$
 (5-23)

Since  $f(Y_0) = 0$ , Eq. (5-22) becomes

$$f(Y) = \left(\frac{df}{dY}\right)_{Y_{O}} \left(\frac{1}{J^{2}} - \frac{1}{J_{O}^{2}}\right) \qquad (5-24)$$

Differentiation of Eq. (5-21) yields

$$\frac{\mathrm{df}}{\mathrm{dY}} = \frac{1}{2J_{\infty}\sqrt{Y}} \left( \frac{1}{1 - J_{\infty}\sqrt{Y}} - 1 \right) \tag{5-25}$$

and

$$\left(\frac{\mathrm{df}}{\mathrm{dY}}\right)_{Y_{O}} = \frac{1}{2\left(1 - \frac{J_{\infty}}{J_{O}}\right)} \tag{5-26}$$

Substituting Eq. (5-26) into Eq. (5-24) and the result into

Eq. (5-20) gives

$$\frac{1}{J^2} - \frac{1}{J_0^2} = 2K \left( 1 - \frac{J_\infty}{J_0} \right) t \tag{5-27}$$

A plot of  $\frac{1}{J^2} - \frac{1}{J_0}$  versus t should yield a straight line at small time with slope  $2K\left(1 - \frac{J_{\infty}}{J_0}\right)$ . For classical cake filtration,  $J_{\infty} = 0$  and Eq. (5-27) reduces to Eq. (5-17).

## 5.2.3 Steady State, t → ∞

If the particles travel outward relative to the fluid  $_{\rm S}$  (U  $_{\rm S}$  > 0) or if the cake is continuously removed, a steady state flux will eventually be established. This steady state flux is given by Eq. (5-12). At steady state, the particles are carried by bulk flow toward the medium at the same rate as the sum of particle transport due to turbulence, centrifugal forces, electrical forces and shear effects.

# 5.3 Expressions for Slip Velocity, U

Three mechanisms contribute to the particle slip velocity, Us. The velocities resulting from each mechanism alone are assumed additive:

$$U_s = U_t + U_r + U_e$$
 (5-28)

where  $U_t$  = particle velocity due to fluid turbulence  $U_r$  = particle velocity due to centrifugal force  $U_e$  = particle velocity due to electric force

## 5.3.1 Velocity Due to Turbulence

The smallest rotation rate of this study, N=1200 rpm, gives  $Ta=1.8\times10^4$ . Hence, without axial flow the fluid is turbulent. It is assumed that with the axial Reynolds numbers used here (Re  $\sim 10^2$ ) the flow is still turbulent.

Particles are transported away from the surface of the filter medium during the motion of eddies from the rotating surface into the mainstream. This turbulent transport is assumed to be characterized by a velocity which is proportional to u<sub>T</sub>, the friction velocity. A similar hypothesis was used by Friedlander and Johnstone (1957) to describe particle deposition from turbulent pipe flows. Hence

$$U_{t} = K_{t} u_{\tau} \qquad (5-29)$$

where K<sub>t</sub> is a constant which should depend upon particle size and density and fluid properties. The friction velocity is defined by

$$u_{\tau} = \sqrt{\tau/\rho} \qquad (5-30)$$

where  $\tau$  is the total shear force acting on the medium (or cake) surface. This shear force is the result of both the axial flow and the rotation of the inner cylinder. For the rates of rotation used here, N > 1200 rpm, the shear force due to rotation far exceeds that from axial flow as shown in Appendix 2. Therefore,  $\tau$  is replaced by  $\tau_r$ , the shear force due to rotation alone. With this substitution and using Eq. (2-17), Eq. (5-30) can be written

$$u_{\tau} = \sqrt{\frac{C_D}{2}} (\Omega R_i)$$
 (5-31)

Consequently,

$$U_{t} = K_{t} \sqrt{\frac{C_{D}}{2}} (\Omega R_{i}) \qquad (5-32)$$

In the present work, the Taylor number is very large, thus it is assumed that the axial flow has essentially no effect on the fluid turbulence and the drag coefficient is given by Eq. (2-24). Substitution of Eqs. (2-21) and (2-19) into Eq. (5-32) yields

$$U_{t} = K_{t} \left(\frac{a}{2}\right)^{0.5} \left(\frac{\mu}{2\rho}\right)^{0.1} R_{1}^{0.8} \Omega^{0.9}$$
 (5-33)

The turbulent transport velocity is proportional to  $\Omega^{0.9}$ .

Taylor (1936) has provided data from which the constant "a" in Eq. (2-24) may be estimated. This constant is a function of  $R_1/R_0$ . Fortunately, he made measurements on an apparatus essentially identical to the one used in this study. In his system,  $R_1=3.20$  cm and  $R_0=4.05$  cm. Using the last point in his Fig. 9 (Re = 2.57x10<sup>5</sup>,  $C_D=1.82x10^{-3}$ ):

$$a = 2.2 \times 10^{-2}$$
 (5-34)

and

$$C_D = 0.022 \text{ Re}^{-0.2}$$
 (5-35)

# 5.3.2 Velocity Due to Centrifugal Force

As a result of the rotation of the fluid within the annular gap, the particles will develop an outward radial velocity,  $V_r$ , if they are denser than the fluid. In the present work, the particles are about 8% denser than the water in which they are suspended. The particles are small enough so that they follow Stokes' law in gravity free fall. Their terminal settling velocity under gravity is approximately  $1.7 \times 10^{-6}$  cm/s yielding a terminal Reynolds number of about  $1.1 \times 10^{-8}$ .

Following the analysis of Friedlander (1977) for a cyclone it is assumed that the particles follow the mean tangential velocity of the fluid. This tangential motion causes an outward force on the particles. Assuming that the particles follow Stokes' law, their radial velocity at a radial position r is

$$U_{r} = \frac{\rho_{p} d_{p}^{2}}{18\mu} \left(\frac{v_{\theta}^{2}}{r}\right) \tag{5-36}$$

where  $v_{\theta}$  is the average tangential velocity of the fluid. Using Taylor's result for  $v_{\theta}$  given by Eq. (2-25) and applying it at  $r = R_{i}$ , the following expression is obtained

$$U_{r} = 0.015 \frac{\rho_{p} d_{p}^{2} R_{i} \Omega^{2}}{u}$$
 (5-37)

The slip velocity due to centrifugal forces is proportional to the square of the rotation rate.

# 5.3.3 Velocity Due to Electric Force

The latex particles used in the present work are negatively charged (Seoud, 1980). Consequently, the particles were made to move away from the membrane by a DC electric field with the rotating cylinder being the negative pole. Following Bier (1959), Moulik et al. (1967) and Henry et al. (1977), the electrophoretic velocity is written as

$$U_{\rho} = K_{\rho}E \tag{5-38}$$

# 5.4 Cake Removal Rate, φ<sub>R</sub>

Little attention has been paid to the removal of filter cakes in axial flow filtration and no models exist in the filtration literature. However, the removal process is analogous to the shearing off of fouling deposits in heat exchangers. Some experimental and modelling work has been carried out on this phenomenon.

According to a model proposed by Kern and Seaton (1959), the rate of removal of dirt deposits in heat exchangers is proportional to the shear stress exerted on the surface of the deposit by the flowing fluid. They assumed that, instead of being removed particle-by-particle, dirt is sheared off in chunks at random planes and that planes of weakness occur at any depth. Using these assumptions, Kern (1966) developed a time-dependent model to describe fouling using classical fluid dynamics and heat exchanger design variables. It was later established experimentally by Taborek et al. (1972) that for

feed solutions containing highly crystalline substances a tenacious bond between the crystals and the wall is formed. The scale offers a high resistance to shear and, in the case of salt solutions of LiSO<sub>4</sub> and CaSO<sub>4</sub>, the shear resistance was so much higher than the fluid shear that the removal rate was negligible compared to the deposition rate. Since the latex particles are not crystalline, Kern's shear stress removal hypothesis is adopted:

$$\phi_{\mathbf{R}} = K_{\mathbf{R}} \tau \qquad (5-39) \ ($$

where  $K_R$  is a dimensional constant which depends on the characteristics of the particles in the cake. As in Section 5.3.1,  $\tau$  is replaced by  $\tau_r$  yielding

$$\phi_{R} = \kappa_{R} \frac{C_{D}}{2} \rho (\Omega R_{i})^{2}$$
 , (5-40)

Utilizing Eqs. (2-21) and (2-19), the following relationship is obtained

$$\phi_{R} = \frac{aK_{R}\rho}{(2)^{1.2}} \left(\frac{\mu}{\rho}\right)^{0.2} R_{i}^{1.6} \Omega^{1.8}$$
 (5-41)

The removal rate is proportional to  $\Omega^{1.8}$ .

# 5.5 Evaluation of Pressure Driving Force, $\Delta P_F$

The pressure difference causing filtration is the difference between the pressure drop between the outside of the cake

and the inside of the inner tube, P<sub>i</sub> - P<sub>ii</sub>, and the pressure difference due to rigid body rotation:

$$\Delta P_{F} = (P_{i} - P_{ii}) - \frac{\rho}{2} \Omega^{2} (R_{i}^{2} - R_{ii}^{2})$$
 (5-42)

The holes in the wall of the inner tube are assumed to be full of liquid which rotates as a rigid body. Hence, if the pressure difference  $P_i - P_{ii}$  just equals that due to rigid body rotation, there is no flow.

In the present apparatus, it was impossible to obtain  $P_i - P_{ii}$  directly. The gauge pressure of the feed as it entered the gap was measured. Assuming that the feed enters at  $P_p$ , the measured pressure difference was

$$\Delta P_{\rm m} = P_{\rm p} - P_{\rm a} \tag{5-43}$$

where P<sub>a</sub> = atmospheric pressure

The driving pressure was obtained by assuming that the filtrate runs down the inside of the inner cylinder in a very thin film, i.e. the inner cylinder is empty. A sketch of the pressure profile in this situation is given in Fig. 5.4. The pressure is atmospheric within the inner cylinder. At the outside of the medium (or cake), the pressure is P<sub>1</sub>. The pressure within the gap has already been described - see Section 2.3.1. The sharp increase in pressure at R<sub>1</sub> is due to the resistance of the medium and the cake.

In Appendix 3, it is shown that

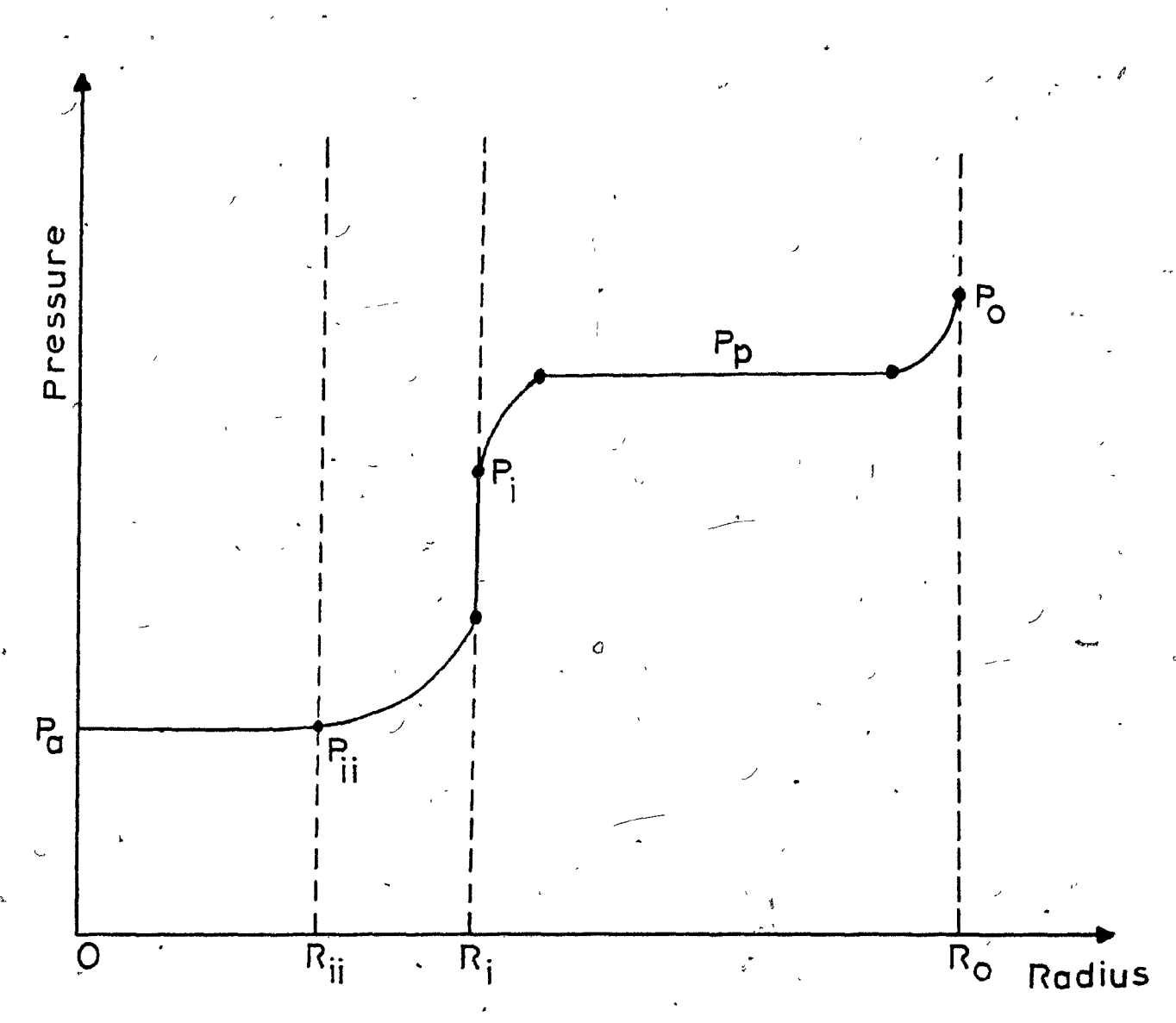


FIGURE 5.4. Pressure Variation in the Radial Direction with Inner Cylinder Empty

$$\Delta P_{\mathbf{F}} = \Delta P_{\mathbf{m}} - \psi \frac{\rho}{2} / (\Omega R_{\mathbf{i}})^{2} \qquad (5-44)$$

with

 $\psi = .0.0453$ 

(5-45)

Hence,  $\Delta P_F$  is lower than  $\Delta P_m$  by an amount which varies from 0.4 kPa at N = 1200 rpm to 2.0 kPa at 2800 rpm.

### CHAPTER 6

### DISCUSSION OF RESULTS

### 6.1 Introduction

The data presented in Chapter 4 showed clearly the beneficial effect of adding an electric field to the tangential flow filters. The filtrate flux increased in the presence of the electric field. At the same time, there was little change in the particle rejection by the filter. Above a certain field strength, (about 100 V/cm for the suspension used here), the flux decreased with increasing field strength.

In this chapter, the flux data are compared to the predictions of the model presented in Chapter 5. The characteristics of the cake are obtained from the fluxes at small times. The effects of rotation rate and electric field strength are compared to the predictions of the model for the fluxes at 90 minutes. The power consumption of the electrofilter and its relationship with the 90-minute flux are also examined.

# 6.2 Behavior for Small Times

Figures 6.1 to 6.5 are plots of  $\frac{1}{J^2} - \frac{1}{J^2}$  versus time as suggested by the small time solution to the model, Eq. (5-27). For N = 0 rpm and E = 0 V/cm, the data are well-represented by straight lines as expected from the cake filtration result, Eq. (5-17). For non-zero rotation rates and/or field strengths, the data are linear at small times and then appear to approach



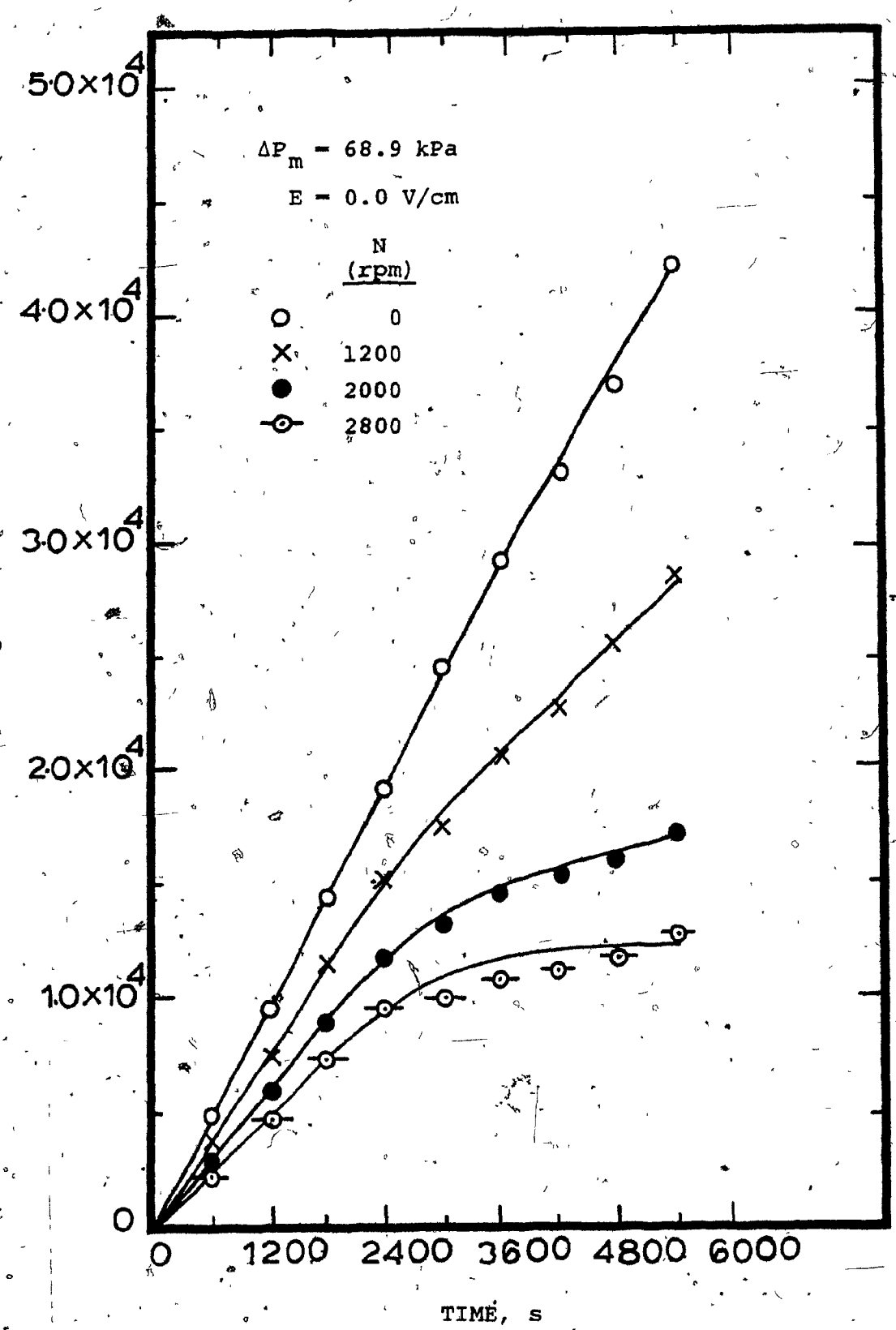


FIGURE 6.1. Plot of  $(1/J^2 - 1/J_0^2)$  Versus Time Depicting Small

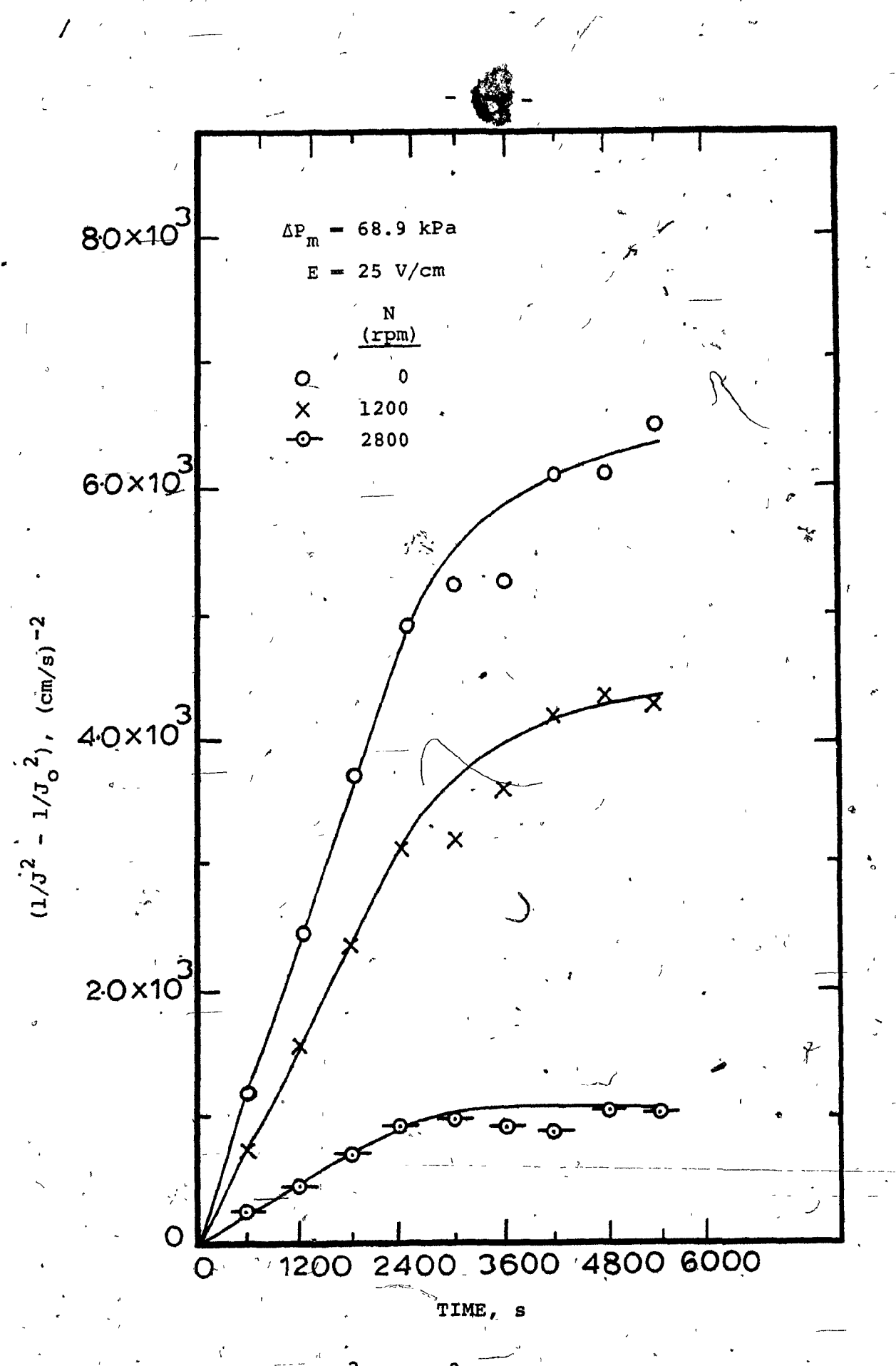


FIGURE 6.2. Plot of  $(1/J^2 - 1/J_0^2)$  Versus Time Depicting Small Time Solution to Model

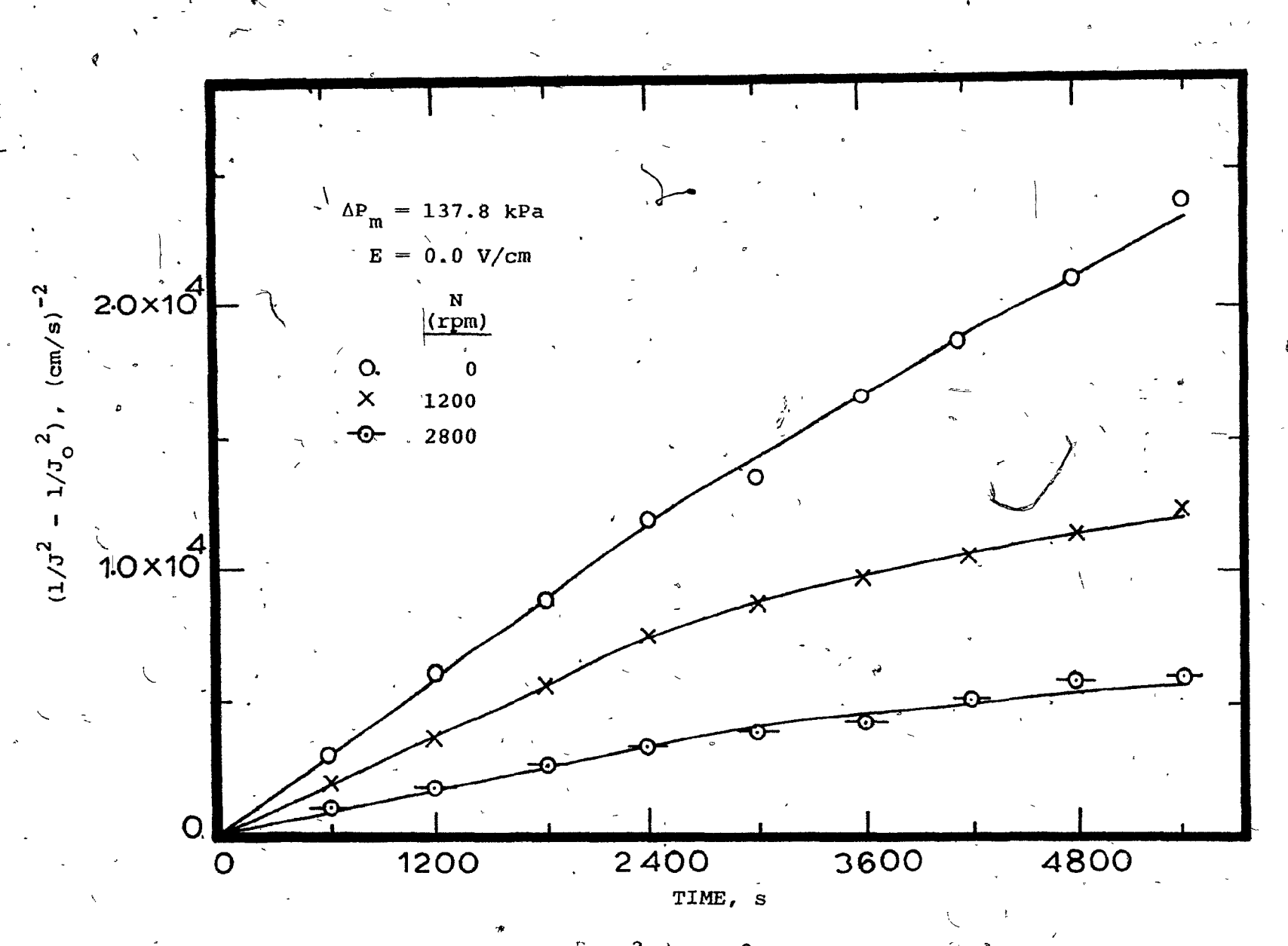
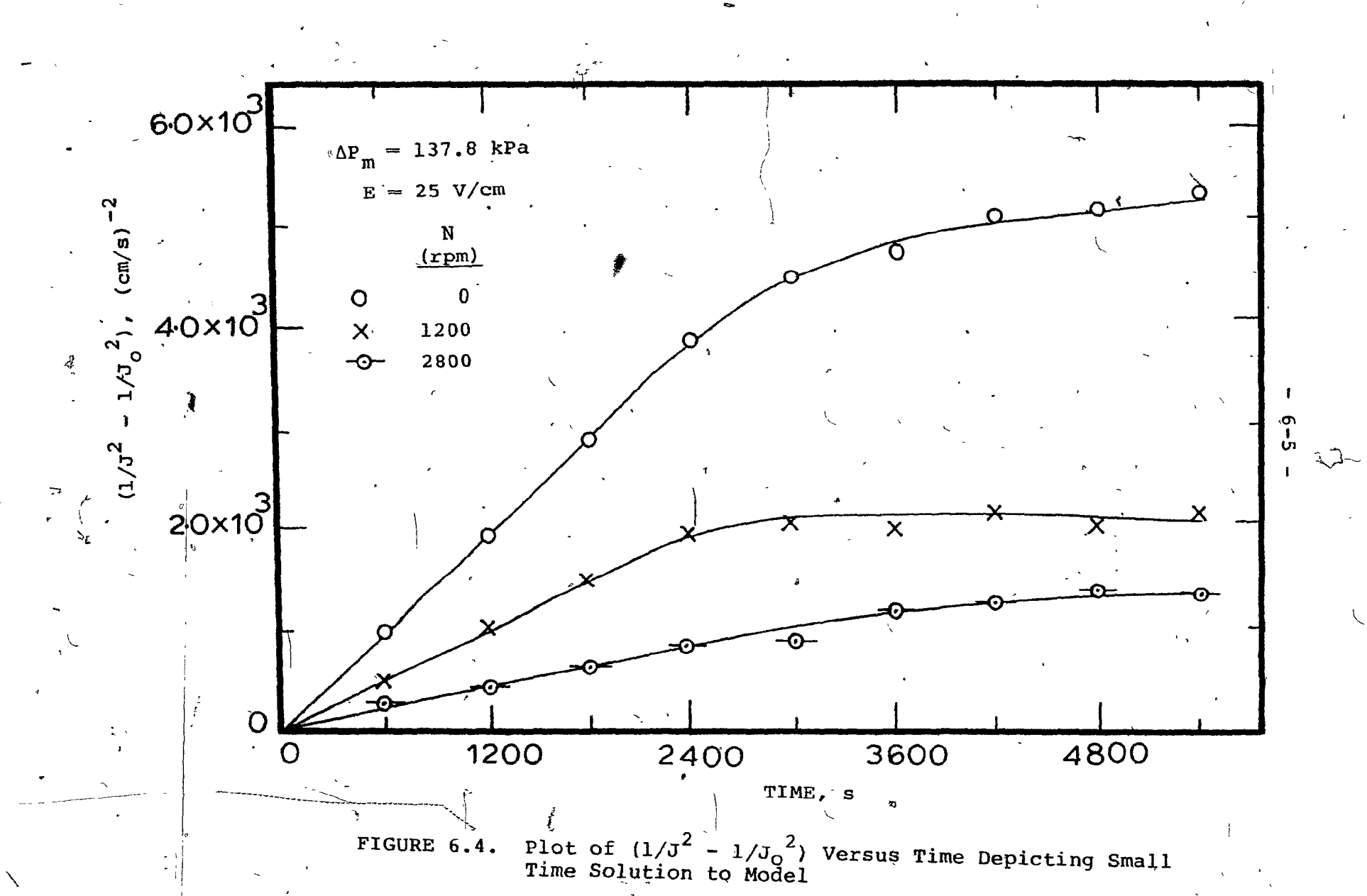
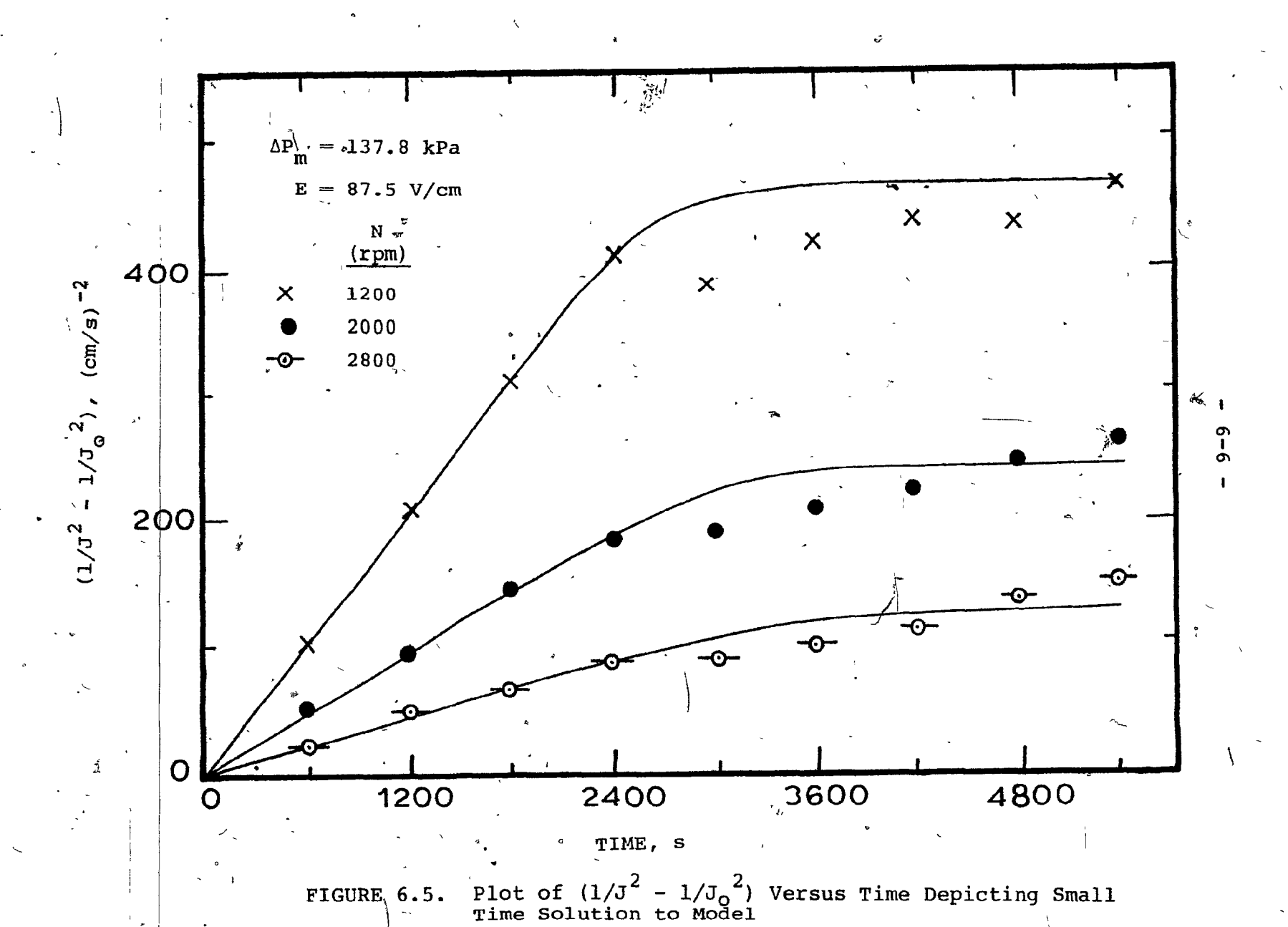


FIGURE 6.3. Plot of  $(1/J^2 - 1/J_0^2)$  Versus Time Depicting Small Time Solution to Model





asymptotic values as time increases. The behavior of all the data was similar to the samples shown in these figures. Qualitatively, the data follow the predictions of the model depicted in Fig. 5.3.

The slope of the curves in Figs. 6.1 to 6.5 at small times is equal to  $2K(1-J_{\infty}/J_{0})$  - see Eq. (5-27). Each run was plotted in the cake filtration form like Figs. 6.1 to 6.5. The slopes of small time were obtained by least squares fit to these plots for times less than or equal to 40 minutes. These slopes are tabulated in Tables Al-1 and Al-2 in Appendix 1.

# 6.2.1 Specific Cake Resistance

The specific cake resistance,  $\alpha$ , is defined by applying Darcy's law to flow through the cake:

$$J = \frac{\Delta P_{F} / \delta_{C}}{\alpha \mu \rho_{p} (1 - \epsilon)}$$
 (6-1)

If the membrane resistance is negligible compared to the cake resistance, Eq. (5-3) reduces to

$$J = \frac{\Delta P_{F}/\delta_{C}}{K_{C}}$$
 (6-2)

Equating Eqs. (6-1) and (6-2) yields the cake resistance per unit thickness:

$$K_{C} = \alpha \mu \rho_{p} (1 - \epsilon) \tag{6 3}$$

Combining Eq. (6-3) with Eq. (5-10) yields

$$\alpha = \frac{K\Delta P_{F}}{11C} \tag{6-4}$$

Let S be the small time slope of Figs. 6.1 to 6.5:

$$S = 2K \left( 1 - \frac{J_{\infty}}{J_{0}} \right) \tag{6-5}$$

then

$$\alpha = \frac{S\Delta P_{F}}{2\left(1 - \frac{J_{\infty}}{J_{O}}\right)\mu C}$$
(6-6)

The specific cake resistance can be computed from the slopes tabulated in Appendix 1,  $\Delta P_F$  as given by Eqs. (5-44) and (5-45) and  $J_{\infty}$ .

For N = 0 rpm and E = 0 V/cm, the particle slip velocity is zero because the axial flow is laminar, hence  $J_{\infty}=0$ . Specific cake resistances for this situation are plotted against the pressure driving force in Fig. 6.6. Also plotted are the data of Doshi and Trettin (1980) for a polystyrene latex with a smaller particle size at a larger concentration and under a larger  $\Delta P_{\rm F}$ . The agreement between the  $\alpha$ -values is good. Both sets of, data show that the cake is compressible because  $\alpha$  increases with  $\Delta P_{\rm F}$ . McCabe and Smith (1967) suggest that for many materials

$$\alpha \sim (\Delta P_{\mathbf{F}})^{\ell}$$
 (6-7)

()

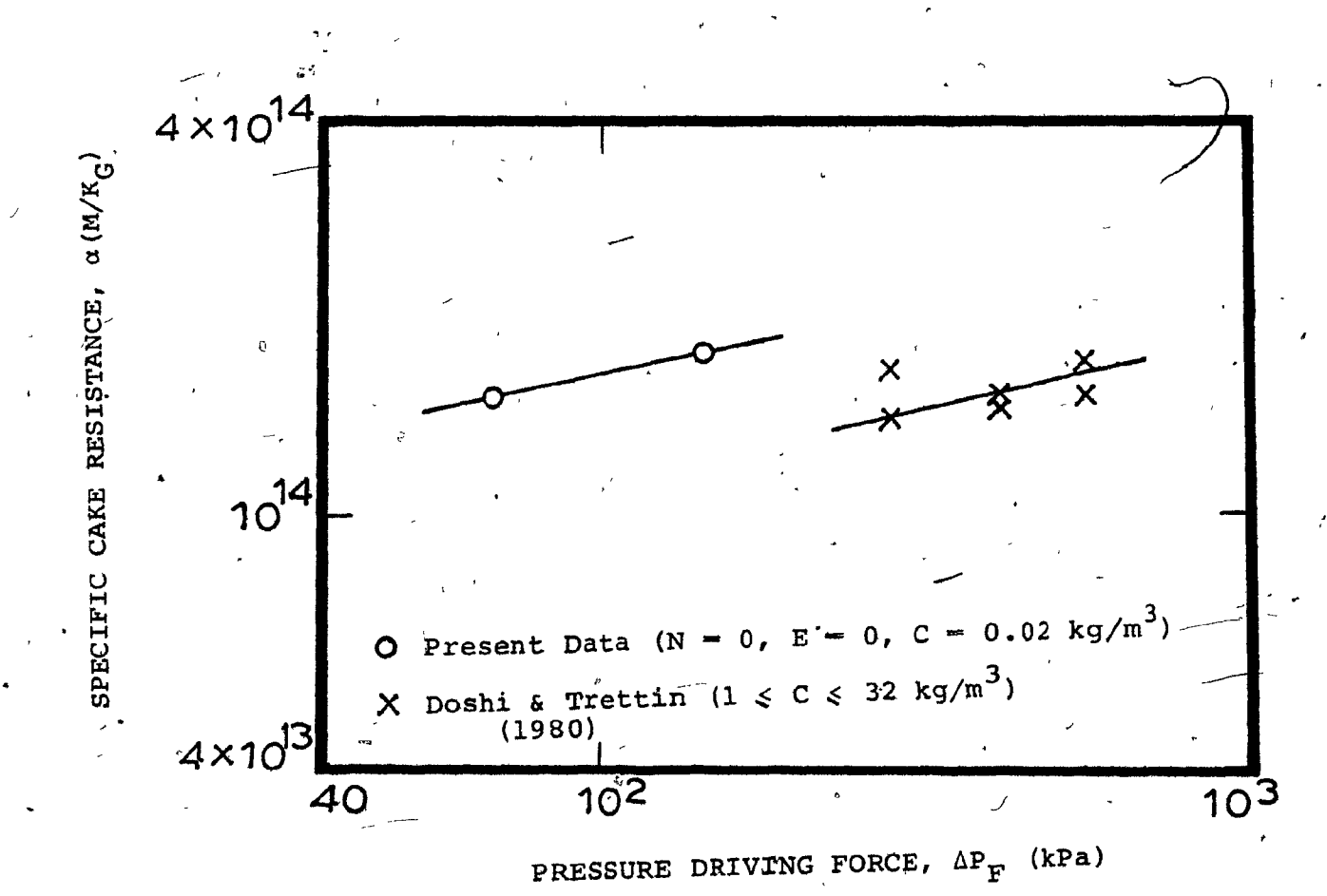


FIGURE 6.6. Variation of Specific Cake Resistance with Pressure Driving Force

with  $0.1 \le \ell \le 1$ . The lines on the plot are drawn with  $\ell = 0.22$ , the value found by Doshi and Trettin. The fit is very good.

For non-zero N and/or E, no  $J_{\infty}$  values are available. In this case,  $\alpha$ -values were calculated using  $J_{90}$  instead. A rough measure of the error is obtained from the  $\alpha$ -values at N = 0 rpm, E = 0 V/cm. In this situation, 25-30% error was incurred when experimental  $J_{90}$ -values were used rather than the true  $J_{\infty}$  value, i.e.  $J_{\infty} = 0$ .

Specific cake resistances calculated from Eq. (6-6) with  $J_{90}$  in place of  $J_{\infty}$  are shown in Fig. 6.7 for one value of the measured pressure difference. Increasing either the rotation rate or the field strength decreased the specific cake resistance. From the Kozeny-Carman equation (Carman, 1956) for a bed of spherical particles, it is readily shown that

$$\alpha = \frac{180(1-\epsilon)^2}{d_p^2 \epsilon^3 \rho_p}$$
 (6-8)

Values of the constant have been found experimentally to lie between 150 and 180. The decrease in  $\alpha$  is probably due to an increase in the void fraction within the cake. Also shown on the ordinate of Fig. 6.7 are values of  $\alpha$  calculated from Eq. (6-8) for void fraction,  $\epsilon$ , of 0.2, 0.3 and 0.4. At higher N and E, the particles approach the cake at a lower rate. Hence, they have time to position themselves in electrostatically favorable positions. Since the particles in the cake are also negatively charged, a very porous structure is favored. At

 $(\bar{\phantom{a}})$ 

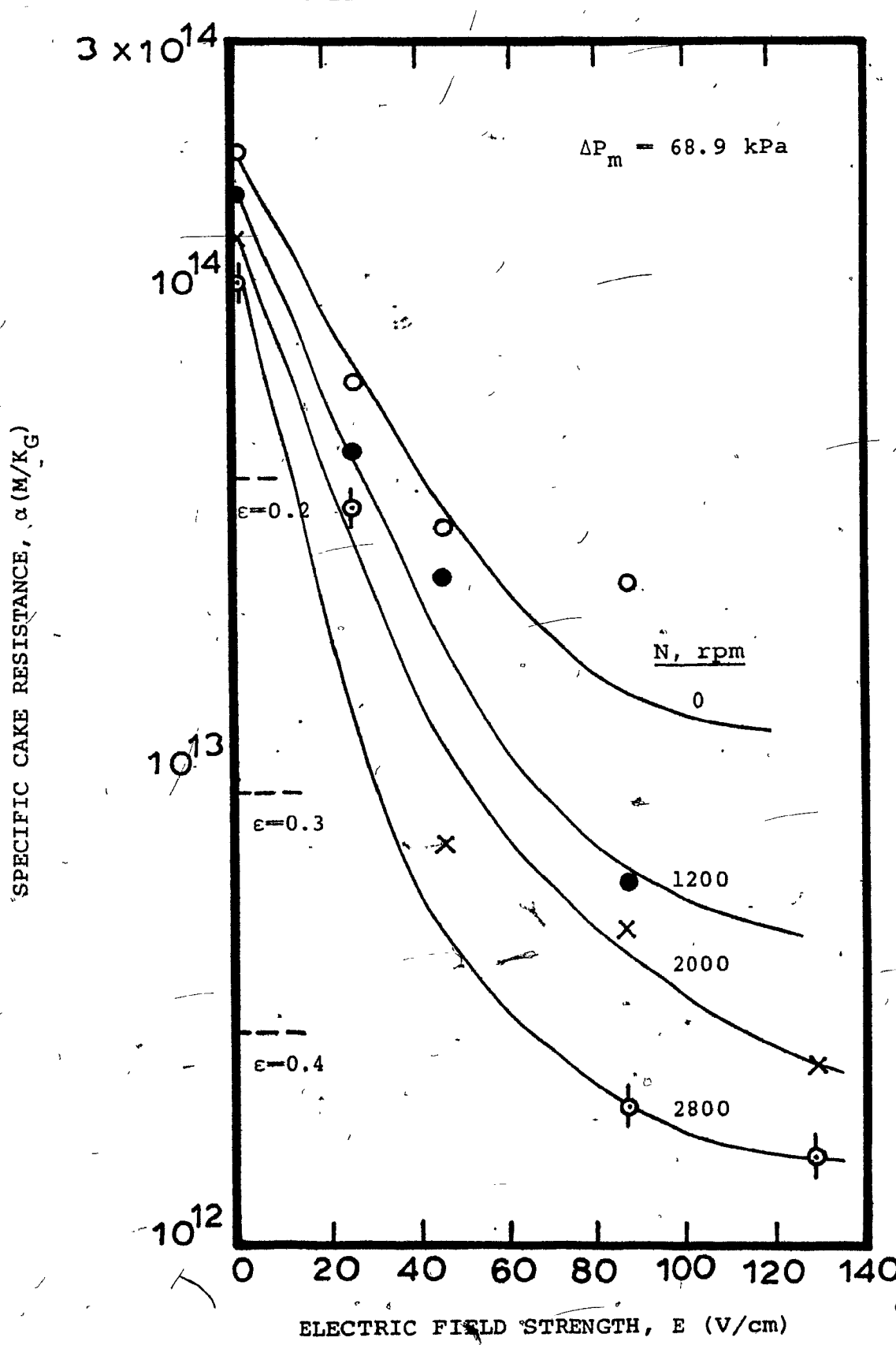


FIGURE 6.7. Variation of Specific Cake Resistance with Field Strength

low N and E, where the rate of arrival of particles at the cake is larger, the particles are forced into more closely packed (lower  $\epsilon$ ), less electrostatically favorable, positions. This yields decreasing  $\alpha$  with increasing values of N and/or E. Doshi and Trettin (1980) also used this mechanism to explain the fact that  $\alpha$  increases with bulk concentration.

The relationship shown in Fig. 6.7 for  $\Delta P_m = 68.9$  kPa was also found for  $\Delta P_m = 137.8$  kPa. Both sets of data were reduced to the same form by plotting the ratio of the cake resistance at a field strength E to that at E = 0 versus E. Figure 6.8 shows that the data for both pressure differences are brought together on these coordinates. At a field strength of 60 V/cm, the cake resistance decreased by a factor of 8 at N = 0 rpm and a factor of 20 at N = 1200 rpm.

# 6.3 Behavior at Long Times

Combining Eqs. (5-12), (5-28), (5-33), (5-34), (5-37), (5-38) and (5-41) yields

$$J_{\infty} = 0.098 \text{ K}_{\frac{1}{p}} \left(\frac{\mu}{\rho}\right)^{0.1} R_{1}^{0.8} \Omega^{0.9} + 0.015 \frac{\rho_{p} d_{p}^{2} R_{1}^{2} \Omega^{2}}{\mu}$$

$$+ 0.0096 \rho K_{R} \left(\frac{\mu}{\rho}\right)^{0.2} R_{1}^{1.6} \Omega^{1.8} + K_{e}^{E} \qquad (6-9)$$

Rotation of the inner cylinder introduces the terms in Eq. (6-9) accounting for turbulence (proportional to  $\Omega^{0.9}$ ), centrifugal force (proportional to  $\Omega^2$ ) and shear at the cake surface (proportional to  $\Omega^{1.8}$ ). The final contribution is due to

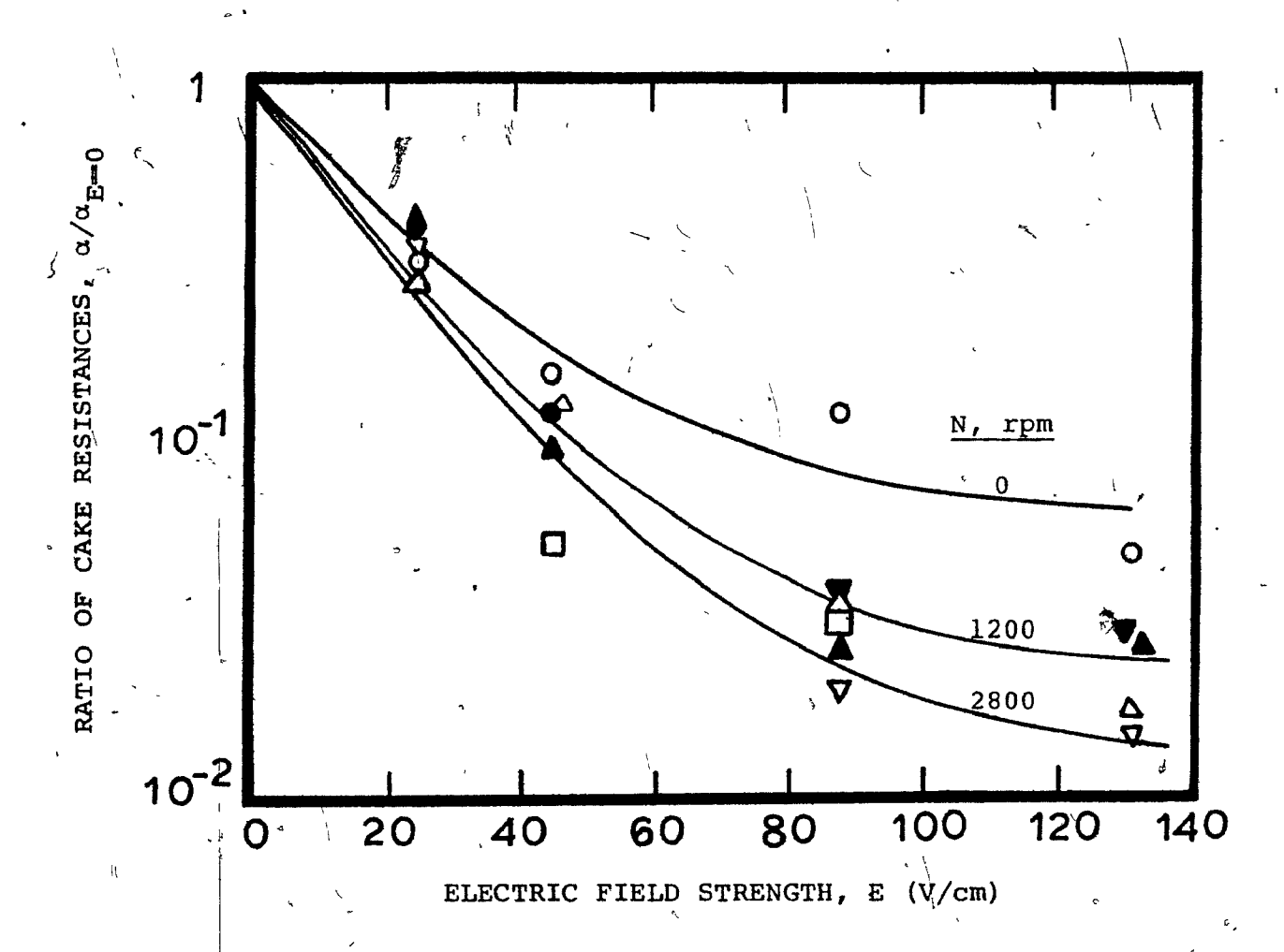


FIGURE 6.8. Variation of Ratio of Cake Resistance with Field Strength

the electric field. Since no experimental values of  $J_{\infty}$  were available, fluxes at 90 minutes,  $J_{90}$ , were used to determine the effect of rotation rate and electric field strength.

### 6.3.1 Effect of Rotation Rate

Of the terms dependent upon rotation rate, only that due to centrifugal force, the second term on the right-hand side of Eq. (6-9), does not contain an arbitrary constant. For the present system at the highest rate of rotation (N = 2800 rpm or  $\Omega$  = 293 radians/s), this term has a magnitude of 1.3x10<sup>-6</sup> cm/s. Since this is several orders of magnitude smaller than the measured  $J_{90}$ -values, it is unlikely that centrifugal force is an important contribution to  $J_{\infty}$ .

Figures 6.9 and 6.10 present  $J_{90}$  as a function of rotation rate raised to the 0.9 power,  $N^{0.9}$ . The plots show a good linear relationship, hence it is likely that the major contribution of rotation to  $J_{\infty}$  is through turbulence. The order of magnitude of  $K_{+}$  is  $5 \times 10^{-4}$ .

Figures 6.9 and 6.10 show a larger effect of rotation rate at larger field strengths. This is not predicted by the model. In Eq. (6-9), there is no interaction between rotation rate and field strength. The effect shown in the figures probably appears because  $J_{90}$ -values were used rather than  $J_{\infty}$ . At 90 minutes, the approach to  $J_{\infty}$  is not the same for each rotation rate and field strength, i.e. at 90 minutes the amount of cake built up and its specific resistance are themselves functions of N and E. This Antroduces the interaction seen in Figs. 6.9 and

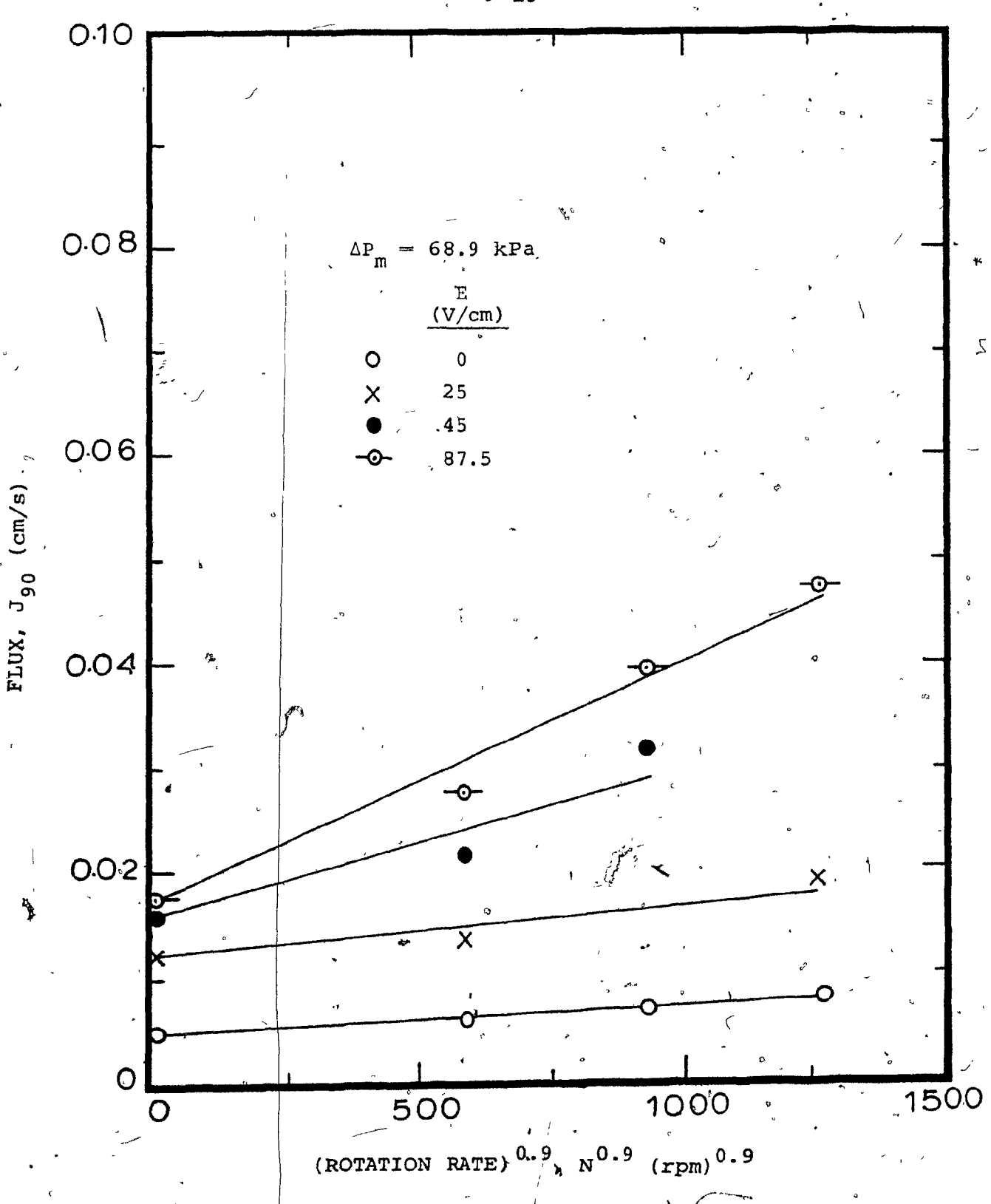


FIGURE 6.9. Variation of Flux with Rotation Rate Raised to the 0.9 Power

۳.

()

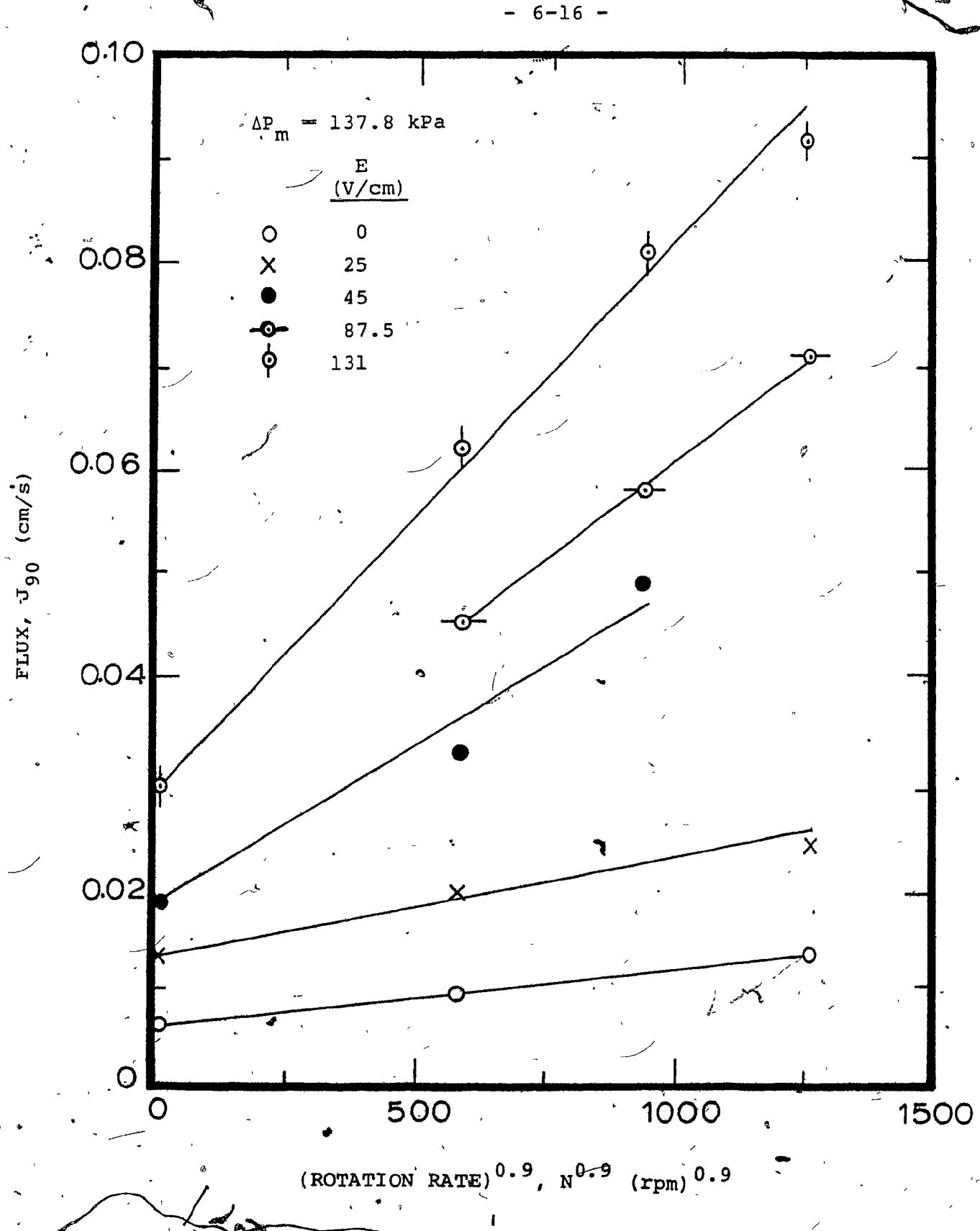


FIGURE 6.10. Variation of Flux with Rotation Rate Raised to the 0.9 Power

6.10. At steady state, the cake should build up until the flux is given by Eq. (6-9).

# 6.3.2 Effect of Field Strength

Equation (6-9) shows a linear dependence of  $J_{\infty}$  on field strength, E: Figures 6.11 and 6.12 show  $J_{90}$  as a function of field strength at the two values of  $\Delta P_{m}$ . The fluxes increased linearly with field strength up to E  $\approx$  100 V/cm. Beyond this field strength, there was a broad maximum and then a decline in flux. The flux decline is probably due to the generation of hydrogen bubbles which accumulated at the surface of the cake, thus clogging the pores.

Fitting the J<sub>90</sub>-points at E < 100 V/cm by least squares yields the following slopes in Figs. 6.11 and 6.12. The slopes in Table 6.1 should equal the mobility of the latex suspension,

TABLE 6.1
Slopes from Plots of J<sub>90</sub> Versus E

Slope,  $\frac{cm/s}{V/cm}$ 

Rotation Rate, rpm	$\Delta P_{\rm m} = 68.9 \text{ kPa}$	$\Delta P_{m} = 137.8 \text{ kPa}$
* '° 0	1.40x10 <sup>-4</sup>	2.90×10 <sup>-4</sup>
1200	2.50x10 <sup>-4</sup>	4.20x10 <sup>-4</sup>
2000	3.70×10 <sup>-4</sup>	5.40x10 <sup>-4</sup>
2800	4.50x10 <sup>-4</sup> .	6.90x10 <sup>-4</sup>

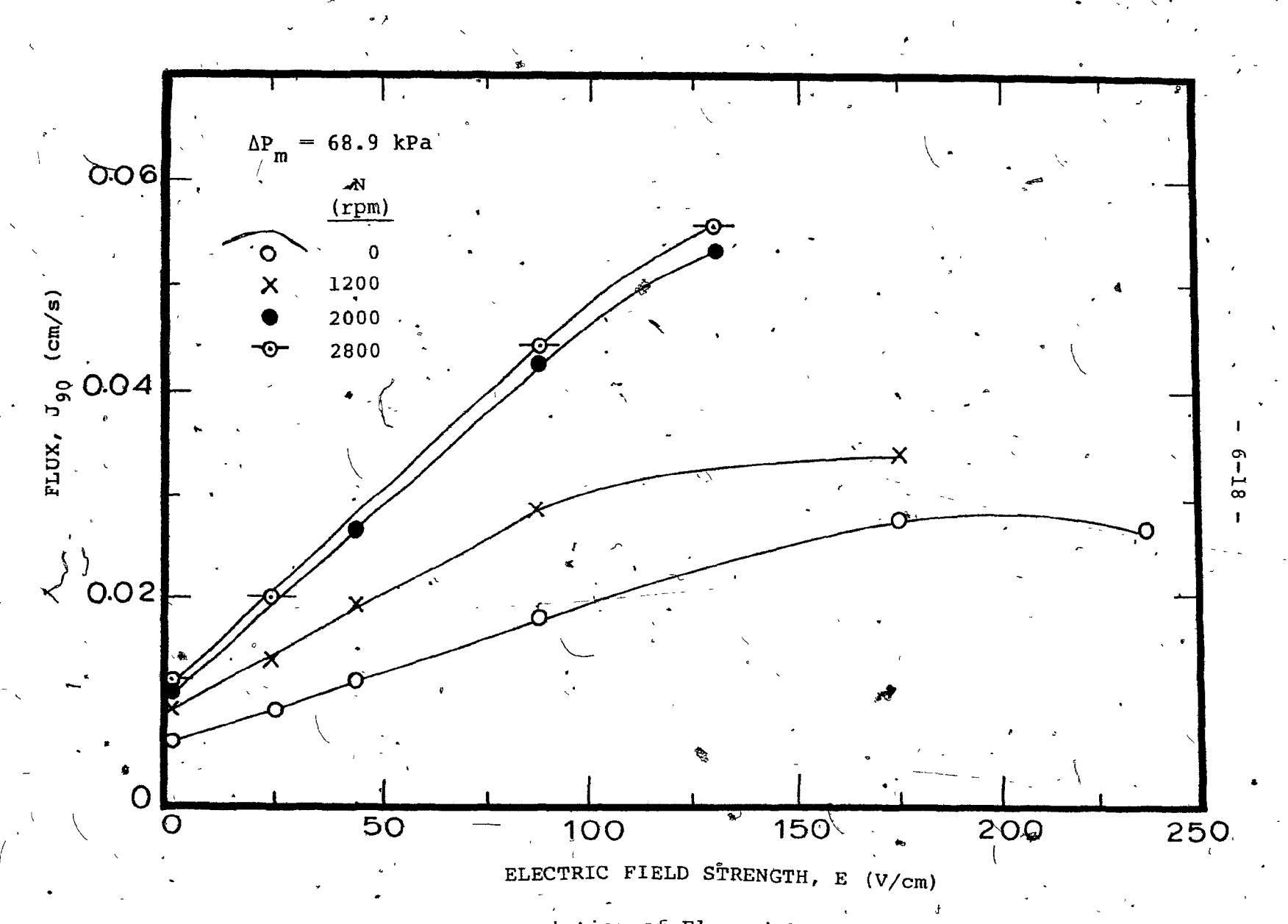
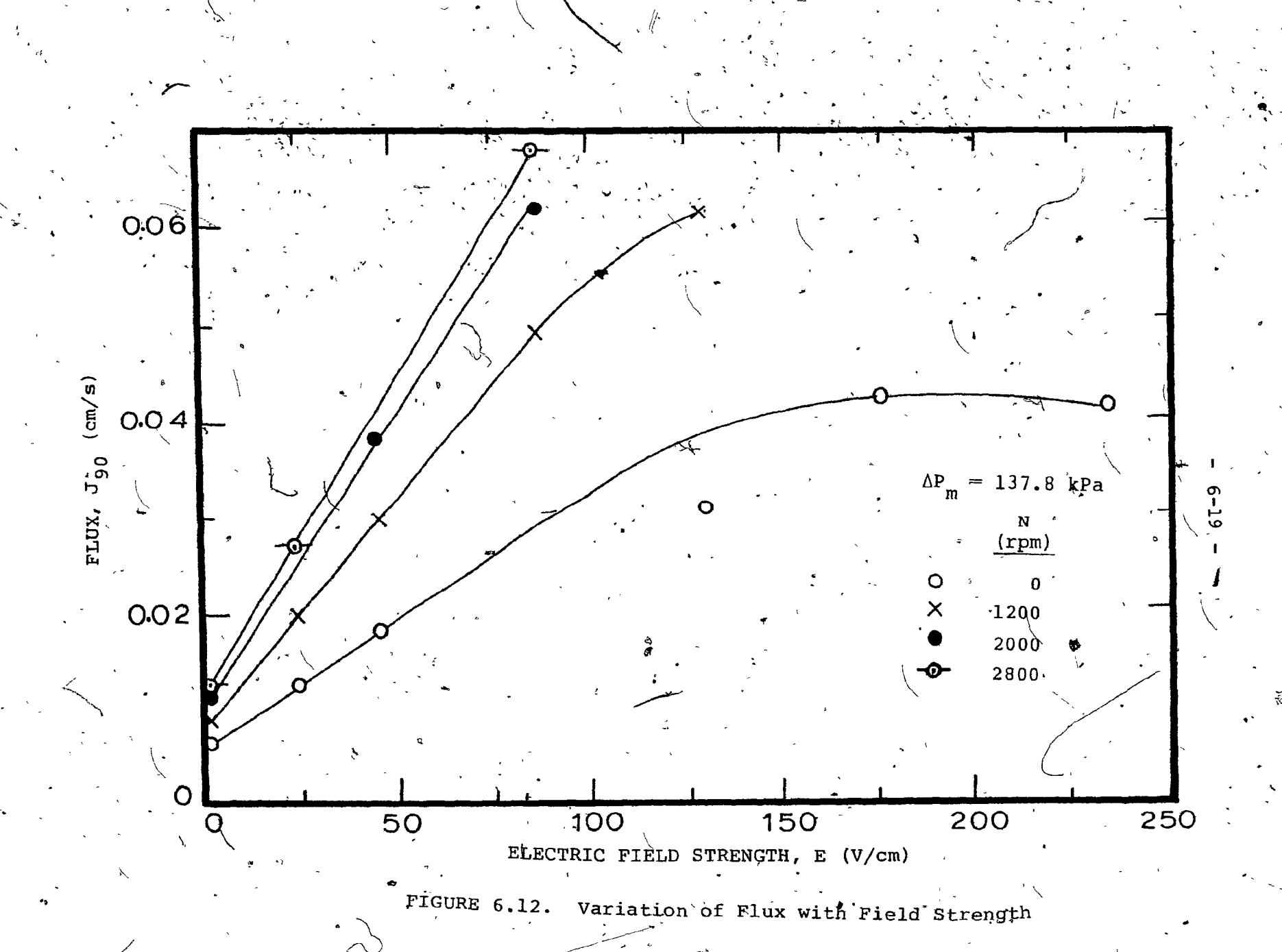


FIGURE 6.11. Variation of Flux with Field Strength



 $\rm K_e = 4.22 {\rm x} 10^{-4} \ \frac{\rm cm/s}{\rm V/cm}$ . As seen in the previous section, there is an interaction of rotation rate and field strength. However, the order of magnitude agreement between the slope and  $\rm K_e$  lends support to the model. It is also possible that there may be an electroosmotic flow through the cake which causes a larger increase in flux with E than the model predicts.

### 6.4 Power Consumption and Flux

A good filter should provide a high flux with a low power consumption. In the tangential flow electrofilter, power is required to rotate the inner cylinder, to maintain the electric field and to pump the suspension through the annular gap. The power required to rotate the inner cylinder goes to overcoming friction in the bearings and to overcoming the shear forces at the surface of the cylinder. Only the power required to overcome surface shear is considered here. The friction in the bearings depends on their design. Power measurements on the actual device are required to account for this.

The power required to overcome shear per unit area of the inner cylinder is given by combining Eqs. (2-18), (2-19) and (5-35):

$$P_r = 0.0096 \rho^{0.8} \mu^{0.2} R_1^{2.6} \Omega^{2.8}$$
 (6-10)

The pumping power is given by the product of the volumetric flow rate of suspension and the axial pressure drop. Assuming fully developed flow and following Bird et al. (1960), the

pumping power per unit outside area of the rotating inner cylinder is

$$P_{\rm p} = \frac{4\mu Q^2}{\pi^2 \kappa R_{\rm o}^{5} F(\kappa)}$$
 (6-11)

where  $F(\kappa)$  is given by Eq. (A2-5) in Appendix 2.

The electrical power is given by the product of the voltage drop between the inner and outer cylinders and the current.

Per unit area of the inner cylinders the electrical power is

$$P_{e} = VI/2\pi R_{i}L \qquad (6-12)$$

Considering the gap between the cylinders as the space between two parallel plates a distance b apart,

$$V = bE = (R_0 - R_1)E$$
 (6-13)

and

$$I = (2\pi R_{i}L)EC_{e}$$
 (6-14)

where  $c_{\rm e}$  = electrical conductivity of the suspension Hence, the electrical power can be written

$$P_{e} = (R_{o} - R_{i}) c_{e} E^{2}$$
 (6-15)

Since the value of  $J_{\infty}$  is proportional to the field strength, the last equation brings out the effect of the conductivity of the suspension on the electrical power requirement.

The total power per unit outside area of the inner cylinder

is

$$P_{\rm T} = P_{\rm r} + P_{\rm p} + P_{\rm e}$$
 (6-16)

The contribution of each of the terms to the total power requirement is given in Table 6.2 for typical values of N and E.

TABLE 6.2

Calculated Power Requirements

					×		
,	, N	E .	Power, W/m <sup>2</sup>				
•	rpm ,	V/cm	Pr	- P.p.,	P <sub>e</sub> ∙	$^{P}\mathbf{T}$	
	0.	. 0	0	3.2x10 <sup>-4</sup>	Ö	3.2x10 <sup>-4</sup>	
ĺ	·: 0	50	0 .	$3.2 \times 10^{-4}$	456	456 ,	
	1200	0	59.5	$3.2 \times 10^{-4}$	. 0	59.5	
	1,200	50 💪	59.5	°3.2x10 <sup>-4</sup>	456	515.5	
i	2800	0	63.8	$3.2 \times 10^{-4}$	Ó	638	
	2800	<sup>′</sup> 50₁	63.8	3.2x10 <sup>-4</sup>	456	1094	

Only when there is no rotation and no field is the pumping power important.

Figure 6.13 shows the value of  $J_{90}$  which results from a given expenditure of power. The power for rotation was computed from Eq. (6-10), while the electrical power was computed from Eq. (6-12) using the measured values of the current and voltage. The pumping power was neglected except for N = 0 rpm and E = 0 V/cm. The flux rises rapidly with power. For N = 0 rpm, the

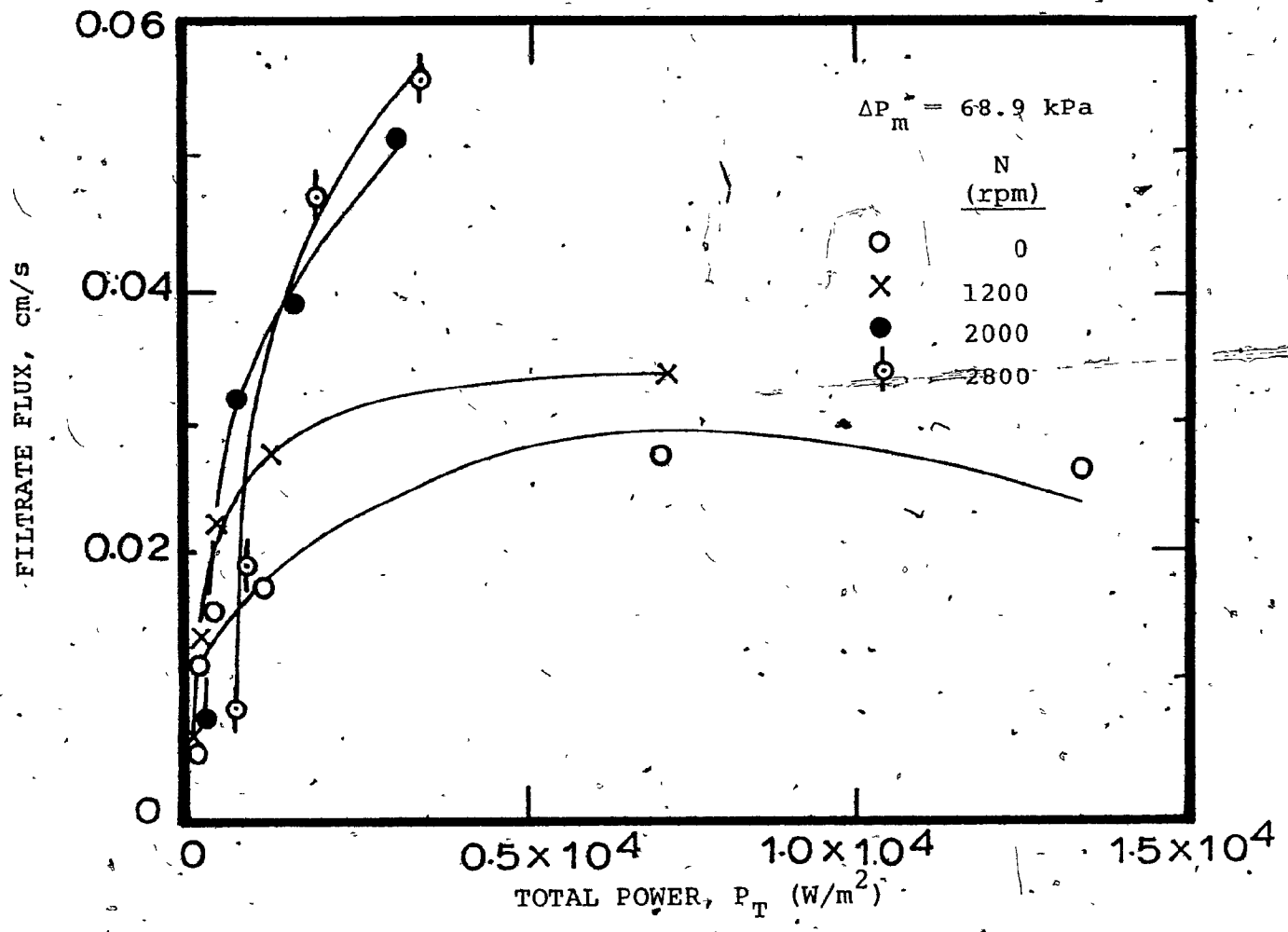


FIGURE 6.13. Variation of Filtrate Flux with Total Power Consumed

flux reaches a broad maximum and then declines due to the generation of hydrogen bubbles as mentioned earlier. This behavior is expected at all rotation rates for sufficiently high electrical power inputs.

An index of filter performance which should not be minimized is the total power expended per unit flux. This index, calculated from J<sub>90</sub>-values, is shown as a function of the electric field strength in Fig. 6.14. For rotation rates of 2000 and 2800 rpm, the power per unit flux passes through a minimum at 40-60 V/cm. The shapes of these curves are in accord with the model as shown below.

Neglecting the pumping power,

$$^{\circ}P_{\mathbf{T}} = a_{1}\Omega^{2.8} + a_{2}E^{2}$$
 (6-17)

where a<sub>1</sub> and a<sub>2</sub> are quantities which may be readily obtained from Eqs. (6-10) and (6-15). Using the results of Section 6.3, the steady state flux may be written

$$J_{\infty} = a_{3}\Omega^{0.9} + a_{4}E$$
 (6-18)

where  $a_3$  and  $a_4$  may be found from Eq. (6-9). Hence

$$\frac{P_{\rm T}}{J_{\infty}} = \frac{a_1 \Omega^{2.8} + a_2 E^2}{a_3 \Omega^{0.9} + a_4 E}$$
 (6-19)

At low field strengths: \*

FIGURE 6.14. Plot of Total Power Per Unit Flux Versus Field Strength

$$\frac{P_{\mathrm{T}}}{J_{\infty}} \rightarrow \left(\frac{a_{1}}{a_{3}}\right)\Omega^{1.7} \tag{6-20}$$

and the power per unit flux increases with rotation rate. At high field strengths:

$$\frac{P_{\mathrm{T}}}{J_{\infty}} + \left(\frac{a_2}{a_4}\right) E \tag{6-21}$$

and the power per unit flux increases with field strength. A minimum in  $P_{\rm T}/J_{\infty}$  at a particular value of E is found by differentiating Eq. (6-19). The minimum value of  $P_{\rm T}/J_{\infty}$  occurs at

$$E = \frac{a_3}{a_4} \left[ \sqrt{1 + \left(\frac{a_1}{a_2}\right) \left(\frac{a_4}{a_3}\right)^2 \Omega} - 1 \right]$$
 (6-22)

and the field strength at which the minimum  $P_{\rm T}/J_{\infty}$  occurs increases with rotation rate. The predictions are in qualitative agreement with the results presented in Fig. 6.14.

#### CHAPTER 7

# CONCLUSIONS

The tangential flow electrofilter is a modification of the tangential flow filter in which a DC electric field is imposed between the rotating inner cylinder and the stationary outer cylinder. In the tangential flow electrofilter, four transport mechanisms are used to minimize the accumulation of particles at the surface of the filter medium. These transport mechanisms are fluid turbulence, centrifugal force, electrophoresis and shear stress at the rotating surface. Turbulence, centrifugal force and electrophoresis move individual particles away from the filter medium, while shear on the surface removes aggregates of particles. A steady state flux results when the particle velocity toward the membrane due to the filtrate flux equals the particle velocity away from the membrane due to the cumulative effect of the four transport mechanisms.

Experiments were conducted with a dilute, aqueous polystyrene latex suspension having a particle size of 0.60 µm and a
zeta potential of -60 mV. Rotation rates up to 2800 rpm and
electric field strengths up to 240 V/cm were employed at two
values of the transmembrane pressure difference, approximately
68.9 kPa and 137.8 kPa. The measured filtrate fluxes and particle retentions showed the following:

(a) Filtrate flux increased with electric field strength up to about 100 V/cm. Rejections were at most 1-2%

lower at higher field strengths.

(b) Filtrate flux increased with rotation rate, while rejections decreased somewhat.

In all cases, the particle rejections were larger than 94%.

A mathematical model was derived for a filtration process in which a cake builds up on the surface of the filter medium. The model takes into account any removal mechanism leading to a steady state filtration flux. In applying the model to the tangential flow electrofilter, all four mechanisms of particle transport were taken into account. Computations from the model showed that centrifugal force was much less effective than the other mechanisms for the rotation rates and equipment size used here.

The small time (t  $\rightarrow$  0) version of the model predicted that a plot of  $(1/J^2-1/J_0^2)$  versus time should yield a straight line near time zero. The flux data for all rates of rotation, field strengths and pressure differences were linear as predicted. The specific cake resistances were obtained from these plots. Without an electric field, the specific cake resistances were similar to those found by Doshi and Trettin (1980) for a commercial latex. Both increasing rotation rate and increasing electric field strength decreased the specific cake resistance, i.e. the cakes were more porous.

The steady state version of the model was used to predict the effects of rotation rate and electric field strength on the filtrate flux. The measured fluxes at 90 minutes,  $J_{90}$ , were compared to these predictions. The  $J_{90}$ -values were roughly ,

proportional to  $N^{0.9}$ , indicating that turbulence may be the major rotating mechanism moving particles away from the filter medium. The  $J_{90}$ -values increased linearly with electric field strength. The rate of increase was in fair agreement with the model prediction. Above a field strength of 100 V/cm,  $J_{90}$  reached a broad maximum and then declined at higher field strengths. This decline is attributed to the generation of hydrogen bubbles which block the pores of the filter. The model does not apply to this situation.

## NOMENCLATURE

, •	
Α '	parameter defined in Eq. (2-13)
a	constant in Eq. (2-21)
a <sub>1</sub> ,a <sub>2</sub>	parameters in Eq. (6-16)
a <sub>3</sub> ,a <sub>4</sub>	parameters in Eq. (6-17)
b ·	"gap" width = R - R, cm
С	concentration of solids in bulk, g/cm,
c <sub>D</sub>	drag coefficient
Ce L	electrical conductivity of the suspension, amp V·cm
C <sub>f</sub>	concentration of solids in feed, g/cm <sup>3</sup>
C <sub>p</sub> ,	concentration of solids in permeate, g/cm3
Cs	saturation concentration of solids, g/cm <sup>3</sup>
Ď	particle diffusivity, cm <sup>2</sup> /s
d <sub>p</sub>	particle diameter, cm
E	electrical field strength, V/cm
Ec	critical electrical field strength, V/cm
F(K)	parameter defined in Eq. (A2-5)
f(Y)	function, see Eq. (5-20)
f(Yo)	function, see Eq. (5-22)
G(κ)΄ .	parameter defined in Eq. (A2-4)
I.	current, amp
J	volumetric filtrate flux per unit area, cm/s
J <sub>D</sub>	diffusion flux of solute away from membrane, cm/s
J <sub>f</sub>	distilled water flux for used Acropor support at $N = 2000$ rpm, $\Delta P_m = 68.9$ kPa, cm/s

```
J_{i}
            distilled water flux for fresh Acropor'support at
            N = 2000 \text{ rpm}, \Delta P_m = 68.9 \text{ kPa, cm/s}
 Jo
            volumetric flux per unit area when t = 0 with poly-
            styrene latex suspension as feed, cm/s
 JO
            distilled water flux when t = 0, cm/s
J<sub>9,0</sub>
            volumetric flux per unit area after 90 minutes of
            operation, cm/s
\mathtt{J}_{\infty}
            volumetric flux per unit area at steady state, cm/s
           parameter defined in Eq. (5-10)
K
            constant in Eq. (3-1)
K
           mass transfer coefficient, cm/s
k
KC
            constant in Eq. (5-2)
Ke
            electrophoretic mobility,
           electroosmotic coefficient as defined in Eq. (2-9)
K_{M}
           constant in Eq. (5-39)
K_R
          . constant in Eq. (5-29)
Kt
           length of inner cylinder, cm
           exponent in Eq. (6-7)
           rotation rate = .60\Omega/2\pi, revolutions per minute
Ν
           pressure, kPa
P
           power required to rotate inner cylinder, W
           electrical power per unit (outside) area of inner
           cylinder, W/m<sup>2</sup>
^{P}_{\mathrm{p}}
           pumping power per unit (outside) area of inner cyl-
           inder, W/m2
           rotational power per unit (outside) area of inner
{}^{p}r
           cylinder, W/m2
           total power consumed (rotational, electrical and
           pumping) per unit (outside) area of inner cylinder,
           W/m^2
           volumetric circulation rate, cm3/s
```

```
radius, cm
           percentage rejection of particles
           radial position, cm
           filter cake resistance, \frac{kPa}{cm/s}
R_{\mathbb{C}}
Re
           Reynolds number = 2R_i \rho u_i / \mu
           filter medium resistance, \frac{kPa}{cm/s}
           parameter defined in Eq. (6-5)
           fractional transmittance
           time, s
           Taylor number, \frac{i}{v}
Тa
           Taylor number beyond which flow ceases to be laminar
Tag
           fractional transmittance of feed
Tf
           fractional transmittance of permeate
           particle velocity, cm/s
           peripheral velocity of rotating inner cylinder = \Omega R_i,
           friction velocity = \frac{C_D}{2} (\Omega R_i), cm/s
           voltage, V
           mean tangential velocity of fluid = 0.52 \Omega R_i, cm/s
           dummy variable, see Eq. (5-19)
           dummy variable, see Eq. (5-22)
Greek Symbols
           specific cake resistance, cm/g
           boundary layer thickness, cm
```

pressure difference due to axial flow, kPa

thickness of cake, cm

ΔΡ

```
\Delta P_{\mathbf{F}}
            pressure difference causing filtration, kPa.
ΔP<sub>m</sub>
            measured pressure difference, kpa
           porosity or void fraction
            zeta potential of latex suspension, V
            dielectric constant of latex suspension
            ratio of radius of inner cylinder to that of outer
           cylinder, R,/R
            fluid viscosity, g/cm·s
           viscosity of latex suspension, g/cm·s
           Kinematic viscosity of fluid, cm2/s
           fluid density, g/cm3
           particle density, g/cm<sup>3</sup>
           density of latex suspension, \sqrt{cm^3}
           shear force on rotating inner cylinder, Pa
τa
           shear force due to axial flow, Pa
\tau_{\mathtt{r}}
           shear force due to rotation, Pa
\phi_{R} .
           rate of cake removal by shear forces at the surface
           of the cake, g/cm<sup>2</sup>·s
           parameter in Eq. (A3-7)
           parameter defined in Eq. (A3-4)
\psi_{\text{II}}
           parameter defined in Eq. (A3-6)
Ω.
           angular velocity of rotation of inner cylinder,
           radians/s
           critical angular velocity, radians/s
```

In this study,  $\mu = \mu_s$  and  $\rho = \rho_s$ .

# Subscripts

44

a	on axis of rotation
e	due to electric force
ʻi ຸ	outside of inner cylinder
ii	inside of inner cylinder
0 ,	inside of outer cylinder
p	~plateau
r	due to rotation
s ,	relative to fluid
t	due to fluid turbulence

#### REFERENCES

- Beechold, H., Ultrafiltration and electro-ultrafiltration in "Colloid Chemistry", Vol. 1 (Alexander, J., ed.), The Chemical Catalog Company, 1926.
- Bier, M., ed., "Electrophoresis", Vol. 1, 263, Academic Press, New York, 1959.
- Bier, M., Electrokinetic membrane processes in "Membrane Processes in Industry and Biomedicine", Plenum Press, New York, 1971.
- Bird, R.B., W.E. Stewart and E.N. Lightfoot, "Transport Phenomena", Ch. 2, John Wiley and Sons, New York, 1960.
- Blatt, W.F., A. Dravid, A.S. Michaels and L. Nelson, Solute polarization and cake formation in membrane ultrafiltration; causes, consequences and control techniques in "Membrane Science and Technology", Ch. 4 (Flinn, J.E., ed.), Plenum Press, New York, 1970.
- Carman, P.C., "Flow-of Gases Through Porous Media", Ch. 1,
  Academic Press, New York, 1956.
- Cooper, F.C., Q.M. Mees and M. Bier, Water purification by forced flow electrophoresis, J. Sanitary Eng. Div., A.S.C.E. 91, 13-24 (1965).
- Dahlheimer, J.A., D.G. Thomas and K.A. Kraus, Application of woven fiber hoses to hyperfiltration of salts and cross flow filtration of suspended solids, Ind. Eng. Chem. Process Design Development 9, 566-572 (1970).
- de Filippi, R.P. and R.L. Goldsmith, Application and theory of membrane processes for biological and other macromolecular solutions in "Membrane Science and Technology", Ch. 2 (Flinn, J.E., ed.), Plenum Press, New York, 1970.
- Doshi, M.R. and D.R. Trettin, Ultrafiltration in an unstirred batch cell, Ind. Eng. Chem. Fundamentals 19, 189-194 (1980).
- Friedlander, S.K., "Smoke, Dust and Haze", Ch. 4, John Wiley and Sons, New York, 1977.
- Friedlander, S.K. and H.F. Johnstone, Deposition of suspended particles from turbulent gas streams, Ind. Chem. Eng. 49, 1151-1156 (1959).

- Grushka, E., K.D. Caldwell, M.N. Myers and C.J. Giddings, Field flow fractionation, Separation and Purification Methods, Vol. 2, Part 1, 127-151 (1973).
- Henry, J.D., Cross flow filtration in "Recent Developments in Separation Science", 2 (Li, N.N., ed.), 205-225, CRC Press, Cleveland, 1972.
- Henry, J.D. and R.C. Allred, Concentration of bacterial cells by cross flow filtration, <u>Dev. Ind. Microbiol.</u> 13, 5-9 (1977).
- Henry, J.D., L.F. Lawler and C.H.A. Kuo, A solid/liquid separation process based on cross flow and electrofiltration, AIChE Journal 23, 851-859 (1977).
- Karnis, A., H.L. Goldsmith and S.G. Masón, The flow of suspensions through tubes. V. Inertial effects, Can. J. Chem. Eng. 44, 181-193 (1966).
- Kern, D.Q., Heat exchanger design for fouling services, <u>Proc.</u>

  3rd International Heat Transfer Conference, Vol. 1,

  170-178, August 1966.
- Kern, D.Q. and R.E. Seaton, Surface fouling ... how to calculate . limits, Chem. Eng. Prog. 55(6), 71-73 (1959).
- Kotera, A., K. Furusawa and Y. Takeda, Colloid chemical studies of polystyrene latices polymerized without any surface-active agents, Department of Chemistry, Tokyo Kyoiku University, Tokyo, 1970.
- Kraus, K.A., Cross flow filtration and axial filtration, paper presented at the 29th Annual Purdue Industrial Waste Conference, Lafayette, Indiana, May 1974.
- Manegold, E., The effectiveness of filtration, dialysis, electrolysis and their intercombinations as purification processes, Trans. Faraday Soc. 33, 1088-1094 (1937).
- Margaritis, A. and C.R. Wilke, Engineering analysis of rotorfermentor, Dev. Ind. Microbiol. 13, 54-57 (1971).
- McCabe, W.L. and J.C. Smith, "Unit Operations of Chemical Engineering", McGraw-Hill, New York, 1967.
- Mikhlin, J.A., Fine particle separation from low-concentrated suspensions on moving porous surfaces under low pressure, Israel J. of Technology 14, 226-230 (1976).
- Mikhlin, J.A. and G.B. Tanny, An investigation of the mechanism of dynamic membrane formation on rotating microporous surfaces, J. Col. Int. Sci. 68, 157-165 (1979).

- Moulik, S.P., F.C. Cooper and M. Bier, Forced-flow electrophoretic filtration of clay suspensions, J. Col. Int. Sci. 24, 427-432 (1967).
- Porter, M.C., Concentration polarization with membrane ultrafiltration, Ind. Eng. Chem. Product R & D 11, 234-248 (1972a).
- Porter, M.C., Ultrafiltration of colloidal suspensions, AIChE Symposium Series 68, No. 120, 21-30 (1972b).
- Porter, M.C. and L. Nelson, Ultrafiltration in the chemical, food processing, pharmaceutical and medical industries in "Recent Developments in Separation Science", 2 (Li, N.N., ed.), 227-267, CRC Press, Cleveland, 1972.
- Reis, J.F.G. and E.N. Lightfoot, Electropolarization chromatography, AIChE Journal 22, 779-785 (1976).
- Schlichting, H., "Boundary Layer Theory", 6th Ed., Ch. XVII, McGraw-Hill, New York, 1968.
- Seoud, H., Ph.D. Thesis, Department of Chemical Engineering, McGill University, Montreal, 1980.
- Strong A.B. and L. Carlucci, An experimental study of mass transfer in rotating Couette flow with low axial Reynolds number, Can. J. Chem. Eng. 54, 295-298 (1976).
- Taborek, J., T. Akoi, R.B. Ritter and J.W. Palen, Predictive methods for fouling behavior, Chem. Eng. Prog. 68(7), 69-78 (1972).
- Taylor, G.I., Stability of a viscous fluid contained between two rotating cylinders, Phil. Trans. 223, 289-293 (1923).
- Taylor, G.I., Distribution of velocity and temperature between , rotating concentric cylinders, Proc. Roy. Soc. Al51, 494-512 (1935).
- Taylor, G.I., Fluid friction between rotating cylinders. I.
  Torque measurements, Proc. Roy. Soc. A157, 546-564 (1936)
- Trettin, D.R. and M.R. Doshi, Ultrafiltration in an unstirred batch cell, presented at ACS Meeting, Washington, D.C., September 1979 (submitted to Ind. Eng. Chem. Fundamentals)

TABLE A1-1

## Small Time Slopes from Cake Filtration Plots

 $\Delta P_{\rm m} = 68.9 \text{ kPa}$ Slope, S (s/m<sup>2</sup>)

E W/cm		N (rpm)		
E, V/cm	0	1200 -	2000	2800
0-	8.00x10 <sup>4</sup>	6.35×10 <sup>4</sup>	4.90x10 <sup>4</sup>	3.90×10 <sup>4</sup>
<b>2</b> 25	2.05x10 <sup>4</sup>	1.32x10 <sup>4</sup>	1.94x10 <sup>3</sup>	$4.02 \times 10^3$
, 45	1.19x10 <sup>4</sup>	6.54x10 <sup>3</sup>	1.16x10 <sup>3</sup>	- ( .
87.5	9.62x10 <sup>3</sup>	1.89x10 <sup>3</sup>	1.16x10 <sup>3</sup>	3.80x10 <sup>2</sup>
131 •	• •••	′ - <del>-</del>	4.75x10 <sup>2</sup>	2.01x10 <sup>2</sup>
175 .	2.76x10 <sup>3</sup>	1.16x10 <sup>3</sup>	~ <b>-</b>	. <del></del>
237.5	3.26x10 <sup>3</sup>	-	_ `	

TABLE Al-2

# Small Time Slopes from Cake Filtration Plots

 $\Delta P_{m} = 137.8 \text{ kPa}$ Slope, S  $(s/m^2)$ 

E W/cm	N (rpm)			
E, V/cm	0	1200	2000	2800
۲۰ ه	4.70×10 <sup>4</sup>	2.91x10 <sup>4</sup>	_	1.28x10 <sup>4</sup>
25	1.57×104	7.90×10, <sup>3</sup>	-	3.33×10 <sup>3</sup>
. 45	6.11x10 <sup>3</sup>	2.58×10 <sup>3</sup>	1.17x10 <sup>3</sup>	-
87.5	-	1.68x10 <sup>3</sup>	7:62x10 <sup>2</sup>	3.60x10 <sup>2</sup>
× 131	2.46x10 <sup>3</sup>	8.55x10 <sup>2</sup> ,	3.56x10 <sup>2</sup>	2.52x10 <sup>2</sup>
175	1.94x10 <sup>3</sup>	<u>-</u>	-	~
237.5	1.68x10 <sup>3</sup>	· -	_	~

#### SHEAR FORCE ON THE INNER CYLINDER

The shear force on the rotating inner cylinder has an axial component,  $\tau_a$ , due to the axial suspension flow as well as a tangential component,  $\tau_r$ , due to rotation. The shear force is given by the vector sum of these two components. The magnitude of the shear force,  $\tau$ , is given by

$$\tau = \sqrt{\tau_a^2 + \tau_r^2} \tag{A2-1}$$

In order to estimate the importance of  $\tau_a$  and  $\tau_r$ , each is assumed to have the value it would have in the absence of the other.

For a volumetric feed flow rate, Q, of 26.7 cm<sup>3</sup>/s, the average axial velocity is 1.46 cm/s and the Reynolds number based on the hydraulic diameter is 130. Therefore, in the absence of rotation, the axial flow is laminar. The equations for the surface shear stress for axial flow through an annulus can be derived from Bird, Stewart and Lightfoot (1960):

$$\tau_{a} = -\frac{4\mu Q}{\pi R} \frac{\left[G(\kappa)\right]}{F(\kappa)}$$
 (A2-2)

where

$$\kappa = R_1/R_0 \tag{A2-3}$$

$$G(\kappa) = \kappa + \frac{1 - \kappa^2}{2\kappa \ln \kappa}$$

$$(A2-4)$$

$$F(\kappa) = (1 - \kappa^4) + \frac{(1 - \kappa^2)}{\ln \kappa}$$

The tangential component of the shear force is given by Eq. (2-20) after substitution of Eq. (5-35):

$$\tau_{r} = 9.58 \times 10^{-3} \, \mu^{0.2} \rho^{0.8} R_{i}^{1.6} \Omega^{1.8}$$
 (A2-6)

Using the physical properties of water at 25°C, a volumetric flow rate of 26.7 cm<sup>3</sup>/s and a rotational speed of 1200 rpm, the following values were computed

$$\tau_{a} = 1.02 \times 10^{-2} \text{ Pa}$$

$$\tau_{r} = 14.5 \text{ Pa}$$

Hence, for all runs with rotation,  $\tau_a$  can be neglected.

# RELATIONSHIP BETWEEN $\Delta P_F$ AND $\Delta P_{ff}$

The pressure driving force causing filtration is the excess pressure difference over rigid body rotation. It is given by Eq. (5-42):

$$\Delta P_{F} = (P_{i} - P_{ii}) - \frac{\rho}{2} \Omega^{2} (R_{i}^{2} - R_{ii}^{2}) \qquad (5-42)$$

In the present work, the measured pressure,  $\Delta P_m$ , was the difference between the feed pressure and the atmosphere. It was assumed that

$$\Delta P_{\rm m} = P_{\rm p} - P_{\rm a} \tag{5-43}$$

To derive the relationship between  $\Delta P_{m}$  and  $\Delta P_{F}$ , two cases were considered.

## Case I: inner cylinder full of liquid

The pressure profile for this case is shown in Fig. A3.1. The pressure is taken to be atmospheric on the axis. Since the fluid inside the inner cylinder rotates as a rigid body (except for the small filtrate flux), the pressure increases quadratically with radius to P<sub>ii</sub> at R<sub>ii</sub>:

$$P_{ii} = P_{a}^{(i)} + \frac{\rho}{2} (\Omega R_{ii})^2$$
 (A3-1)

The pressure continues to rise across the wall of the inner

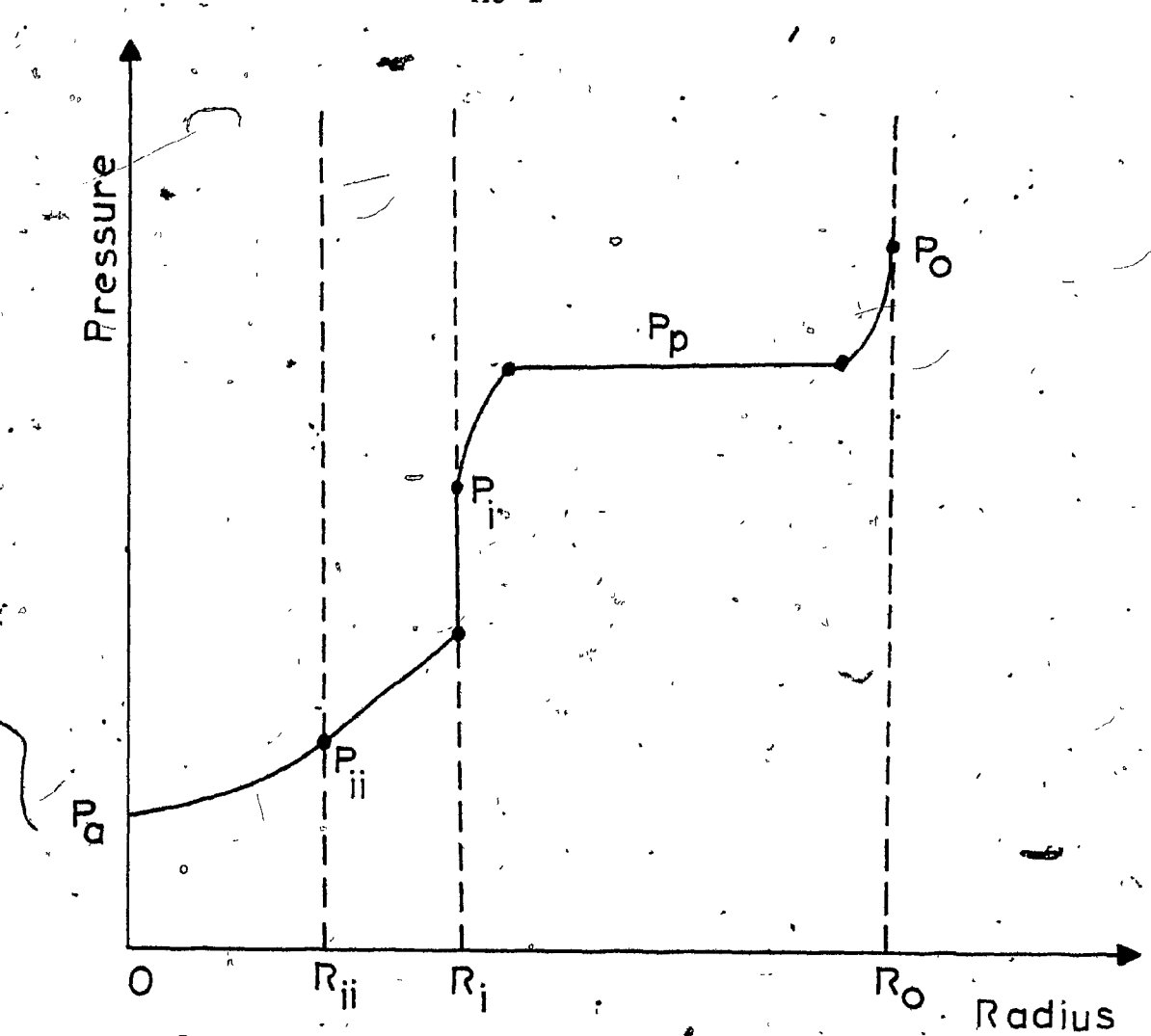


FIGURE A3.1.' Pressure Variation in Radial Direction with Inner Cylinder Full

tube. The sharp pressure increase at R<sub>i</sub> is due to the resistance of the medium and the cake. The pressure profile across the gap is described in Section 2.3.1.

Combining Eqs. (2-23), (2-24), (A3-1) and (5-43) yields

$$\Delta P_{F} = \Delta P_{m} - \frac{\rho \Omega^{2} R_{i}^{2}}{2} \psi_{I} \qquad (A3-2)$$

where

$$\psi_{I} = 1 - 0.27 \left[ \left( \frac{R_{i}}{R_{o}} \right)^{2} \left( \frac{1.9 R_{i} + 0.1 R_{o}}{0.9 R_{i} + 0.1 R_{o}} \right) - 1 \right]$$
 (A3-3)

For the present apparatus:  $R_{ii} = 3.05$  cm,  $R_{i} = 3.25$  cm,  $R_{o} = 4.05$  cm and  $\psi_{I} = 0.926$ .

### Case II: inner cylinder empty

The pressure profile for this case is sketched in Fig. 5.4 and discussed in Section 5.4. For this case

$$P_{ii} = P_{a} \tag{A3-4}$$

replaces Eq. (A3-1). The final result is-

$$\Delta P_{F} = \Delta P_{m} - \frac{\rho \Omega_{R_{i}}^{2}}{2} \psi_{II}$$
 (A3-5)

0 where

$$\psi_{II} = \psi_{I} - (R_{ii}/R_{i})^{2}$$
 (A3-6)

For the present apparatus:  $\psi_{II} = 0.0453$ .

#### Discussion

The form of the equation for  $\Delta P_{\mathbf{F}}$  can be written as follows.

$$\Delta P_{F} = \Delta P_{m} - \frac{\rho \Omega^{2} R_{i}^{2}}{2} \psi \qquad (A3-7)$$

The pressure driving force decreases as the rotation rate increases. The large difference between  $\psi_{\rm I}$  and  $\psi_{\rm II}$  shows that

the condition within the inner cylinder can have an important effect by reducing the driving force for filtration.

In the present work, experiments were carried out at two values of  $\Delta P_m$ : 68.9 kPa and 137.8 kPa. Table A3-1 gives the values of  $\Delta P_F$  predicted by the two cases for four values of the rotation rate (with  $\rho=982$  kg/m³).

TABLE A3-1 .
Filtration Pressure Difference

 $\Delta P_{F}$ , kPa

Rotation Rate	$\Delta P_{m} = 68.9 \text{ kPa}$		$\Delta P_{m} = 137.8 \text{ kPa}$			
rpm	Case I	Case II	Case I	Case II		
0	<u>6</u> 8.9	68.9	137.8	137.8		
1200	61.3	الم 68.5	130.2	137.4		
2000	47.8	. 67.9	116.7	136.8		
2800	27.6	66.9	9635	135.8,		

For the small pressure differences used here, the effective driving force for filtration is reduced significantly if the inner cylinder runs full.

To test this analysis, predictions of the decrease in flux with increasing rotation rate were compared with flux data for distilled water. Since there is no cake when using distilled water,

$$J = \frac{\Delta P_{\mathbf{F}}}{R_{\mathbf{M}}}$$

where  $R_{M}$ , the membrane resistance, is not a function of the rotation rate. Denoting the flux at the same  $\Delta P_{m}$  without rotation as  $J^{O}$  and combining Eqs. (A3-7) and (A3-8) yields

$$\frac{J}{J^{\circ}} = 1 - \frac{\rho \psi \left(\Omega R_{1}\right)^{2}}{2\Delta P_{m}}$$

(A3-9)

Assuming Case I and using ( $\rho = 982/kg/m^3$ ), the following comparison between the predictions of Eq. (A3-9) and measurements is obtained

TABLE A3-2
Fluxes for Distilled Water

Flux Ratio, J/JO

Rotation	$\Delta P_{\hat{m}} = 68.9 \text{ kPa}$		$\Delta P_{m} = 137.8 \text{ kPa}$			
Rate rpm	Predicted Eq. (A3-9)	Measured	Predicted Eq. (A3-9)	Measured		
_ 0	1.00	1.00	1.00	1.00		
1200	0.89	0.77	0.95	0.87		
2000 °	0.70	0.62	0.85	0.71		
280,0	0.40	0.50	0.70	- 0.63		

The agreement between the predictions and the data is fair. Equation (A3-9) predicts that the quantity  $(1 - J/J^0)$  should be proportional to  $\Omega^2$ , while the data show a more linear relationship. This is probably due to the fact that the inner cylinder was not completely full. At the higher fluxes, the inner

tube ran more full. Therefore, with the very much lower fluxes obtained in the filtration runs it is believed that Case II is the more likely. Hence, in the latex experiments the driving force was essentially independent of rotation rate.

# COMPARISON OF POWER REQUIREMENTS FOR ROTATION OF THE TANGENTIAL FLOW FILTER AND THE ROTORFERMENTOR OF MARGARITIS AND WILKE

The tangential flow filter is similar to a device used by Margaritis and Wilke (1971) to remove liquid from a fermentation broth. The power requirements for the rotation of the present design are plotted in Fig. A4.1 for several diameters of the rotating inner cylinder. In all cases,  $R_{\rm o}/R_{\rm i}=1.25$ . A similar plot from Margaritis and Wilke is included as Fig. A4.2.

Table A4-1 presents a comparison between the rotational power requirements of the present design and the rotorfermentor. The tangential flow filter requires less power for rotation than Margaritis and Wilke's device.

TABLE A4-1

Power Requirements for Rotorfermentor (RF)

and the Tangential Flow Electrofilter (TFE)

Power per unit length, W/m

		1,				
Rotation Rate		* .	D (	cm)	* 1	,
	2.	54 5.08		10.16		
rpm	.TFE	, RF	TFE 🕏	' RF	TFE	RF
500	0.036	0.195	0.449	1.95	5.23	29.2
1000	0.234	1.17	3,12	13.7	36.4	234

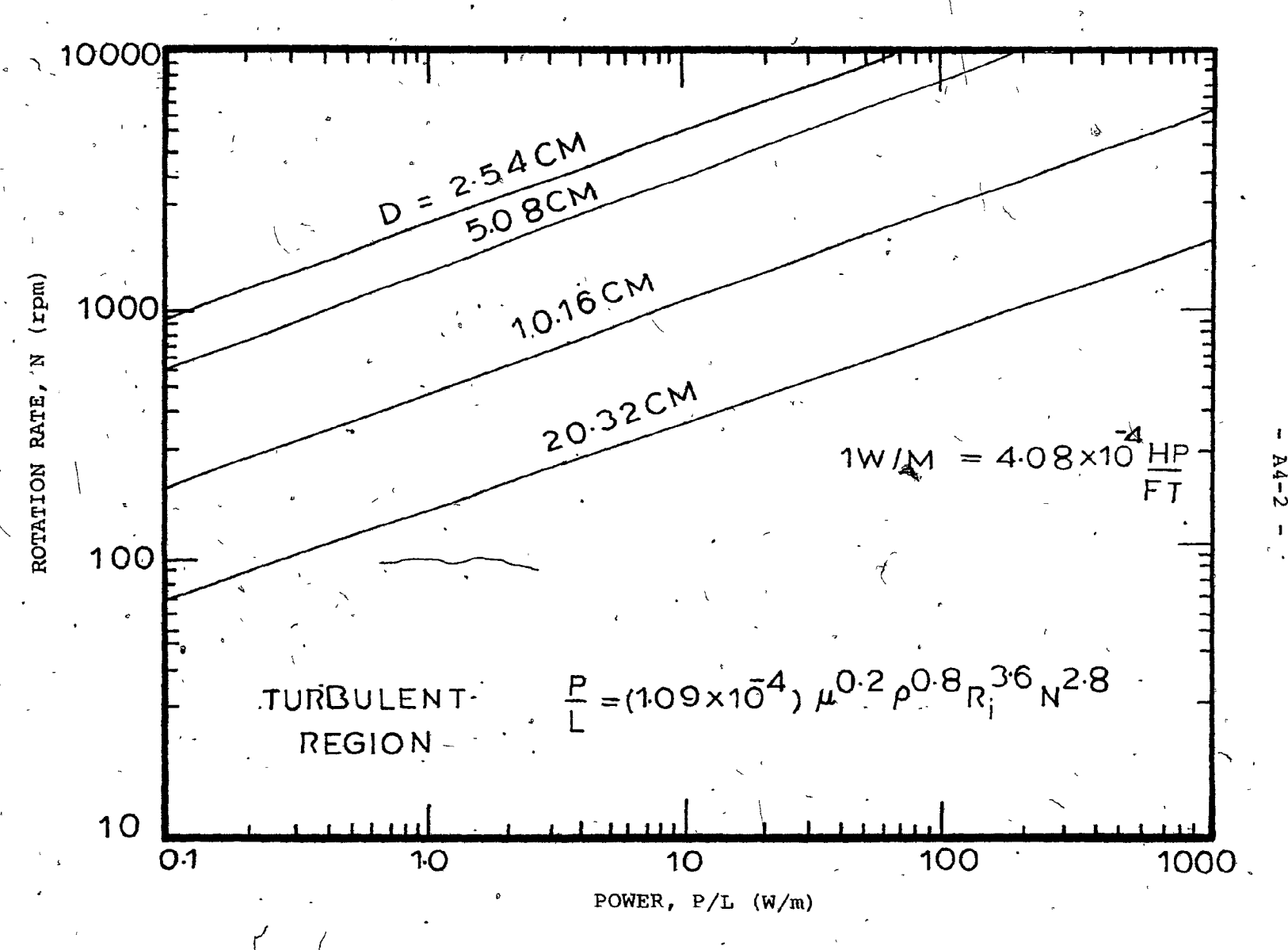


FIGURE A4.1. Plot of Rotation Rate Versus Power Per Unit Length for Tangential Flow Electrofilter

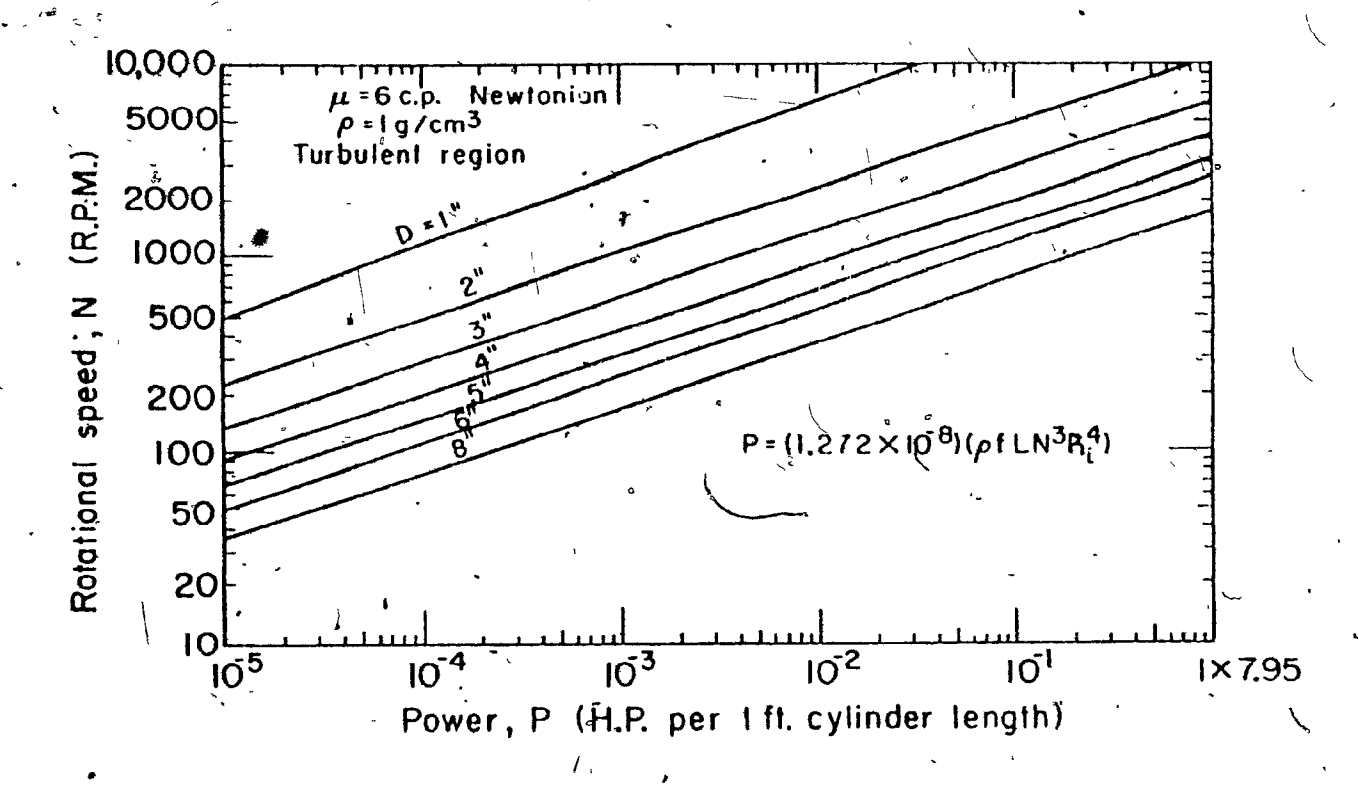


FIGURE A4.2. Plot of Rotation Rate Versus Power Per Unit Length for Margaritis and Wilke Rotorfermentok